THE APPLICATION OF THE SAG POWER INDEX TO ORE BODY HARDNESS CHARACTERIZATION FOR THE DESIGN AND OPTIMIZATION OF AUTOGENOUS GRINDING CIRCUITS

Peter Amelunxen

Department of Mining, Metals and Materials Engineering,

McGill University, Montreal

Advisor: Dr. André Laplante,

McGill University, Montreal

October 2003

A thesis submitted to McGill University in partial fulfillment of the requirements of the degree of Masters of Engineering, Department of Mining, Metals and Materials Engineering.

Your file Votre référence
ISBN: 0-612-98509-1
Our file Notre référence
ISBN: 0-612-98509-1

ABSTRACT

The SAG Power Index test (SPI) is a tool for forecasting autogenous mill performance. Much effort has been directed towards the development of the process models relating SPI to throughput estimates, but little has been directed towards ore body modeling. Blending studies are presented showing that the SPI is not additive, affecting the geostatistical procedures. A method is given to ensure that additivity is respected during geostatistical interpolation. A procedure for relating mean SPI precision to sample spacing is given. This procedure is combined with a study of the process model error to estimate the precision of the mean throughput forecasts. A case study from Chino Mines is discussed. The relative throughput error is between 20 and 26 percent for perfect knowledge of SPI. For 100 m sample spacing at Chino, one third of the error is due to the process models and the rest to the SPI estimates.

RÉSUMÉ

L'essai d'indice de puissance SAG (SPI pour « SAG Power Index » en anglais) sert à prédire la capacité des broyeurs SAG. Plusieurs modèles de processus unitaires ont été développés pour permettre cette prédiction, ce qui n'est pas le cas des modèles géostatistiques de la distribution des valeurs de SPI dans les gisements. Des études de mélange d'échantillons montrent que le SPI n'est pas une variable additive, ce qui complique son utilisation en géostatistique. Nous présentons une méthode qui résout ce problème en restituant au SPI son additivité. Nous présentons une procédure qui fait le lien entre la maille de détermination du SPI et la précision du SPI moyen. Nous présentons une étude de cas pour la mine Chino. Nous combinons cette procédure à une étude des erreurs des modèles de procédés utilisés dans la prédiction de la capacité des circuits de broyage SAG pour en estimer la précision, qui se situe entre 20 et 26%. Lorsque la maille d'échantillonnage à Chino est de 100 m, un tiers de l'erreur de prédiction provient des modèles de processus unitaires et deux tiers des erreurs de SPI.

TABLE OF CONTENTS

LIST OF FIGURES

LIST OF TABLES

LIST OF EQUATIONS

1 INTRODUCTION

Beginning in the middle of the 20th century a trend began to emerge in the design and construction of comminution circuits. Large-diameter autogenous (AG) and semi-autogenous grinding (SAG) mills began to replace the two-stage process of secondary crushing and rod-milling. Autogenous mills brought with them lower operating costs, but at a price. The lower steel charges in the autogenous mills and their dependence on large ore pieces for grinding media rendered them susceptible to production swings caused by abrupt changes in ore hardness and competency.

Initially, the transition to autogenous milling forced the design engineers to cope with the design complexities of large-diameter mills without adequate scale-up technology. The practice developed to perform large-scale pilot-plant studies, an expensive and lengthy prospect often requiring hundreds of tonnes of ore sample. However, the same ore hardness variability that caused the production swings in the full-scale mills created problems in their pilot counterparts. If autogenous milling is so susceptible to abrupt ore changes within the ore body, how could the design team be certain that the ore used for the pilot plant was representative of the ore that will be processed by the full-scale installation?

Driven by lower operating costs, the diameters of autogenous mills and their capital costs have steadily increased[1] over the past 25 years, adding to the risk and cost of design errors and exacerbating the problem of inadequate scale-up technology.

As the risk increased, engineers began to adopt the Bond work index, product of a 10-kg test long-used for ball mill scale-up, for use in conjunction with pilot plant work. The Bond test, when performed on samples collected from the ore body, provided a measure of the ore hardness variability. This measure could be used to "correct" the pilot plant

[1] For example, during the five years from 1975 to 1980, only 3 wet autogenous mills with diameter greater than 35 feet (10.67 m) were installed worldwide. Between 1995 and 2000, 13 were installed worldwide (Jones 2001).

results and thereby avoid design errors that would have resulted from a sampling problem. Although an improvement over an exclusive pilot-plant-based design, this method, still in use today, is flawed because the Bond test was developed as a model for ball mill scale-up, and therefore has difficulties measuring hardness variability for autogenous mills.

The 1970's and 1980's saw the introduction of various alternative tests for autogenous mill scale-up. They include the McPherson autogenous work index test, the JKMRC technology[2], and the Media Competency test. These tests have become useful for predicting AG/SAG behaviour, but they suffer from large sample mass requirements (although not quite as large as pilot plant work). The costs of diamond drilling and the small diameter of core samples make it an expensive prospect to use these tests for ore body characterization. The SAG Power Index[3] (SPI) test was developed in an attempt to adequately model AG/SAG mills while providing a cheaper alternative for characterizing ore bodies.

The test employs a small laboratory mill (30.5 cm diameter) to grind a 2 kg of sample from a fixed starting size to a fixed product size. The SPI, measured in minutes, is the time it takes to grind the ore, and it is used to calculate the energy requirements of a full-scale mill in a manner similar to the Bond method for ball mills. It has gained acceptance for AG/SAG circuit design, and much work has been done to examine its feasibility for use in AG/SAG circuit modeling and scale-up. A computer program called CEET[4] was developed to perform the scale-up calculations on a virtually unlimited data set of SPI values, facilitating the use of the index in geologic models and mine block models. To date, however, no detailed examination has been undertaken to investigate its application to ore body characterization; *i.e.* how should the SPI values be incorporated into the block models in the first place?

---

[2] Which includes drop-weight tests, abrasion tests, and a modeling suite

[3] The SPI is a proprietary test exclusively marketed by Minnovex Technologies Inc., a Toronto-based mineral processing technology company. This thesis was performed with technical and financial support from Minnovex.

[4] Refer to Section 2.1.4.3 for detailed description of CEET and the nature of the scale-up calculations

There are two main issues that have not been addressed. The first involves the question of additivity of the SPI index. Geostatistical or geometrical interpolation procedures assume that the parameter being interpolated can be linearly averaged. Gold grades, for example, are additive. If one were to blend a high-grade gold ore with an equal amount of low-grade ore, the grade of the resulting blend would be the average of the grades of the parent ores. Permeability, on the other hand, is not an additive parameter and is therefore more difficult to model geostatistically. Preliminary work performed in 1997 suggested that the SPI may not be additive[5], *i.e.* that blends are "softer" than the weighted average predicts. This research project investigates the additivity of the SPI by performing SPI tests on a series of blended and unblended ores. The results are presented in Section 3.

The second main issue involves determining the proper size and scope of an ore body sampling campaign. Simply stated: for a given ore body, how many samples should be collected and tested for SPI? Some ore bodies have been characterized with as few as 15 samples and others with as many as 1300. Answering this question is linked to the precision that would result from different scopes of sampling campaigns and the direct needs of the mine. There are two main sources of error in the calculations used to convert SPI to throughput (or mill power and diameter, if for design). One is a result of the geostatistical interpolation procedure and is a function of the distance between samples (*i.e.* the number of samples and the spatial variability of ore hardness). The other is the imprecision of the calculations used to convert SPI measurements to mill capacities. Quantifying these errors is prerequisite to determining the proper scope of a sampling program.

To answer the question of error attributable to geostatistical interpolation of SPI values, this work presents a method for calculating the precision of mean SPI values in an ore zone as a function of the spacing between SPI samples. This method can be used to optimize the scope of a sampling campaign such that the acceptable error levels of the throughput estimates are achieved.[6] An example from Chino Mines is used to illustrate

[5] See Section 2.3.2

[6] It is assumed that the mine knows what level of precision is desired. This is associated with the cost of the imprecision in forecast or design errors.

the procedure. Note that the geostatistical technique itself is not original, but its application to ore hardness measurements is. It is presented in Section 4.1.

The errors that are associated with the conversion of SPI to mill capacities are presented in Section 4.2. This is done through an error propagation study that uses Monte-Carlo simulation. This study is the author's original work.

Finally, the investigations into SPI additivity, geostatistical error, and model error are integrated into a proposed macroscopic procedure for applying SPI technology to ore body hardness characterization. This is discussed in Section 5.

While this thesis focuses on the SPI test for autogenous mill characterization, a similar approach can be used for the Bond work index for ball mill design, or kinetic parameters for flotation or leach circuit design.

The body of the thesis is divided into 3 sections. Section 2 contains a review of literature pertinent to the work presented. It is subdivided in three—one part reviewing grinding and SPI technology, one reviewing geostatistical techniques, and one describing previous work on blending and additivity. Section 3 presents the results of the work conducted on blended samples to investigate additivity. Section 4 is a summary of the investigations into geostatistical error and model error.

Conclusions, recommendations, and suggestions for future studies are summarized in Section 6, and acknowledgements can be found in Section 7. The bibliography is listed in Section 8.

2 LITERATURE REVIEW

The referencing style used in this thesis is as follows. References appearing in parenthesis *outside the last sentence of a paragraph* apply to the paragraph itself. References inside the sentence apply only to that sentence.

2.1 SPI TEST

The SPI test is a laboratory-scale batch test that employs a 30.5 cm diameter rotating mill to measure the grindability of a 2 kg ore sample for use in design and production planning of full-scale SAG mills (Starkey *et al.* 1994). The simplicity of the test and its capacity to provide a good estimate of the hardness variability (regional or across entire ore bodies) has made the test an attractive supplement to traditional metallurgical test work (Kosick *et al.*, 2001).

This section details the historical background of the SPI test.

2.1.1 Need for the SPI test

This section describes the significant developments in the field of comminution leading to the current state of the science.

2.1.1.1 DEVELOPMENT OF PRIMARY AUTOGENOUS GRINDING

Autogenous grinding was originally developed as a dry technology (*i.e.* water was not added to the ore) in the first decade of the 20th century. Pioneering work was done by Graham on so-called "tube mills" in a paper published in 1907 and summarized by Bond in 1985 in a detailed history on the topic (published in the SME Mineral Processing Handbook, from which the following is excerpted). Tube mills were tumbling mills between 1.2 and 1.8 meters in diameter and 6.1 and 6.7 meters in length, and although they were established for the grinding of fine ores with coarser pebbles, they

nonetheless contained many of the features found in current SAG milling including trommels, liners (consisting of silex or flint blocks and cemented into place with portland cement), and grate- and overflow-discharge designs (Bond 1985). Tube mills predominated in South Africa, with only a few commercial installations in the Americas prior to the 1920's, when they were supplanted by ball milling (although their use continued uninterrupted in South Africa) (Bond 1985).

Primary autogenous rock grinding[7] was developed in the 1930's and 1940's. The Hadsel mill, developed in California by Hadsel and marketed briefly by Hardinge (Hardinge Company)[8], consisted of a rotating large-diameter Ferris wheel structure with interior buckets for lifting and dropping rock onto iron liners (McPherson 1989). It was originally operated wet; however, the excessive wear impelled Hadsel to develop a dry version, which later became the foundation of the Aerofall mill[9]. Hardinge then developed (*circa* 1940) the Hardinge Cascade mill, which was marketed as a dry mill before being converted to the wet cascade mill in 1950. (Bond 1985)

The parallel development of primary autogenous milling in South Africa consisted principally of a trend towards ever-larger diameters of tube mills, accompanied by the corresponding increase in feed particle size (Bond 1985). This trend was accelerated with the introduction of the Hardinge and Aerofall technology during the experimentation of a 5.2-m mill at Daggnfontein Mine (Anglo American) in South Africa (McPherson 1989). One problem with the large-diameter, short-length mills marketed by Aerofall and Hardinge was that they could not be manufactured in South Africa at the time. The solution, championed by Union Corporation, was to manufacture longer wet autogenous mills with smaller diameters (McPherson 1989). The result of the combination of manufacturing circumstance and history with tube mills is now evident in the prevalence

---

[7] The practice of feeding all of the rock together, without any prior size separation, into a large primary tumbling mill, as opposed to "secondary" or "intermediate" autogenous grinding (the practice of using 2 to 6 inch pebbles to grind 1/8-inch ore feed) to which tube mills were applied.

[8] from 1932 until 1936.

[9] Consolidated Mining & Smelting Co (Cominco) acquired rights to build the dry Hadsel mill in Canada and in the early 1940s released the rights to an employee (David Weston), who established Aerofall Mills Ltd in Toronto and made numerous improvements.

of "long mills", or AG and SAG mills with larger lengths (relative to their diameter) than their counterparts in the Americas (Bond 1985, McPherson 1989).

Beginning in the mid 1950's and proceeding throughout the following decades, primary autogenous milling began to supplant traditional rod-mill/ball-mill grinding by replacing secondary and tertiary crushers and the rod mill or mills (and sometimes part of the ball milling process as well). The primary incentive is a reduction in capital and operating costs due to fewer pieces of equipment and lower steel consumption. In some cases (such as the early applications to coarse-grained specular hematite) autogenous grinding also provided improved metallurgical results. These benefits came at the cost of increased sensitivity (*i.e.* tonnage variability) resulting from changes in ore hardness. (Bond 1985)

It soon became apparent, however, that many of the naturally harder ores (such as taconite or many hard-rock base-metal deposits) showed increased resistance to comminution by abrasion. Furthermore, extremely soft ores were observed in which insufficient coarse material was present for autogenous grinding. Either case resulted in the generation of too much fine material (depending on grate sizes) and therefore depressed metallurgical performance. As a result, it became common to add 10 to 13 cm steel balls to supplement the grinding process. This became known as semi-autogenous grinding, or SAG milling, the results of which were less production of fines and lower sensitivity to changes in ore hardness. (Bond 1985)

2.1.1.2 SEMI-AUTOGENOUS GRINDING

Today's most common form of a semi-autogenous grinding circuit consists of a single-stage primary crusher, typically a large gyratory crusher, that reduces the run-of-mine ore to under 25-cm (top size). The material is transferred to the SAG[10] mill circuit from the coarse ore stockpile on a belt conveyor.

The SAG mill rotates between approximately 70% and 85% of critical speed and the material is passed through the mill where it undergoes grinding—generally at about 65 to

[10] For the remainder of this work, SAG will refer to both fully-autogenous (AG) and semi-autogenous milling unless otherwise noted.

75 percent feed density—and out onto the classification mechanism via the grates and/or pebble ports. The grates and pebble ports are typically 2 to 8 cm in width and designed to help the SAG mill retain the ore charge until it has undergone significant grinding. The classification device can either be a trommel screen fixed to the discharge end of the SAG mill or a vibrating screen deck, or (in some cases) both. The goal of the classification mechanism is to separate product-size material from unfinished material. The product, or screen-undersize, is promoted to the secondary grinding circuit while the unfinished material, or screen-oversize, is returned to the SAG feed, often via a pebble-crushing circuit. This material is generally called "critical-size" material. The circuit configuration described above is called an "ABC" circuit— the acronym connoting the "autogenous mill/ball mill/pebble crusher" arrangement—and is the circuit depicted in Figure 2-1.

The secondary grinding circuit generally consists of one or more ball mills in series or parallel, operating in closed circuit with a series of cyclones arranged in cyclopacks. Figure 2-1 shows a typical flowsheet.

A good description of a conventional semi-autogenous grinding circuit (the new Batu Hijau concentrator in Indonesia) can be found in McLaren *et al.* (2001).

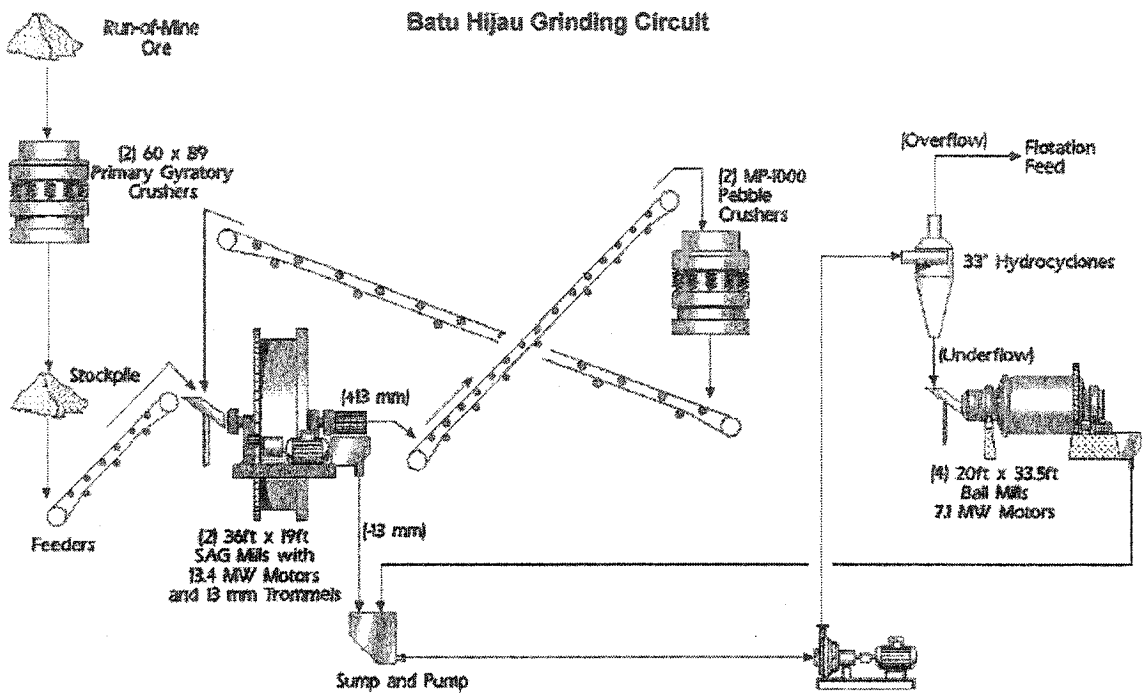

Figure 2-1 Batu Hijau grinding circuit, from McLaren et al. (2001)

2.1.1.3 DESIGN PRACTICES OF AUTOGENOUS GRINDING

The design of the comminution circuit is recognized as one of the most important steps in the design stage of a beneficiation plant. As such, the existing literature and practice is both broad and deep. This document only addresses the areas that are relevant to the evolution of the SPI test.

Of the four principal design phases generally identified between the conception and commissioning of a green-fields comminution circuit—financial appraisal, pre-feasibility, feasibility, and detailed engineering—it is principally during the feasibility stage that the SPI test is prevalent in modern plant design practice. The circuit configuration and equipment size determines capital and operating costs of an installation, which in turn drive the economic feasibility. Indeed, in Design and Installation of Comminution Circuits (Mular and Jergensen, editors, 1982, pp. 1) Barratt and Sochocky write:

"The selection of an appropriate comminution circuit for a specific ore is one of the most important decisions in the design of a processing plant. The importance is related to the

fact that the capital and operating costs for crushing and grinding plants generally represent, as is well known, the major portion of the plant costs." Furthermore, "The most important step in the development *is the analysis and understanding of the ore characteristics.*" (text italicized by the author)

Hence, the effort to produce a feasibility study can be broadly grouped in two classes. The first is the effort of understanding the ore characteristics. The second is the design of a circuit appropriate for those characteristics.

Some possible circuit configurations are (after Barratt and Sochocky, 1982):

- Single Stage Autogenous
- Autogenous – Ball Mill
- Autogenous – Ball Mill - Crusher
- Single Stage Semi-Autogenous
- Semi-Autogenous – Ball Mill
- Semi – Autogenous – Ball Mill – Crusher

Once the circuit arrangement has been selected, the size of the grinding mills required to process the design tonnage must be selected. This is the second major deliverable of the feasibility study (without considering the cost-related consequences on down-stream unit operations).

In practice the mill shell sizes are selected such that the design tonnage is achieved in a multitude of circuit configurations (which are generally identified at the pre-feasibility stage) using bench-scale and pilot-scale testing programs, and the most cost-efficient circuit is selected based on budgetary quotes for the pieces of equipment considered and their respective sizes.

The principal parameters describing the characteristics of the ore body are:

- Hardness
- Abrasiveness
- Friability

- Mineralization
- Liberation Size
- Chemistry

While the chemistry and the mineralization to some extent affect the comminution circuit design (the presence of alkalis, for example, may create sliming problems), the predominant variables are the liberation size (which dictates the size requirements of the finished product), and the trio of hardness, abrasiveness, and friability, which together dictate the amenability of the mineral to grinding and hence the mill diameter (and power) required to grind the material to the product size (Barratt and Sochocky, 1982). These three variables are measured by the gamut of metrics generated by the various pilot- and bench-scale test work options, namely (Mosher and Big, 2001):

- Pilot Plants
- Media Competency Tests
- Drop Weight Tests
- Autogenous Mill Work Index Test (McPherson Test)
- SAG Power Index (SPI)
- Bond Impact, Rod Mill and Ball Mill Tests
- Abrasion Index Test

The nature of each test, their respective mill diameters and required top size, and the sample mass required for each are listed in Table 2-1 (after Mosher and Big, 2001).

Test	Top Size (mm)	Closing Size (mm)	Sample Requested (kg)	Sample Used (kg)	Test Type	Mill Diameter (m)
Pilot Testing	100 - 150	varies	~ 10000	varies	Continuous	1.83
Media Competency	165	n/a	750	400	Batch	1.83
Bond Impact	75	n/a	20 50x75 mm rocks	7.5	Single Particle	n/a
Drop Weight	64	n/a	75	24	Single Particle & Batch	n/a
MacPherson Autogenous	32	1.2	135	100	Continuous	0.45
SAG Power Index (SPI)	19	n/a	10	3	Batch	0.305
Bond Rod Mill	13	1.2	20	10	Locked	0.305
Bond Ball Mill	3.3	0.149	10	4	Locked	0.305

Table 2-1 Existing test work options for SAG circuit design

Pilot Plants

Pilot plants are the favored design tool for determining power requirements of SAG mills, although they also can be used to provide insight into ball charge, power split[11] (by changing the SAG product size), and pebble-crushing requirements. Pilot plant testing (after Mosher and Bigg, 2001):

- makes it possible to work with samples that are relatively similar in feed size to the full-scale operation,
- allows direct examination and comparison of some important operating variables (mill speed, screen slot size, ball charge, and feed density),
- requires the least amount of direct scale-up, and
- is the most accepted method.

The main drawback to pilot plant testing is the large amount of coarse material required for testing. For green-fields projects it is necessary to dig a pit, sink a shaft, or drill an adit to obtain sufficient coarse material for testing. This can be a considerable expense and, as a result, it is not unreasonable for a pilot plant program to require over a year of time and a million dollars (Rowland 1989). Furthermore, the fact that a single or several samples are collected from one or a few places in the ore body creates a significant risk of designing a plant based on a misrepresentative sample of ore. Indeed, most pilot plant design failures on record have been attributed to insufficient testing of ore types (Digre, 1989; *e.g.* Sherman 2001)[12].

Media Competency Tests

As implied by the name, media competency tests measure the resistance of coarser ore particles to breakage in a high-aspect-ratio (diameter to length) tumbling mill. There are several different versions of the test (Kilborn, Allis-Chalmers, or Amdel-Orway), but they share the same characteristic of testing larger particles for resistance to impact breakage. In this respect they are a compromise between pilot plants, which require a

[11] The "power split" is the ratio between installed SAG mill power and installed ball mill power.

[12] Another contributing factor to pilot plant-based design is the smoothing of hardness variability resulting from the large sample mass required.

large amount of coarse sample, and bench-scale tests which require a small amount of fine sample. (Mosher and Bigg 2001)

The Kilborn test is performed in a 910 x 610 mm test mill. The mill is charged with 125 kg of 35 mm balls and 5 kg of silica sand at 60% to 65% solids and operated for 24 hours in semi-continuous form (*i.e.* ground ore is removed and replaced with fresh rock pieces). The pulp density is checked every 30 minutes and the level is checked every 60 minutes; rock pieces or water are added as necessary. (Wyslouzil 1982)

The test procedure developed by Allis-Chalmers in Milwaukee is a batch test in which large rock pieces are milled in a 183 cm (6 ft) by 30 cm (1 ft) drum for a fixed number of revolutions, then the charge is screened to determine the breakage rate of the coarse particles (McPherson and Turner, 1980; Mosher and Bigg, 2001).

The Amdel-Orway test is called the Advanced Media Competency Test and also uses a 183 cm diameter by 30 cm length tumbling mill. The mill rotates at 26 rpm and approximately 200 kg of sample are required (The actual test requirement is eleven pieces of rock each of the following size fractions: -102+76 mm, -76+51 mm, -51+38 mm, -38+25 mm, -25+19 mm). The sample is placed in the mill and the mill is rotated for 500 revolutions, after which the sample is sized and the number of rock pieces remaining in each of the feed size classes determined. Bond rod-mill work index tests, Bond ball-mill work index tests, abrasion tests, and impact tests are performed on the products of the test. (AMMTEC, 2002)

Drop Weight Tests

The most prevalent drop-weight test used in the mineral processing industry was developed by the Julius Kruttschnitt Mineral Research Centre in Queensland, Australia, and is marketed by their commercial arm, JKTech. The test requires 75 kg of screened sample with a top size of 64 mm. The JK Drop Weight Tester consists of a 20 kg steel weight which is raised to a known height and released such that it falls with a known amount of energy onto a rock particle of a certain size. The test is repeated between 10 and 30 times for each of approximately 15 size/energy combinations. The broken particles are collected and screened, and the percentage of the progeny particles that

are finer than one tenth of the size of the original particle is determined. This is called the t_{10}. The energy as determined from the height of the drop-weight is known as the E_{CS} (JKTech 2003). The t_{10} is then plotted against the E_{CS} and an exponential equation of the form:

$$t_{10} = A\,[\,1 - e^{-bE_{CS}}]$$

Equation 2-1

is fitted using least-squares techniques. The constants A and b are curve-fitting parameters that together are an indication of ore hardness. (Mosher and Bigg, 2001)

In addition to the A and b parameters, which indicate the amenability of the ore to breakage by high-energy impact, a low-energy parameter called the t_a (similar in definition to the t_{10} described above) is generated by a proprietary tumbling test and used in conjunction with the A and b parameters defined above.

The behavior of ore in a full-scale mill is modeled using the breakage rates determined as described above. The energy input in the full scale mill (as determined by the mill diameter, the amount of balls and coarse particles, and the rotational velocity) per particle (as determined by feed rate and feed size distribution) is combined with models for mass transfer of slurry within the mill and classification of particles at the grates to determine the discharge size distribution of the mill. An iterative procedure is then used to test various mill sizes, grate configurations, and ball charges for optimum performance. (Leung *et al.* 1987)

Autogenous Mill Work Index (McPherson test)

Approximately 150 kg of sample no finer than 3.2 cm are required for the McPherson test. The sample is crushed naturally to 100% minus 3.2 cm and fed into a 45-cm air-swept mill designed by Aerofall Mills, Ltd. (McPherson *et al.* 1989). The mill is charged with 8% by volume graded ball charge (18.2 kg) and mill load is controlled by varying the feed rate based on sound such that a 28% load by volume in the mill is maintained. The mill is operated in a dry, continuous, closed-circuit fashion with a 14-mesh screen (1180 μm) until steady-state conditions are achieved, after which the mill is surveyed over a 1-hour period and the autogenous work index calculated based on the feed and product size distributions and the measured power input according to the equation:

$$A_{wi} = W / (10/P_{80} - 10/F_{80})$$

Equation 2-2

where A_{wi} is the autogenous work index (kWh/tonne), W is the power input to the mill (kW/tonne), and the P_{80} and F_{80} are the 80%-passing size of the product and feed size distributions, respectively. (McPherson *et al.*, 1989; Farrow and Smith, 1982)

The McPherson test is a dry test requiring significantly less sample than traditional pilot plant test programs and hence is much cheaper from a time and cost perspective. However, 150 kg of sample are still difficult to acquire if one must confine the collection to drill core. Another drawback to the test is the small feed size, necessitating a correction using a database of measured plant operations when the autogenous work index exceeds a certain value. (McPherson *et al.* 1989; Rowland, 1989)

SPI Test

As stated, the goal of the above tests was to provide a metric for measuring the hardness, friability, and abrasion properties of mineral ores in order to infer the operating characteristics of full-scale SAG mills. In this regard the above tests provide an invaluable suite of tools for autogenous mill design, and are an improvement over the standard Bond-based methods used since the development of SAG milling in the 1950's. The acceptance of these tests has meant that the principal concern when designing grinding circuits is no longer *how to measure the pertinent ore properties*, but *whether the ore body's characteristics are adequately represented by the samples tested.* The SPI test was developed originally as a complement to the above tests in an attempt to eliminate the problem of sample representativity, but through extensive calibration over the past several years, it is now used as a complete design and forecasting tool by itself.

The test employs a 30.5 cm diameter by 10.2 cm wide grinding mill charged with 5 kg of steel balls. Two kilograms of sample are crushed to 100% minus 1.9 cm and 80% minus 1.3 cm and placed in the mill. The mill is run with several screening iterations until the sample is reduced to 80% minus 1.7 mm (10-mesh). The length of time required to achieve 80% minus 10-mesh, in minutes, is called the SAG Power Index, or SPI. In addition to the SPI, the test generates a parameter called the P_{64}. The P_{64} is the 80%-

passing size of the material that is finer than 10-mesh at the end of the test[13]. It is related to the abrasive properties of the ore. (Starkey *et al.* 1994; Starkey and Dobby, 1996)

The SPI is used in a proprietary transformation equation that has been calibrated with an extensive database of plant surveys to generate the operating specific energy (kWh/tonne) for the full-scale mill (Starkey and Dobby, 1996; Kosick and Bennett, 1999).

The advantage of the SPI test is therefore tied to the fact that the test only requires a 2-kg sample[14], a quantity that for most properties can be easily collected from existing drill core. Hence, the test can be viewed as an addition to the suite of tools described above, the primary difference being that it can easily be employed to measure hardness distributions in the ore body.

Bond Rod- and Ball-Mill Tests

The standard rod-and ball-mill work index tests were developed by Bond beginning in the 1920's and became the most widely-used metric for ore hardness by the early 1960's (Mosher and Bigg, 2001).

The tests employ a standard Bico-Braun rotating bench-scale ball mill charged with 20.185 kg of graded balls (or rods, in the case of the rod-mill index test). A standard volume of 100% minus 6-mesh (3.36 mm) is placed in the mill with the ball charge and the mill is operated in a closed-circuit locked-cycle fashion with a closing screen size equal to that of the proposed ball mill circuit (generally 150 μm). After each grinding cycle, the ground product is removed and replaced with fresh feed. The cycles are repeated until a steady-state system is achieved; *i.e.* the circulating load is unchanged at 250% after 2 or 3 cycles. (JKMRC 1999)

---

[13] Because by definition at test completion exactly 80% of material is finer than 10 mesh, 80% of this is 64% of the original 2-kg sample (80% x 80% = 64%), hence the name P_{64}.

[14] The SPI test itself requires 2 kg of sample, however 3 kg are requested for crusher-index determination and other considerations.

Once steady state is achieved, the work index is calculated by way of an equation employing the 80%-passing size of the product from the last cycle (P_{80}, in microns), the 80%-passing size of the feed (termed the F_{80}, also in μm) and the grams per mill revolution of product generated. (Deister, 1987)

The main drawbacks to the test are that it requires a somewhat larger sample than the SPI test (approximately 10 kg minimum) and it is recognized to be unreliable for predicting SAG performance due to the finer particle sizes and higher proportion of impact breakage that predominates in the test (Mosher and Bigg, 2001).

2.1.2 Development of SPI test

The SPI test was created in 1991 with the construction of a prototype mill in Canada. The first practical application was performed with the second prototype mill, constructed in Iran to address a question regarding ore sample representativity at Gol-E-Gohar. A 50-tonne sample of very soft ore believed to represent the entire ore body was used for SAG testing. Relative SPI values collected for test work on drill core showed this to be an extremely soft and misrepresentative portion of the ore. The success in identifying the soft nature of the sample drew the attention of Kvaerner-Davy and MinnovEX Technologies, Inc., the latter endeavoring to develop an industrial calibration database of test results for absolute kWh/tonne prediction.

The development of the calibration database, undertaken with financial support from MITEC (Mining Industry Technology Council of Canada, now part of Camiro), began in earnest in 1994 and the results were released in April 1995, in the form of a straight-line equation derived from grinding line surveys at five Canadian SAG plants (Starkey, 1997). This equation was deemed valid for operating closed-circuit SAG mills with no pebble crusher and nominal 15-cm feed size (Starkey and Dobby, 1996).

An empirical database that quantitatively demonstrated the applicability of the test to semi-autogenous milling allowed MinnovEX to commercialize the SPI test.

2.1.3 Commercialization of the SPI test

Between 1997 and 2000 the SPI test calibration database grew at a rapid pace as a by-product of commercial autogenous mill optimization projects undertaken at MinnovEX. Nearly 200 calibration points were collected from a variety of grinding circuit configurations in operation at more than 25 mining properties, including many configurations with pebble crushers or fine feed. As of 2000, the SPI database was routinely used to quantify the effects of fine feed, pebble crushing, or both (Kosick *et al.* 2001).

While expanding the SPI database, MinnovEX in partnership with 13 major international mining companies undertook to develop a computer algorithm that could be used to apply the autogenous mill specific energy calculations (used to convert SPI values to mill power draws, specific energies, and tonnages) on a block level. The idea was to use SPI measurements taken from drill core and interpolate them into a three-dimensional model of the ore body (a "block model" in mining jargon) and then apply a computerized algorithm to determine the throughput or specific energy estimates for each block from their respective SPI values. This procedure allows the engineer to generate a 3-dimensional map of the ore body hardness, SAG mill throughput predictions, and specific energy requirements on a block-by-block basis. This provides a much greater understanding of the ore hardness characteristics and therefore a greater degree of latitude in selecting the cheapest circuit—indeed, a whole new degree of freedom is given to the design process (that of being able to select a given *time period* or specific *ore volume* upon which to base the design, something which previously had not been economically feasible due to the large sample sizes required for the alternative tests). (Kosick *et al.* 2001; Custer *et al.* 2001; Dobby *et al.* 2001)

The computer program is called CEET, an acronym for Comminution Economic Evaluation Tool.

The SPI test procedures and CEET Algorithm are described in more detail in Section 2.1.4.3 below, but the reader is referred to the referenced publications for the complete descriptions of the various CEET components.

2.1.4 The SPI: State of the Science

The SPI test, procedures, and interpretation methodology are the intellectual property of MinnovEX Technologies Inc. This section does not present a detailed description of the test equipment and procedure; this can be found in the referenced publications. The purpose of this section is to provide the background information essential for the subsequent ore body characterization work.

2.1.4.1 GENERAL TEST PROCEDURES

Equipment

The SPI laboratory mill is a 30.5 cm diameter steel mill with a TEFC 120V electric motor, V-belt drive, and a Dodge gear reducer coupled to the 2.54 cm drive shaft. The mill is charged with a 15% by volume charge of steel balls and a 2-kg sample of ore (Starkey and Dobby, 1996). An illustration of the SPI mill is shown in Figure 2-2.

Figure 2-2 SPI test mill being discharged

In addition to the mill, the following screens and pans are required (internal documentation, MinnovEX, 2001):

- 46.7 cm (18-in) pan
- 46.7 cm (18-in) Tyler 10-mesh (ASTM #12) screen
- 46.7 cm (18-in) ASTM standard 1-inch screen (for catching the balls)

- 20.3 cm (8-in) ASTM standard screens numbers ¾-in, ½-in, 3/8-in, #3, #6, #12[15], #20, #40, #70, #100, #140, Pan

The following ancillary equipment is required (internal documentation, MinnovEX, 2001):

- Rotap Sieve Shaker
- Laboratory jaw crusher with 2.54 cm closed-gap setting
- Digital Balance
- Drying oven
- Pans and sample bags
- Dust masks, gloves, and other safety equipment

Procedures

To perform an SPI test, the 2-kg charge is crushed to 100% minus 19 mm and 80% minus 12.7 mm by repeated closed-circuit crushing in the laboratory jaw crusher. The sample is then screened using the Rotap sieve shaker and the screens with sizes described above. In general, after crushing approximately 80% to 90% of the total feed sample is coarser than a Tyler standard #10 mesh (1.7 mm).

The test is performed by placing the crushed 2-kg sample in the mill with the ball charge and running the mill for series of grinding iterations. The sample is removed and screened after each iteration. If the ore has not yet been reduced to 80%-passing 1.7 mm, the entire sample is returned to the mill for another grinding iteration. This sequence is performed until more than 80% passing 1.7 mm is achieved, and the SPI (the time required to reach 80%-passing 1.7 mm) is then interpolated from the grinding iterations.

Once the technician determines that less than 20% of the sample is coarser than a Tyler standard #10 mesh, the test product is screened on the ASTM sieve set given above to

[15] ASTM standard #12 has the same 1700 µm mean opening as the Tyler standard #10 screen typically referred to as the standard "closing size" of the SPI test.

determine the final screen analysis of the product (internal documentation, MinnovEX, 2001).

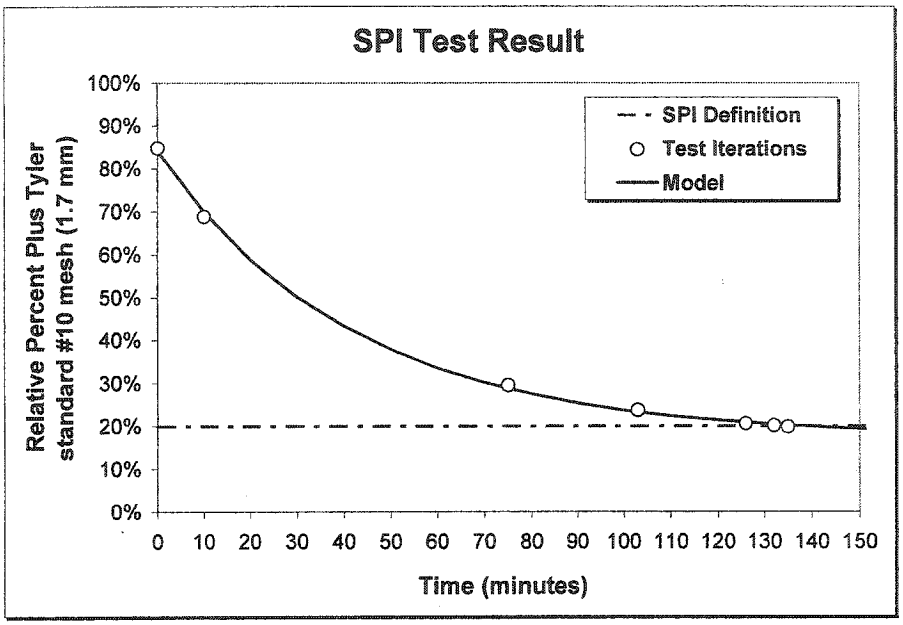

Figure 2-3 SPI test curve for a typical ore

2.1.4.2 CALCULATING THE SAG MILL SPECIFIC ENERGY

To calculate the autogenous mill specific energy from the SPI, the following must be known (in addition to the SPI):

- Autogenous mill product size (T_{80})
- Approximate mill feed size
- Autogenous circuit configuration (*i.e.* pebble crushing and circulating load, ball charge, *etc.*)

The procedure involves the following two steps (Custer *et al.*, 2001; Dobby *et al.*, 2001):

1. Determine the specific energy for the product size and reference circuit, which is usually a SAG mill operating in closed circuit with no pebble crusher and 6-inch feed size.[16]
2. Adjust the specific energy calculated for the reference circuit to reflect the characteristics of the target circuit (*i.e.* finer feed, pebble crushing *etc.*).

Reference Circuit

The primary SPI calibration equation was originally developed for 6-inch feed and no pebble crushing. Figure 2-4 shows the SPI standard circuit with the primary variables.

The F_{80} in Figure 2-4 is defined as the size, in inches unless otherwise specified, for which 80% of the feed is finer. The T_{80} is defined as the size, in microns unless otherwise specified, for which 80% of the product is finer. (Kosick and Bennett, 1999)

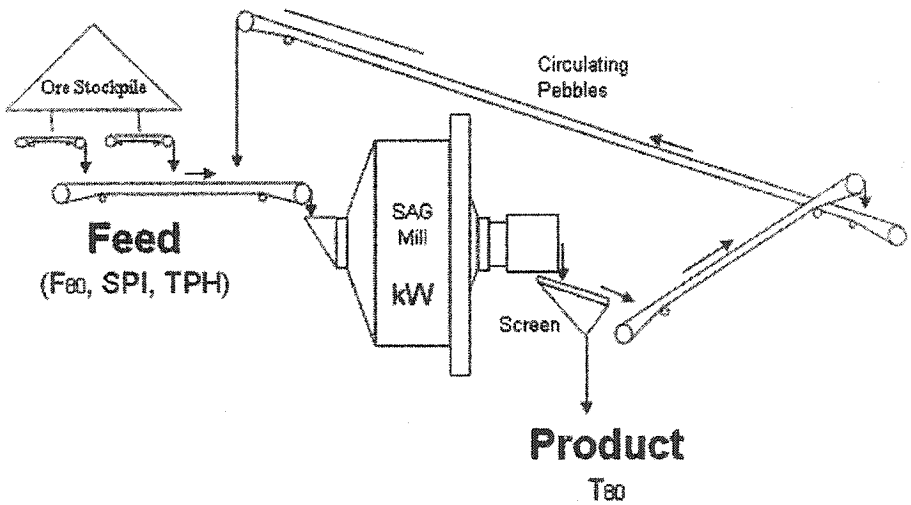

Figure 2-4 SPI standard circuit

The primary calibration equation was developed by sampling and testing the SAG mill feed for SPI and F_{80} while sampling the product for T_{80} and monitoring the mill power draw (kW) and mill feed rate (TPH). This process, repeated for many operating SAG mills operating at 6-inch F_{80}'s, provided enough data to generate the primary calibration

[16] This particular reference circuit (wet SAG grinding in closed circuit with a screen, no pebble crusher and nominal 6-inch feed) is often termed the "standard circuit" and the SPI that calculates the kWh/tonne for this circuit is called the "primary calibration equation"

equation through multivariate regression. The equation is (Kosick and Bennett, 1999; MinnovEX 2001):

$$E = C_1 * (SPI / \sqrt{T_{80}})^{C2}$$

Equation 2-3 SPI equation (standard form)

Where E is the mill specific energy in kWh/tonne and the values of the constants C_1 and C_2 are protected by MinnovEX for competitive reasons. Figure 2-5 shows a predicted-versus-actual scatterplot of the primary calibration database. The ordinate represents the specific energy observed in the plant during the sampling program, and the abscissa is the specific energy found by applying Equation 2-3 to the SPI and T_{80} values determined from test work on the feed and product plant samples (Kosick and Bennett, 1999).

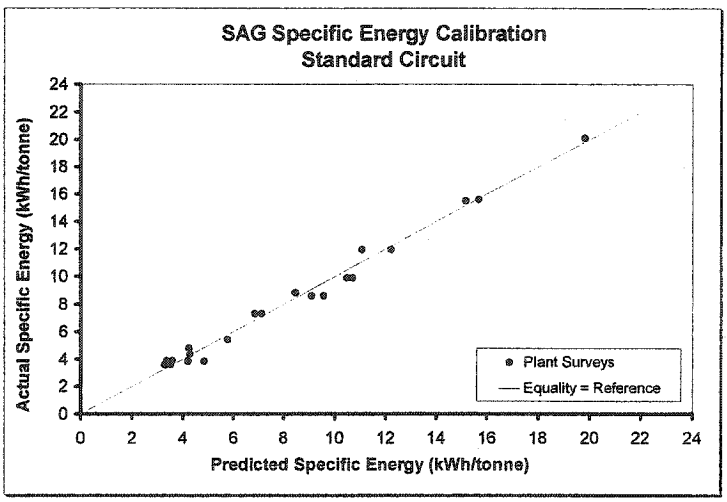

Figure 2-5 Primary calibration scatterplot (after Kosick and Bennett, 1999)

Target Circuit

Given the product size and SPI values, once the specific energy requirements are determined for the standard circuit as described above, the values are adjusted to reflect the difference in specific energy that can result from a change or changes in the configuration of the circuit (*e.g.* adding a pebble crusher) or the operating parameters (*e.g.* receiving a finer feed). One would intuitively suspect that finer feed and/or pebble crushing would result in lower SAG mill specific energies than predicted by the standard equation and hence survey points from operating plants should fall below the equality line that represents the standard circuit. Figure 2-6 shows a selection of survey points

that illustrate the effects of finer feed and pebble crushing. The specific energies do not include the energy expended in the pebble crusher, conveyor belts, or pumps.

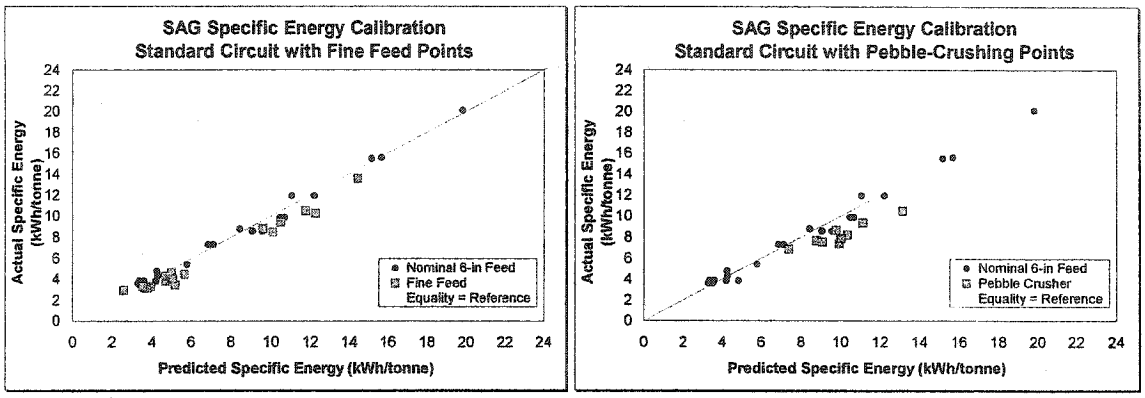

Figure 2-6 SAG specific energy scatterplots showing effects of fine feed and pebble crushing (Kosick et al., 2001; MinnovEX 2001)

The general method for accounting for differences between the target circuit and the reference circuit (such as those depicted by Figure 2-6) is to include a sub-model as a multiplier in Equation 2-3. The sub-model, F_{SAG}, is a function that varies based on the number and magnitude of the parameter differences, and is introduced as follows (Dobby *et al.* 2001)[17]:

$$E = C_1 * (SPI / \sqrt{T_{80}})^{C2} * F_{SAG}$$

Equation 2-4 SPI calibration equation (common form)

The sub-model F_{SAG} incorporates some or all of the effects of finer feed, pebble crushing, differences in circulating loads, differences in ball charges (or fully autogenous grinding), extremely fine grinding, low aspect-ratio mills, and open-circuit grinding. Grinding circuit audits performed on industrial-sized circuits are required for calibrating the sub-model for the target circuit. There are sufficient data in the MinnovEX database to model fine feed or pebble crushing conditions without necessarily collecting plant data; however, when other conditions (such as fine grinding, low-aspect ratio mills, or open circuit SAG mills) are investigated it might be wise to first perform some calibration

[17] Note that the same technique is applied to the Bond equation to "correct" for differences between the Bond standard circuit (2.44-m diameter wet ball mill closed with cyclones and fed by a rod mill). *See* Rowland and Kjos, Mineral Processing Plant Design, *ed.* Mular and Bhappu, Ch. 12, "Rod and Ball Mills", pp 263-267. SME-AIME, 1980)

work before attempting to estimate the value of F_{SAG}. (after Kosick *et al.* 2001; Bennett *et al.* 2001)

Throughput or Power?

Once the specific energy requirement, in kWh/tonne, is calculated for a given block or sample of ore, the throughput is calculated by dividing the SAG power by the ore's specific energy:

$$P / E = T$$

Equation 2-5

where P is expected mill power draw (kW), E is the specific energy requirement (kWh/tonne) and T is the throughput (tonnes/hr). For the design of an autogenous circuit, the target throughput is multiplied by the specific energy to determine the required power:

$$T * E = P$$

Equation 2-6

If the goal is design, it is general practice to let the manufacturers or engineering firms size the SAG mill such that the mill diameter and motor are sufficiently large to draw or deliver the required power. If the goal is production forecasting, the power used must be the actual power delivered to the mill shell (*i.e.* minus transformer, motor, gear reducer or VFD, and pinion inefficiencies).

2.1.4.3 CEET

CEET is the computer program that is used to apply the calculations described in the previous section to large collections of samples or blocks that represent the ore body. In addition to the SAG model described above, it incorporates a ball mill model (an empirically corrected form of the Bond ball mill model) and a data set that is preferably generated from geostatistical distribution of SPI and Bond work index data. The general functionality is best described by a series of steps (Kosick *et al.* 2001; Custer *et al.* 2001):

1. Three input sets are created. The first is the required block model containing a list of SPI and Bond work index pairs, their x, y, and z coordinates, and various other ore properties. The second is a fixed data set residing in CEET that consists of various circuit configurations, equipment sizes, and operating and capital cost parameters. The third is a list of input variables selected and submitted by the user to describe his or her design criteria (*i.e.* average throughput target, maximum and minimum allowable tonnages, desired average product size, maximum allowable product size, *etc.*).
2. For each block in the block model CEET calculates the comminution circuit performance (*i.e.* tonnage, required kW, *etc.*) and cost.
3. The results of Step 2 are summarized over the entire block model to generate a result for the whole block model for each flowsheet.
4. The user examines the results. If designing a circuit, the flowsheet with the lowest capital cost or operating cost can be selected as per his or her design criteria. If it is a production planning project, the resulting tonnages and product sizes are readily available for each block and can now be imported into the mine planning software.

The CEET output and the user input values that customize the SAG and ball mill models are entered and retrieved via HTTP and FTP internet connections. The reader is referred the cited publications for more detailed information on the functionality and application of CEET.

2.1.4.4 CEET II

The reader will observe from Section 2.1.4.2 that quantitative knowledge of the T_{80} and F_{SAG} is required to calculate the required specific energy. Quantitative knowledge of the feed size and pebble crusher circulating load is required to estimate the value of F_{SAG} (Equation 2-4). Prior to CEET II, this knowledge was acquired either by performing a series of sampling surveys around the grinding circuit (for existing plants) or estimating them from the database (for design projects). The difficulty with this solution is tied to the fact that the T_{80}, feed size, and circulating load are heavily dependent upon ore characteristics. The resulting specific energy calculations would therefore be valid for

material similar to that processed during the sampling campaign, but may not be so when applied to ore still buried in the pit.

The first CEET version addressed this issue (rather poorly) by assuming a constant F_{SAG} and T_{80} value for the entire block model. CEET II improved this by introducing sub-models for feed size, circulating load, F_{SAG}, and T_{80}. These four models are described below in detail, as they will be referenced in the error analysis of CEET presented in Section 4.2.1.

Feed Size

The feed size predictor relates the 80%-passing and 50%-passing points of the feed size distribution (F_{80} and F_{50}, respectively, in mm) to the hardness of the ore and the closed-side setting of the primary crusher (CSS in Figure 2-7). Two parameters, the SPI and the SPI Crusher Index[18] (C_F), quantify the ore hardness. Figure 2-7 shows the F_{80} model on the left and the F_{50} model on the right. The curves are exponential regressions fitted with a least squares procedure. The x-axes are equal to $C_F^{n1}SPI^{n2}CSS^{n3}$, where values of n_1, n_2, and n_3 are proprietary. (Dobby *et al.* 2001)

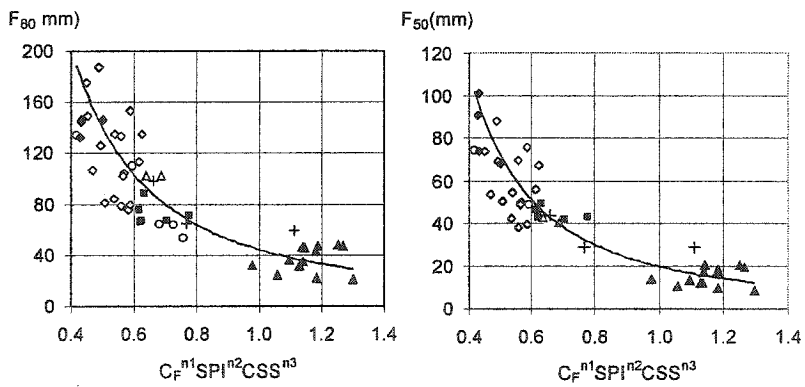

Figure 2-7 Feed size models developed for CEET II (Dobby et al. 2001)

[18] The SPI crusher index C_F is an index test developed as part of the CEET II effort that describes the breakage of ore during the crushing iterations undergone by the SPI test feed sample (Dobby *et al.* 2001).

Circulating Load

The circulating load model is based upon the feed size distribution, grate and pebble port apertures, the slot width of the trommel or vibratory screen, and the ore hardness as defined by the SPI. The feed size distribution is determined using the feed size sub-model described above.

Knowledge of the feed size distribution, the average grate/pebble port size, and the screen or trommel slot width permits the calculation of the relative mass present in the coarse (plus grate-size), fine (minus slot width), and intermediate size fractions of the feed ($\theta_3, \theta_1, \theta_2$ respectively). A semi-empirical model relates the pebble crusher circulating load (PCCL) to the ore hardness (SPI) and the relative mass of the two coarsest size classes[19] (θ_2 and θ_3). The form of the model as published by Dobby *et al.* (2001) is given by:

$$PCCL = a\,(\theta_2 + b\theta_3 / SPI^C)^D\, SPI^E$$

Equation 2-7 PCCL Model

Dobby *et al.* determined the values of the calibration constants a, b, C, D, and E using a database of measured circulating loads and operating characteristics. Figure 2-8 shows a scatterplot of the predicted circulating load versus those in the database (Dobby *et al.* 2001).

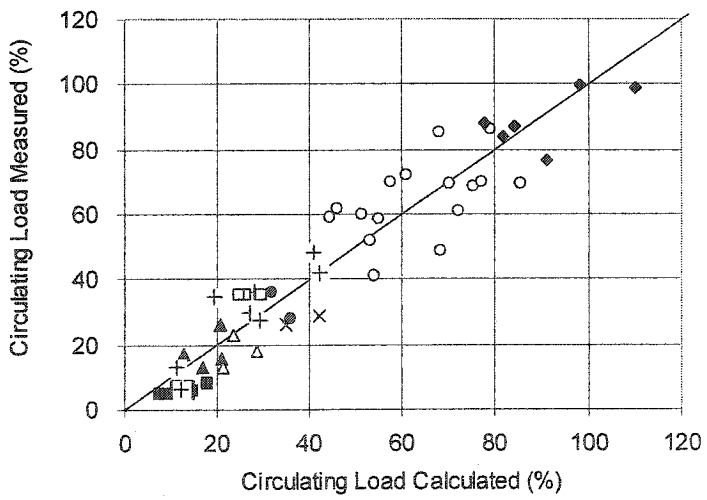

Figure 2-8 Circulating load sub-model scatterplot

[19] The finest size class is material finer than the slot width of the trommel or screen, hence it has no effect on the circulating load.

F_{SAG} sub-model

The F_{SAG} sub-model in Equation 2-4 is a function of the feed size and pebble crusher effectiveness. Its value is determined using an unpublished formula derived from the database of sampled grinding circuits (Dobby *et al.* 2001).

T_{50} and T_{80} Models

For simplicity this section describes only the T_{80} model with the explanation that the T_{80} calculations are identical in form if not function.

The T_{80} model estimates the T_{80} from the feed size distribution, the ore hardness as quantified by the SPI, the size of the grate or pebble port apertures, the slot width of the trommel or screen, the ball charge in the mill, the pebble crusher circulating load, and the pebble crusher product size (Dobby *et al.* 2001).

The feed stream is divided into the same three size categories used for the circulating load model. The pebble crusher discharge is a fourth stream with a portion, θ_4, finer than the screen or trommel apertures. Each stream will produce a portion of the mass flow in the product stream and hence will contribute to the T_{80}. The magnitude of this contribution is based on their mass and their particle size. Their mass is known from the size distribution and the screen or trommel slot width. Their particle size, characterized by the 80%-passing size in the case of the T_{80} calculations, is calculated using a series of empirical equations. These equations in their published form are (Dobby *et al.* 2001):

$$T_{80}(A) = a_1 D_1 SPI^{b1} SF \text{ (fine material in feed)}$$
$$T_{80}(B) = a_2 SPI^{b2} SF \text{ (intermediate material in feed)}$$
$$T_{80}(C) = a_3 P_{64}^{b3} SF \text{ (coarse material in feed)}$$
$$T_{80}(D) = a_4 D_2 SPI^{b4} SF \text{ (fine material in pebble crusher product)}$$

Equation 2-8 T_{80} equations

In these equations, the constants a_1, a_2, a_3, a_4, b_1, b_2, b_3, and b_4 were determined from calibration with the plant database, SF is a function of the steel charge in the mill, and D_1 and D_2 are the 80%-passing sizes of fines in the mill feed and pebble crusher product

(respectively). The final T_{80} is calculated by weighted sum of the four components, namely (Dobby *et al.* 2001):

$$T_{80} = T_{80}(A)\,\theta_1 + T_{80}(B)\,(PCCL \times \theta_4) + T_{80}(C)\,(\theta_2 - PCCL \times \theta_4) + T_{80}(D)\,\theta_3$$

Equation 2-9 T_{80} equation

Because these four sub-models are based in part upon measured ore properties, the design team could now account for regional differences in feed sizes, product sizes, and crusher effectiveness (Dobby *et al.* 2001).

CEET II was completed in partnership with commercial mining companies in the year 2001 and has since been used in a large number of commercial projects (Kosick *et al.* 2001).

2.1.4.5 COMMERCIAL PROJECTS

Today the SPI technology described above is in common usage in design and production planning programs. Since the commercialization of CEET in 2000, many large base-metal operations are using the SPI test as part of large-scale projects for production management. Many (if not most) new autogenous grinding circuit design projects used the SPI test and CEET technology for guiding the sample selection or even the design criteria. (Kosick *et al.* 2001; Custer *et al.* 2001; Lane *et al.* 2001)

To date (June 2003) over 6,000 SPI tests have been performed on approximately ten mineral types and nearly fifty grinding lines.

2.1.5 The SPI Technology in a Historical Context

The following summary is a compilation of material presented by JKMRC (1996) and BMHB (1985) with the exception of the SPI-related analysis, which is the author's work.

2.1.5.1 HISTORICAL COMMINUTION MODELS

The modeling of comminution circuits has historically been dependent on the computational power available to perform calculations. Before the advent of discrete element modeling and population balance methods the only comminution models were

simple energy relationships that related the energy input to the degree of size reduction (expressed in terms of percent passing size). Today these energy models, far advanced from the early days described below, are the most common tool used for the macroscopic design and shell sizing of grinding circuits. (JKMRC 1996)

It has always been clear that more energy is required to achieve a similar relative size reduction as the product becomes finer, resulting in the simple differential equation

$$dE = -k\left(\frac{dx}{x^n}\right)$$

Equation 2-10

where E is the energy input, K and n are constant, and x is the particle size in cumulative percent passing. The difficulty that arose involves the estimation of the value of the exponent n. (JKMRC 1996)

In 1867, Rittinger argued that the incremental energy input is proportional to the amount of new surface area created, hence n = 2. Substituting 2 for *n* in Equation 2-10 and integrating yields "Rittinger's Law" (after BMHB 1985):

$$E = k\left(\frac{1}{x_2} - \frac{1}{x_1}\right)$$

Equation 2-11 Rittinger equation (general form)

Kick studied coarser comminution, arguing in 1883 that the energy input for crushing an ore is constant for a given reduction ratio, hence n = 1. Substituting 1 for n in Equation 2-10 yields "Kick's Law" (BMHB 1985; JKMRC 1996):

$$E = k * \ell n\left(\frac{x_1}{x_2}\right)$$

Equation 2-12 Kick equation (general form)

In 1952 after extensive experimental work on ball mills, Bond suggested that the energy is proportional to the length of the new crack tip formed, resulting in the intermediate value of n = 1.5 and his "third law" of comminution (BMHB 1985; JKMRC 1996):

$$E = k\left(\frac{1}{\sqrt{x_2}} - \frac{1}{\sqrt{x_1}}\right)$$

Equation 2-13 Bond equation (general form)

In 1961, Hukki, after reviewing a wide range of comminution devices, concluded that no single relationship was adequate, and proposed the graph shown in Figure 2-9. At crushing sizes, Kick's relationship was appropriate. At intermediate sizes, traditionally reserved for rod- and ball-mill grinding, Bond's equation worked well; and at finer sizes, Rittinger's ideas about surface area were more plausible. (JKMRC 1996)

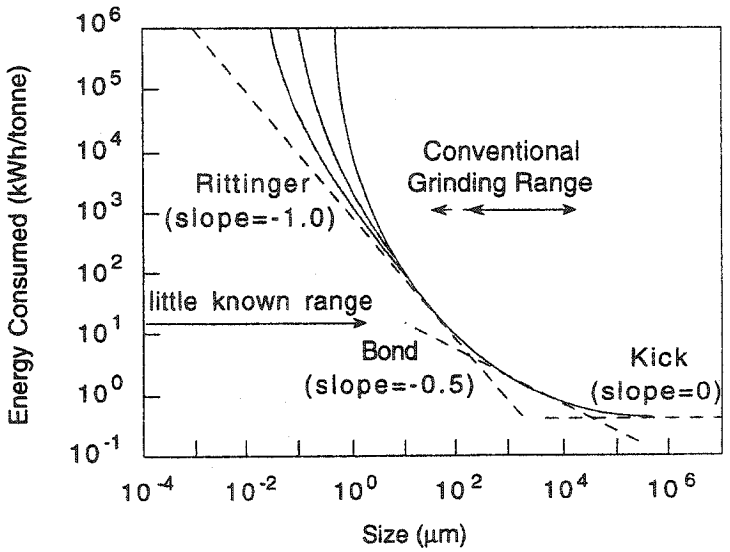

Figure 2-9 Relationship between energy input and particle size (JKMRC 1999)

In modern comminution, it is suspected that all of these underlying ideas are incorrect. Compelling evidence provided by the material science field suggests that cracks initiate at points of weakness or flaws in the atomic structure of the material. It is assumed that most rocks contain a distribution of flaws of various sizes, from geological faulting or jointing down to dislocations in the crystal structures on the atomic scale. For large particles there are plenty of flaws available. For finer particles, the larger flaws would tend to become external particle surfaces. It is this underlying trend that produces different n-values at different particle size. (JKMRC 1996)

But even if the underlying elements of the theories of Bond, Kick, and the other researchers are not correct, their observations regarding increased incremental energy expenditure with decreasing particle size are. This is true regardless of whether they are based on physical theories about crack phenomena or on the statistical properties

relating to the size and occurrence of the particles and their imperfections. (JKMRC 1996)

Note that the above theories do not incorporate effects of particle transport, expenditure of energy that does not result in breakage, or deviations of the slope of the product size distribution from the typical. For this reason it is necessary to correct the energy models either empirically or with a series of plant surveys as per suggestions in contemporary literature (*e.g.* Rowland 1980; Dobby *et al.* 2001). (JKMRC, 1996)

2.1.5.2 SPI MODEL IN A HISTORICAL CONTEXT

The SPI test is a batch laboratory-scale test created for the energy modeling of SAG mills, *i.e.* product size ranges intermediate to ball-milling (Bond's theory) and coarse crushing (Kick's theory). The typical product size of a SAG mill varies between 1mm and 10mm. This region in Figure 2-9 is the area where the tangent created by Bond's value of n = 1.5 and Kick's tangent (n = 1) diverge from the energy curve suggested by Hukki. This divergence may be one of the reasons for observed lack of correlation between the Bond equation and traditional SAG milling[20,21].

The SPI test, like the Bond equation, is calibrated empirically with an extensive database of operating SAG mills. The general form of the calibration equation can be liberally rewritten from Equation 2-3[22] as:

$$E = k * \left(\frac{1}{x_2^{c1}} - \frac{1}{x_1^{c1}} \right)$$

Equation 2-14 SPI equation (general form)

---

[20] As a semantic correction, it might be stated that the divergence of the Bond model in Figure 2-9 and the observed lack of correlation between Bond tests and SAG milling are both results of a common cause, namely, the value of n for this model does not correctly reflect for the size range in question the propensity for breakage of a particle, i.e. its flaw size distribution and occurrence function.

[21] It might also be noted that a similar divergence between Bond's and Kick's theories near the range of particle sizes traditionally involved in tower mills (*i.e.* vertimills) may explain the observed lack of correlation between the Bond equation and tower mill performance, and may provide insight into the form of a still-nonexistent tower mill model.

[22] By applying the exponent C_2 to the terms within the parentheses and introducing the second term in the parentheses in Equation 2-14 above, which reduces to zero for large values of x_1

where c_1 is the value of n – 1 in the above analysis. The absolute value of c_1 is protected for competitive purposes, but it is in the range of approximately 0.2 to 0.4—precisely where one would suspect from examination of Figure 2-9. In other words, it appears that the empirical development of the SPI equation has resulted in a value of n that is substantiated by the values arrived at by historical researchers working with neighboring particle size ranges. In this context, the SPI equation can be viewed as an integral part of the spectrum of energy models for mineral comminution.

It is interesting to note that while the equation used by MinnovEX to calculate the autogenous mill specific energy does not utilize the second term in parenthesis (Equation 2-14), typical F_{sag} values used for fine feed size compensate. In other words, for a given SPI and transfer size, both Equation 2-4 and Equation 2-14 would yield the same result.

2.2 GEOSTATISTICS

The body of knowledge termed geostatistics is broad and deep, and as such a complete review of the practice is beyond the scope of a Masters thesis, especially one that focuses on industrial comminution. This section endeavors to present the reader who is unfamiliar with geostatistics with a macroscopic understanding of those parts of the practice that are relevant to this work.

The information contained in this Section has been compiled from various sources including (first and foremost) the course notes and seminar presented by Michel Dagbert, Geostat Systems International Inc. during March 5 – March 7, 2001 in Toronto, Ontario. Other sources include Isaaks and Srivastava (1989), and David (1988). All figures have been extracted from Dagbert (2001), with permission.

2.2.1 Background

Geostatistics came about more than 40 years ago in the Witwatersrand gold mines where Krige proposed a statistical correction to the traditional way of estimating the average grade of a block of ore by the arithmetic mean of a limited number of channel cuts in drives, raises and stope faces around the block. As Krige's work was supported

by large numbers of samples, it was experimental in nature. Matheron formulated the theory ten years later, introducing the variogram (a tool for analyzing spatial variability of ore grades) and an estimation method based on it called "kriging" (in recognition of Krige's early work in South Africa).

The next two decades saw the application of these tools to a large variety of deposits from fairly regular sedimentary iron ore to highly variable uranium or precious metals. They have been refined too. The last decade has seen the emergence of more robust ways of analyzing the spatial continuity of the mineralization using alternate formulations of the variogram. Variants of the kriging method have also been proposed. Emphasis is being put on the estimation of block recoveries (tonnages and grades above various cut-offs) rather than just a single block grade average. In some mining operations with poorly visible ore, geostatistics has proven to be a powerful method of processing grade control sample data. Finally, as this report will attest, it is now being applied to ore hardness indices and rate constants for kinetic models of separation processes, thereby enabling the design of a grinding or flotation circuit based on the geostatistically-distributed properties of the ore body as a whole.

In this section several geometrical interpolation methods and their characteristics are introduced. The concept of estimation error is discussed and it is shown that kriging is simply a statistics-based interpolation method that aims to minimize the estimation error. Finally, alternative methods for geostatistical estimation are summarized.

2.2.2 Geometrical Interpolation Methods

The three main geometrical interpolation methods discussed here are *nearest-neighbor* (also known as the *method of polygons* or *polygonal estimation*), *inverse-distance* methods, and *moving-window average* methods. Strictly speaking, these methods are the same in that nearest-neighbor interpolation weights nearby samples by the inverse of the distance, raised to the power of infinity, whereas moving window average methods weight them by the inverse of the distance, raised to the power of zero. Generally "inverse-distance" weighting methods are assumed to be in-between somewhere, with most common exponents taking on the value of 2 or 3, the higher values giving proportionally more weight to the nearest sample or samples.

2.2.2.1 NEAREST NEIGHBOR

The nearest neighbor method is known as polygonal estimation because the general algorithm consists of calculating the *polygon of influence* surrounding each sample point. The polygon is defined by its vertices, each of which occurs at the intersection of the perpendicular bisectors between the sample point and its neighbors. By definition, each sample point can have only a single polygon of influence. Furthermore, any point in the polygon of influence of a sample is closer to that sample than it is to any other nearby sample. Once the polygon has been identified, the value of each point in that polygon is attributed the value of the sample point around which it is drawn[23].

Although it is uncommon to apply nearest-neighbor estimation for ore reserve estimation and grade control, the method is commonly used to *decluster* raw sample sets prior to conducting statistical analysis. Declustering is the procedure by which nearby samples are given lower weighting factors than samples that are more spatially dispersed. Because nearby samples will (hopefully) show similar values, this will be reflected in the statistical calculations. If the nearby samples are each given the same weighting factor as the more dispersed samples, calculated averages will be biased towards the values of the nearby samples and calculated variances will be lower than the estimated variance of the population (ore body). Declustering using polygonal estimation is a convenient method for calculated weighting factors that reflect the actual ore that each sample represents in the deposit.

The nearest-neighbor method is the only geometrical interpolation method that does not require a search neighborhood or *search ellipsoid* of some kind.

Figure 2-10 shows a plan view of hypothetical drill core intercepts in a bench of an open pit gold mine (units are g/tonne of gold). Crosses are the drill-hole intercept coordinates and numerals are their assay grades. Figure 2-11 shows the polygons of influence surrounding each drill core intercept.

---

[23] The process of dividing a polygon into many points is known as *discretization* and the points are referred to as *discretization points* or *discretization nodes*.

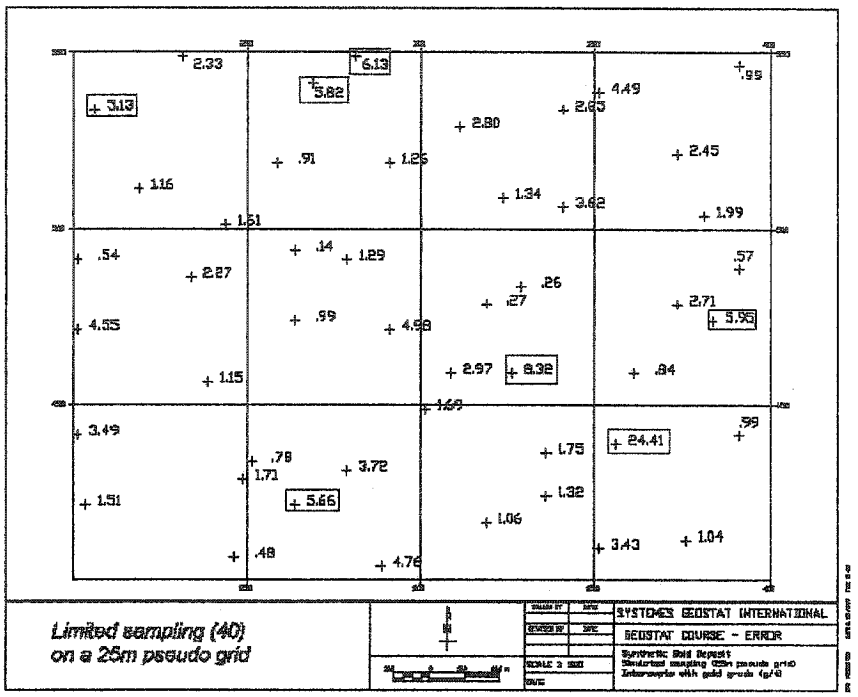

Figure 2-10 Map of intercepts available in a test portion of a bench with measured gold values (g/t Au) shown (Dagbert 2001)

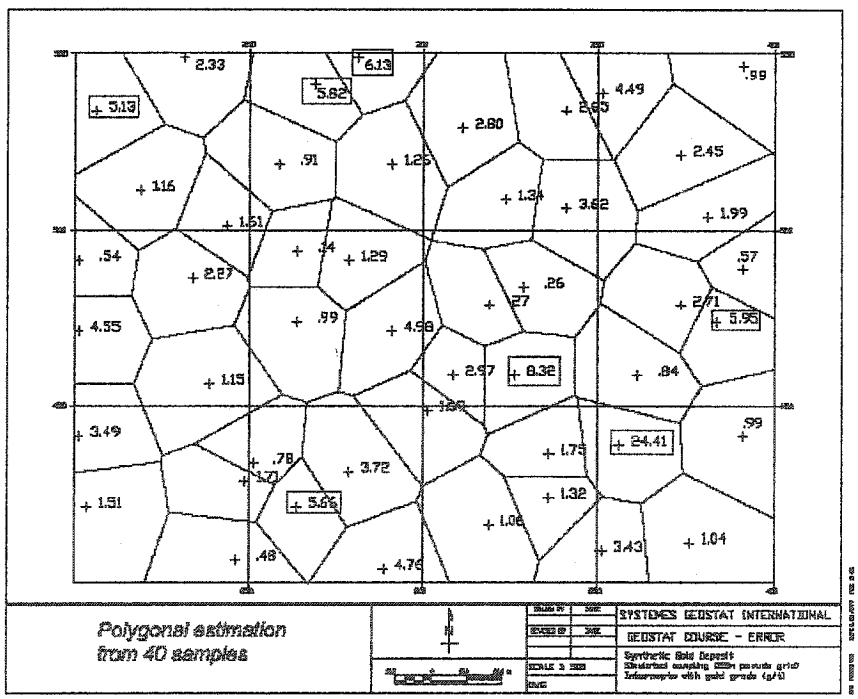

Figure 2-11 Polygons of influence for the test portion (Dagbert 2001)

2.2.2.2 INVERSE DISTANCE

Inverse distance is probably the most often-used of the geometrical techniques. It is simple and most geostatistical programs include this as an interpolation option. In its simplest form, the estimated value of a point or node is calculated by proportioning the value of nearby samples according to the inverse of their distance from the node. *Inverse Distance Squared*, the most common form, proportions the sample values by the inverse of its squared distance from the node, inverse distance cubed by the inverse of the cubed distance from the node, and so on.

A benefit to inverse distance squared is that different exponents can be used in different directions to account for *anisotropy*[24]. For example, in a coal deposit it might make sense to use inverse distance squared in the horizontal directions to account for the increased grade continuity, but inverse distance to 4^{th} power in the vertical due to both the (observed) reduced thickness in this dimension and a better (theoretical) understanding of the sedimentary genesis of the deposit. An alternative method used for accounting for anisotropy is to use smaller search radii in the directions with less continuity.[25]

Inverse distance methods are generally used when insufficient data are available for more detailed geostatistical and variability studies, or when the variable of interest is difficult to model using geostatistical methods. Because of the practice of averaging, it is impossible for any node to have a value greater than the maximum or lower than the minimum of the sample values within the search neighborhood. This inevitably results in a certain amount of *smoothing*, resulting in a histogram of calculated node values that will be narrower (*i.e.* lower standard deviation) than that of the sample set itself. This phenomenon should be considered during the interpolation analysis.

---

[24] *Anistropic* behavior means that the variable of interest can change more quickly in one or more directions. Variables that have the same degree of continuity in all direction show *isotropic* behavior.

[25] Note that in general deposits are assumed to be isotropic unless there are clear reasons suggesting otherwise (such as in the coal seem example described).

2.2.2.3 MOVING WINDOW AVERAGES

The general practice of using the method of moving averages for geometrical interpolation consists of defining a set of search radii or a search ellipsoid. The calculated node value is then equal to the average sample values that are within the search ellipsoid.

To a limited extent, anisotropy can be incorporated by varying the length of the search radii that define the ellipsoid. Smoothing is also a factor in this method.

The practice of moving window averaging for grade estimation is rare, however it is sometimes applied to ore hardness, separation efficiency (for processing unit operations such as flotation or dewatering) and other variables with less impact on the project economics than ore grade. By far the most common method for applying this technique is to identify different lithologic or otherwise-defined ore class boundaries and assign the average value for the samples collected from that unit to all nodes within those boundaries. This practice generates reasonable estimates of the average values for those units, however it does not generate any information on the variability of the variable within the lithologic unit or ore class.

Figure 2-12, Figure 2-13 and Figure 2-14 show variations of gold grade in g/tonne in a hypothetical test bench as comparison between the "real" grades (as determined from 1200 simulated values) and the estimated grades calculated using polygonal estimation and inverse distance squared. Note that:

- The polygonal estimation reflects the natural distribution of the gold grades shown in Figure 2-12. There is no smoothing of the histogram of gold grades.
- The inverse-distance squared method shows more continuous variability in gold grade, but has a higher degree of smoothing.

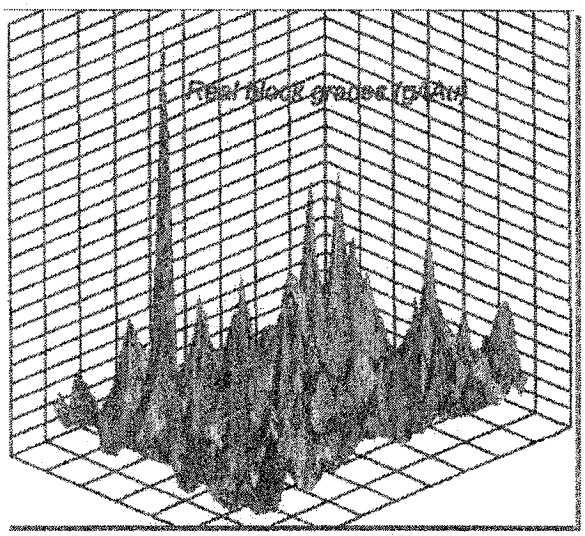

Figure 2-12 Real block grades in a bench. Horizontal grids are on 5 m intervals. Vertical is g/tonne Au on unit intervals beginning from 0 g/tonne Au (Dagbert 2001).

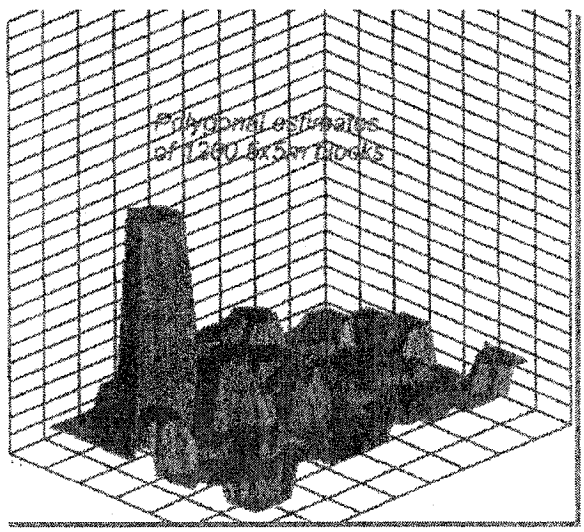

Figure 2-13 Variations of gold grade in the bench according to the nearest neighbor method, same axes as Figure 2-12 (Dagbert 2001)

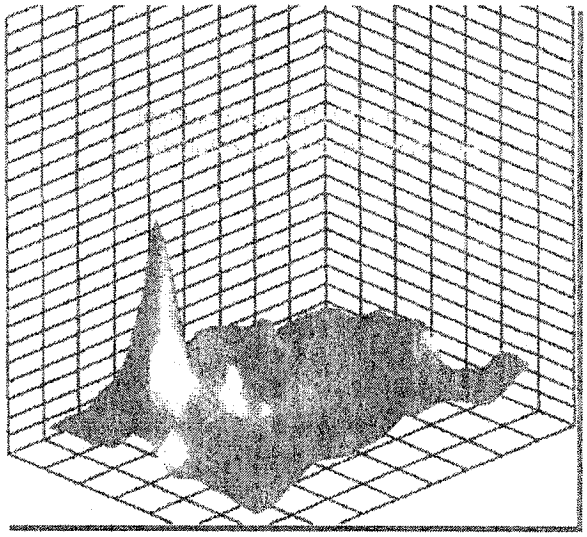

Figure 2-14 Variations of gold grade in the test portion of the bench according to the inverse distance squared method. Same axes as Figure 2-12 (Dagbert 2001)

2.2.3 Geostatistical Methods

This section describes selected geostatistical methods used for ore reserve estimation and grade control. The first part of this section introduces the concept of estimation error. The second part explains the geostatistical tool called the variogram, which is used to calculate the expected estimation error for a node from samples separated by distances. The third part explains the basis of kriging, which is simply a statistical procedure that calculates the appropriate weighting factors for the nearby samples such that the estimation error of the node is minimized. Finally, some alternative forms of node interpolation and simulation are summarized in the fourth part.

2.2.3.1 ESTIMATION ERROR

It is apparent from Figure 2-13 and Figure 2-14 that neither the inverse distance squared method nor the polygonal estimation method produce perfect estimates of the gold grades shown in Figure 2-12. It can therefore be stated that the estimates derived from a small number of samples are not true values. The difference between the true value and the estimate is the estimation error. It can be positive (under-estimation) or negative (over-estimation). If the estimation error is large, then serious ore classification problems may occur. Obviously, at the time of the estimation the error is not known, otherwise there would be no error.

Figure 2-15 and Figure 2-16 show the histograms of errors for the polygonal estimation method and the inverse distance squared method discussed above. A glance at the histogram shows that the dispersion of the histogram of errors due to the polygonal estimation method is greater than that due to the inverse distance squared method. This is known as the *error variance* or the average squared difference between each value and the mean of the histogram. The square root of this variance is the *standard error* (standard deviation of the errors) and is a good measure of the overall magnitude of errors. In the example discussed, the standard error for polygonal estimation is 3.96 g/t and 2.57 g/t for inverse distance squared.

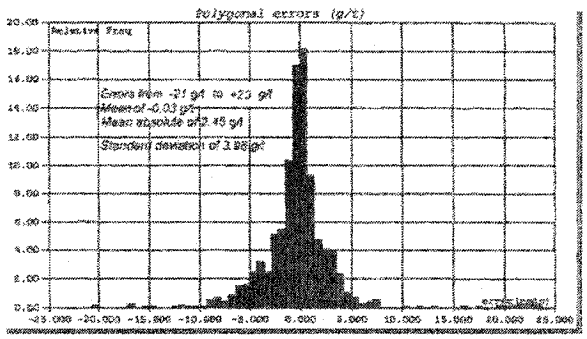

Figure 2-15 Histogram of errors due to the polygonal estimation method, g/t Au(Dagbert 2001)

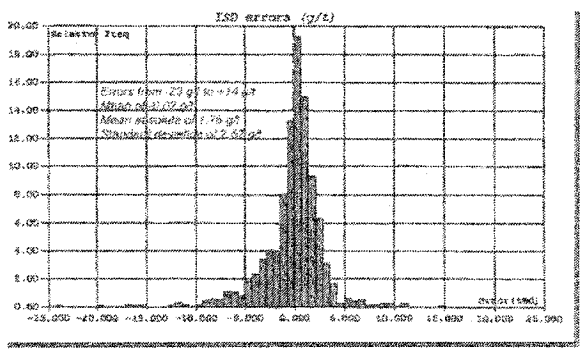

Figure 2-16 Histogram of errors due to the inverse distance squared method, g/t Au(Dagbert 2001)

It is important to point out that the *mean residual error*, or the average value of the above histograms, is zero. This signifies that these methods are *unbiased* methods for point estimation, *i.e.* the sum of the weights used for nearby samples equals unity.

2.2.3.2 THE VARIOGRAM

The previous section has shown that a convenient way to characterize the magnitude of estimation errors is through the standard variance of the histogram of errors. The variance is the average squared difference between the true value and all possible estimates for that value; hence a way to appraise that squared difference is to look at squared differences between sample values themselves. If the differences between samples are high, even at small distances between those samples, then it is expected that the differences between the true value and estimates derived from those samples will be high as well. This is the concept behind the variogram: to analyze differences between samples to be able to predict differences between estimates and true values. The variogram looks at squared differences between samples simply because the selected measure of the error is also a squared difference, the variance.

Practically, samples are classified according to how distant they are from each other. As it is expected that the differences between samples increase with increasing distances, it is customary to classify samples for analysis into groups with similar distances.

Figure 2-17 shows a conceptual view of what a variogram is. Equally sized channel samples have been taken along a straight portion of a drift at 3 m intervals. Considering all the pairs of samples at 3 m distances, the squared differences between the two sample values in each pair are averaged. This is the first point in the variogram; it shows the average squared difference of sample values separated by a distance of 3 meters. Repeating this procedure for samples separated by 6 meters gives the second point in the variogram. The same process is repeated for pairs at 9 meters, 12 meters, 15 meters, and each time a new variogram value is generated. The result is a diagram showing the average squared difference between samples as a function of the distance between those samples. The very interest of the variogram is the **rate of increase of those differences**. If the rate is low, two samples may have very similar values even if they are far apart, resulting in an estimation error that is likely to be low. On the other hand, if the average difference between samples increases rapidly with distance, the estimation error is likely to be high.

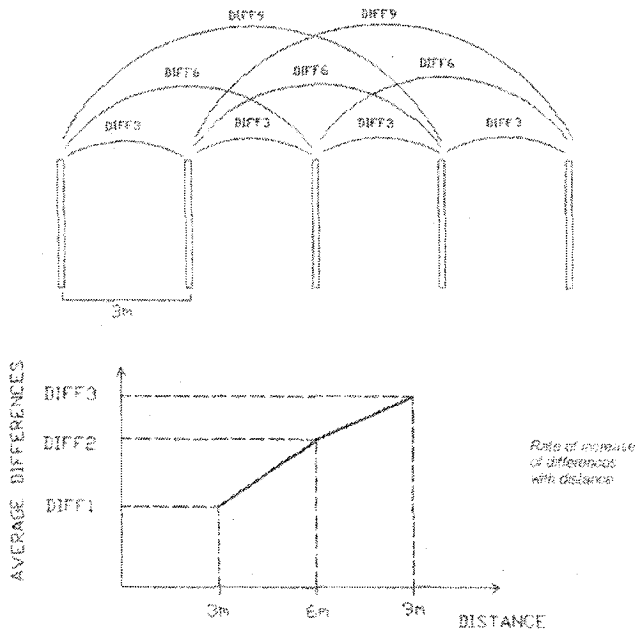

Figure 2-17 Calculation of a variogram from regularly spaced samples in one direction.

Some further notes on the variogram are:

- The variogram depicted in the example above has been computed in a single direction. In practice, *directional* variograms should be calculated in 3 directions to account for any anisotropy. If the same variogram is used in all 3 dimensions, it is said to be an *omni-directional variogram* and the variable exhibits isotropic behavior.
- The variogram is not exactly the average squared difference between samples but only half of it. The 0.5 scaling factor is meant to adjust the variogram such that it is of comparable units to the variance. This 0.5 factor explains why the variogram is sometimes referred to as the *semivariogram.*
- The total number of possible pairs between N samples is defined by N(N-1)/2. Hence with 1000 samples, 500,000 possible pairs can be investigated. In practice not all pairs are examined as pairs separated by large distances are generally of little interest and only specific directions are analyzed. Furthermore, because of sampling practicalities, it is necessary to define the distance for sampling pairs with a lag or tolerance in order to generate sufficient sample pairs within a distance class. These two points combine to make variogram

computation a very tedious process if it were to be performed by hand. Computer programs are generally used.

- Implicit in the variogram calculation method is the assumption that the variation of differences between samples with distance and direction is the same everywhere (for example there are no places where the difference at 10 meters in a given direction is always around 5 whereas in another place this difference is always around 10). This is called the *stationarity* assumption and a lot of geostatistical theory depends on it.
- The calculated variogram is not used in kriging. Rather, a model or curve (called the *model variogram*) is fit to the calculated variogram to approximate its shape. The equation of the curve is used for kriging

General terminology regarding the variogram is as follows. The point where the variogram intercepts the y-axis, or variogram axis, is known as the *nugget effect* (Figure 2-18). It can be thought of as the average squared difference between adjacent samples. The differences are due to the natural variability of the variable being measured (*natural nugget effect)* plus any sampling variance, testing/assay variance, and other errors that propagate into the testing procedures (*human nugget effect*). The term originally came from gold deposits, where adjacent drill holes were often observed to have very different gold assays due to the presence of a relatively small amount of large "nuggets" in one of the holes.

The *sill* of the variogram is the plateau where the average difference between samples tends to level out. The *apparent sill*, shown in the model, is the estimated sill based on the calculated variogram. The *nested sill*, which is equivalent to the calculated variance of the entire sample set, can also be used for variogram modeling. The *range* is the distance along the x-axis at which the average distance reaches the sill. It can be thought of as the distance between samples beyond which there is no statistical relationship between their values.

For good estimation (low standard errors) it is desirable to have a variogram with a low nugget effect, a low sill, and a low slope (and hence a high range).

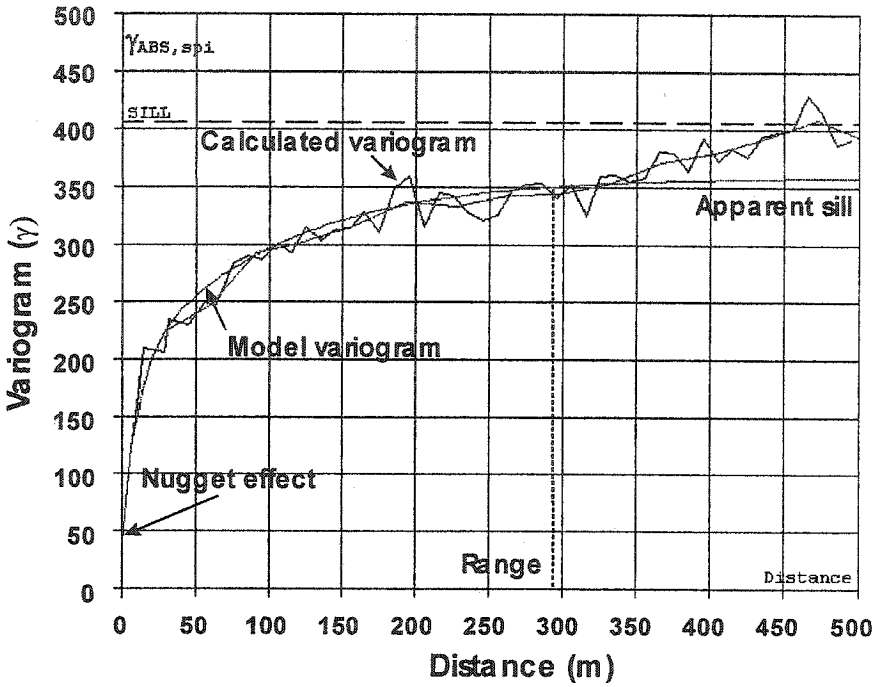

Figure 2-18 Properties of a variogram

2.2.3.3 KRIGING

The main feature that distinguishes kriging from the estimation methods discussed in Section 2.2.2 is that it does not use a pre-ordained weighting system that is dependent upon the estimation method used (*i.e.* as inverse distance squared uses a weighting system for nearby samples based on the inverse of the squared distance). Instead, kriging is a calculation method for the set of weights for the nearby samples such that the error variance, or standard deviation of the error, is minimized. As with the three geometrical interpolation methods discussed, the sum of the weights in a single kriging system must equal unity, therefore the kriging method is also unbiased. For these reasons, kriging is often associated with the acronym *B.L.U.E.*, for "best linear unbiased estimator" (it is linear because the estimate is a weighted linear combination of the available data).

A brief description of the procedure is as follows. It can be shown that the estimated grade/value of a point or node, given *n* number of nearby samples, is a function only of the values of those samples and weighting system that we apply to them. This can be expressed by the (unbiased) equation:

$$V = \sum_{i=1}^{n} w_i \bullet V_i \text{ and } \sum_{i=1}^{n} w_i = 1$$

Equation 2-15

Where V is the estimated point value, V_i is the measured value of the nearby sample *i*, and w_i is the weight applied to the sample *i*. Furthermore, it can be shown that the error variance of the estimate is a function only of the weights applied to the nearby samples, the variance of those samples, and the variogram as described in section 2.2.3.2. It is given by the formula:

$$\sigma_R^2 = \sigma^2 + \sum_{i=1}^{n} \sum_{j=1}^{n} w_i w_j C_{ij} - 2\sum_{i=1}^{n} w_i C_{i0}$$

Equation 2-16

Where σ^2_R is the error variance, σ^2 is the variance of nearby samples, and the *C* represents the variogram function[26]. Knowing the general formula for the error variance as a function of the variogram, local variance, and the weighting system, we solve for the weights such that the error variance is minimized. This is done by setting the *n* partial first derivatives of the error variance with respect to the weights equal to zero and solving. This produces a system of n equations and n unknowns. However, not just any system of weighting factors is acceptable; the unbiased condition dictates that only a weighting system in which the individual weights sum to one is acceptable. This has the effect of adding another equation to the system; the problem therefore becomes one of constrained minimization, the solution of which is not as straightforward.

The constrained minimization problem is solved through the introduction of a Lagrange parameter, thereby converting the constrained minimization problem into an unconstrained one. The Lagrangian is introduced in the following manner:

$$\sigma_R^2 = \sigma^2 + \sum_{i=1}^{n} \sum_{j=1}^{n} w_i w_j C_{ij} - 2\sum_{i=1}^{n} w_i C_{i0} + \underbrace{2\mu\left(\sum_{i=1}^{n} w_i - 1\right)}_{0}$$

Equation 2-17

[26] Actually it represents what is called the *covariance* function, similar in nature to the variogram. Detailed explanations of this and other equations can be found in Isaaks & Srivastava, chapter 12

Because the sum of the weights equals zero, the Lagrange term has the net effect of adding zero to one half of the equation.

The n + 1 equations (n equations plus the unbiased condition) and n + 1 unknowns (n weights plus μ, the Lagrange term) are known as the *ordinary kriging system*. It is solved for the individual weights, which are subsequently applied to the nearby sample values to generate the node estimate.

2.2.3.4 OTHER GEOSTATISTICAL METHODS

Block Kriging

The previous discussion described the method of *ordinary kriging*. Block kriging is a modification of the ordinary kriging process intended to account for the fact that in general the mining industry is not concerned with the estimated value of a point, but rather the average estimate of an entire block. Block kriging is simply a method of discretizing the block into many discretization points and using ordinary kriging for each point. The estimated points are then "re-combined" into a single block average. Because of the averaging that occurs in a block, the larger the blocks are, the more smoothing that occurs.

Multiple Indicator Kriging

Multiple indicator kriging is the process of kriging "histograms" into each block with the intent of evaluating the amount of smoothing that occurs during the kriging process. The general procedure is to assign different indicator cut-offs and create a variogram for each one. An indicator cut-off is an "arbitrarily" chosen grade, for example in a gold deposit the gold grade indicator cut-offs could be 1 g/t, 2, g/t, 3 g/t, and so on. For the 1 g/t cut-off, a unit value of 1 is assigned to all sample assays greater than the cut-off, and 0 is assigned to those lower than the cut-cut-off. The variogram is then calculated for all of the 1's and 0's, which are subsequently kriged into each block. The same process is applied to all of the cut-offs, resulting in a different value for each cut-off. These values become the histogram, effectively a kriged distribution for all of the cut-offs chosen.

Conditional Simulation

As the name implies, this method is not an interpolation method but a simulation method. It is computer-intensive, but has gained popularity with the increased computer processing power of the last decade. Although it is beginning to be used for reserve estimation, it is most often employed for short-term production forecasting from blast hole drill chips (due to the usually smaller blocks used in the model[27], the increased assay availability[28], and the limited number of blocks requiring interpolation[29]).

The idea behind conditional simulation is to simulate assay or core composites in the block model using nearby samples such that the global histogram of assays and the variogram derived thereof are both preserved (hence it is "conditional"). Because the method simulates assay values, the block grids are generally much smaller. The benefits to conditional simulation are that the effect of smoothing is not present because no averaging occurs in the process; therefore predicted economic repercussions such as ore dilution and the effects of blending in the mining and stockpiles processes can be evaluated. However, this also results in the fact that only a "simulated" value is given for a single node and not the "best linear unbiased estimate." The result is that upwards of 20 or 30 individual simulations should be performed if the best estimate of a single block is desired. This adds significantly to the computer power needed (due to the smaller grids and increased number of iterations needed) and is the main drawback of conditional simulation.

2.3 ORE BLENDING

There are two main issues that generally arise during any discussion of ore blending. The first issue centers around the industrial practicality of ore-blending programs: what are the benefits and detriments? The second involves the laboratory and theoretical

---

[27] Which is in turn due to increased knowledge of mining selectivity in the immediate short-term and closer assay spacing

[28] Diamond drill holes generally have spacing intervals an order of magnitude greater than those of blast hole drills

[29] A single blast "parcel" or pattern will have only a fraction of the blocks contained in the entire deposit, smaller blocks notwithstanding. This significantly reduces the computer time required for the simulation.

issues that might arise when attempting to perform test work on blended samples or modeling of blend behavior in a process plant.

2.3.1 Full-Scale Blending

Perhaps the single most important benefit to blending is attributable to the fact that the process plant houses a number of very different unit processes connected together in series configuration. Each unit process, be it autogenous grinding, secondary grinding, flotation, or dewatering, has its own capacity or capacities, depending on the properties of the mineral. When only one of these processes is operating at maximum capacity during the processing of any given ore, there is a production bottleneck in the process plant and the remaining unit operations will be operating below capacity, resulting in idle capital and probably increased specific operating costs. (After Mitchell and Holowachuk, 1996)

The obvious solution to the problem is to widen the bottleneck through process improvements. If for some reason this is not possible, the alternate solution is to implement a program of ore blending such that an ore that would create a bottleneck at one unit process is blended with an ore that would create a bottleneck at another unit process. The resulting blend would serve to reduce both hypothetical bottlenecks and increase the overall plant production over what would be achieved by processing each ore exclusively. (Bennett et al 2001; Mitchell and Holowachuk, 1996)

This problem can be particularly acute in SAG grinding for two somewhat associated reasons.

Firstly, in SAG grinding the ratio of impact to abrasion/attrition grinding is different than it is in secondary ball-mill grinding due to differences in typical mill diameters, feed sizes, and ball charges. It was shown (Section 2.1.1.3) that rock can exhibit various different properties of ore hardness that may not be correlated, such as friability and abrasiveness. Relative differences in these properties from one ore to the next will lead to relative differences in maximum capacities from the SAG mill to the ball mill circuit. For example, it is common for an ABC grinding circuit that is milling hard, coarse ore to produce a larger relative amount of fine material in the primary mill product. Because

the ore is hard and coarse, more primary milling time is required (*i.e.* lower throughputs) and hence the product becomes finer (due to higher residence time in an abrasion-dominated environment). The combination of low throughput and fine product creates under-loading of the ball mills. The opposite scenario occurs when the SAG mill receives fine, soft material. This tends to flow through the SAG mill and out the grates before much grinding actually occurs, resulting in a high flux of coarse material to the ball mills. In this scenario the ball mills are the bottleneck and the SAG mill is under-loaded. (Bennett *et al.* 2001)

The second reason has to do with the variability of feed particle size to the mills. Feed size fluctuations are much more erratic in primary milling than they are in secondary milling (after the ore has already passed through a grinding machine, grates and a screen, and possibly a pebble crushing circuit with a circulating load). Feed size variations change the abrasion/attrition ratios in the autogenous mills significantly, and lead to performance efficiency problems in the grinding circuit as a whole (after Hart *et al.* 2001).

The effects of a program of ore blending can be evaluated by performing SPI and Bond tests on the problematic ores and then calculating the SPI and Bond work index for the blend based on the proportion of each ore used to create it. This procedure raises the important question of additivity: can SPI and Bond Wi values be averaged linearly? Recall that in Section 2.2.3.3 the geostatistical method of kriging was discussed, and it was noted that kriging itself results in a linear average of the surrounding data points. As such, if SPI and Bond Wi values are not additive there would be repercussions on the geostatistical method used. The next section describes some preliminary work undertaken to answer the question of additivity of the SPI.

2.3.2 Modeling of Blends

The first study[30] that was conducted to investigate blending was initiated by the author in 1997 under the auspices of MinnovEX and NSERC, (Natural Sciences and Engineering Research Council of Canada). It was a preliminary scoping study into the effects on ore

[30] Amelunxen, P., "Minnovex SPI Grind-Time Variations in Hard/Soft Ore Combinations", MinnovEX Technologies / NSERC study, Toronto, Ontario, 1997.

blending. The work was performed before some important quality control procedures were implemented on the general SPI procedure and as a result the sample preparation procedures can be criticized somewhat:

- The parent ores were crushed to SPI feed size prior to blending.
- The ratios of the different size classes were not controlled[31], except for the plus 2.54 cm material and minus 2.54 cm material.

The above caveats notwithstanding, the project conclusively determined that the SPI of a blend will be lower than the linear average SPI of the parent ores used to create it. It is therefore not an additive parameter.

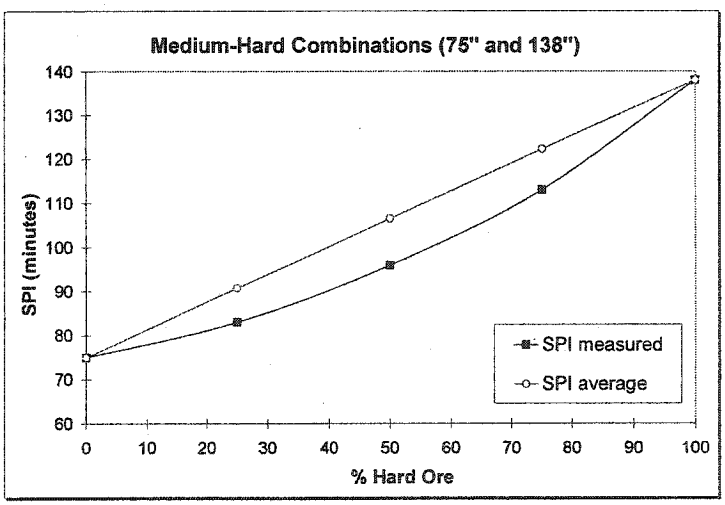

Figure 2-19 Blend results, 1997 NSERC study (Amelunxen 1997)

Figure 2-19 shows results from a typical blend suite. The straight line shows the SPI calculated by linear average based on the percent hard ore shown on the x-axis. The curved line shows the measured SPI values of the blend.

2.4 ROSIN-RAMMLER EQUATION

The Rosin-Rammler equation was published in 1933/34 as a technique for use in determining the particle size analysis of coal powder. There has been some confusion

[31] "Controlled size class" blending indicates that material was screened into different size classes and the size classes were individually blended in the correct proportions

on the general form of the Rosin-Rammler equation; one common form (particularly on the Australian continent) as published by Taggart (1945) and JKMRC (1999) is given by:

$$R = 100 - e^{-(x/a)^m}$$

Equation 2-18 Rosin-Rammler formula A

In Equation 2-18, R is the cumulative percent passing size x, and a, and m are constants[32]. Often, however, the size parameter a is expressed as $1/b$ (*e.g.* Lynch and Lees, 1985), giving the equation:

$$R = 100 - e^{-(bx)^m}$$

Equation 2-19 Rosin-Rammler formula B

The equation has also been expressed without the constant b raised to the power of m, as in BMHB (1987):

$$R = 100 - e^{-bx^m}$$

Equation 2-20 Rosin-Rammler formula C

Given the confusion, the author has not hesitated to take some liberties with the general form of the equation as well. This explanation is provided for clarity.

All equations are fitted using least-squares regression techniques.

[32] The constant a is sometimes referred to as the size parameter, or modulus, of the curve and is the 36.79% cumulative percent passing size.

3 THE BEHAVIOR OF BLENDS

The question of additivity is important for at least one simple reason. All geostatistical and geometrical interpolation techniques that are used for modeling ore bodies are based on the additivity of the parameter in question. The process of calculating a parameter's average for a cell or moving window, computing a variogram, or calculating a kriged value is performed under the implicit assumption that the parameter can be mathematically averaged. For metal assays such as gold grade or copper concentration, it is intuitive that the parameter is additive, but what about for index-type tests such as the SPI, where the value is expressed in units of "minutes"?

The simplest way to prove that an ore property is additive is to create a physical blend of two different ores, and measure the value of that property in the parent and progeny samples. If the calculated average is the same as the value measured on the blend, the property is additive. This approach has shown (Section 2.3.2) that the SPI is not an additive parameter. This stems from the fact that the reduction of ore in a laboratory mill can be characterized by a non-linear curve of grind versus time, whereas the SPI is only one point on this curve (*see* Section 2.1.4.1 and Figure 2-3). It has been observed that, within experimental errors, the SPI of a blend of samples is always lower than the calculated average would predict.

This section will show that the observed difference between the SPI of a blend and that of the parent ores can be fully explained by considering the entire curve of grind versus time when calculating the average. This curve is described in Section 3.1 in detail and a model or models are derived to represent it. Section 3.2 shows how the models of two parent ores can be combined to predict the behavior of the blend. Section 3.3 presents the results of experimental blending work that show agreement between the predicted behavior of a blend of ores and the measured behavior. Section 3.4.3 provides some suggestions for improving the SPI test in light of the current analysis, and the geostatistical implications that should be considered.

3.1 MODELING OF THE SPI TEST

The SPI test is a series of grinding iterations on a 1.7 mm screen. When 80% of an initial 2 kg charge has been ground to minus 1.7 mm, the test is complete and the time required for grinding the ore to this point is the SPI. Figure 3-1 shows the typical grinding iterations of an SPI test. The y-axis is the percent of the initial SPI charge remaining in the plus 1.7mm portion of the charge.

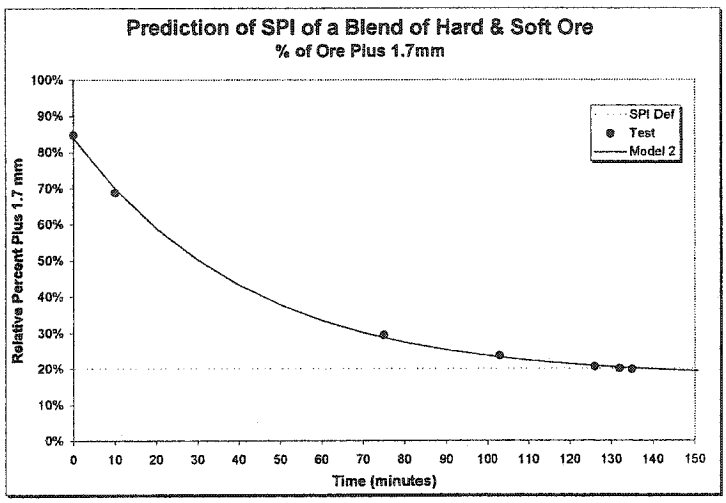

Figure 3-1 SPI test grind curve

Several models can be used to represent the SPI grinding behavior:

$$P = c_1 + c_2 e^{-c_3 t}$$

Equation 3-1

$$P = c_1 e^{-c_2 t^{c_3}}$$

Equation 3-2

$$P = c_1 + e^{-c_2 t^{c_3}}$$

Equation 3-3

where P is the percent of material retained on the 10-mesh screen, c_1, c_2, and c_3 are constants, and t is the grinding time, in minutes.

Equation 3-1 is a simple exponential function that converges on 0 + c_1 where c_1 is the percentage of the test feed that is already finer than 1.7 mm at zero minute. Equation 3-2 and Equation 3-3 are forms of the Rosin-Rammler equation. They converge on 0

and 0 – c_1, respectively. Figure 3-2 shows the three models extrapolated far past the test completion point to illustrate the differences in the convergence of the models.

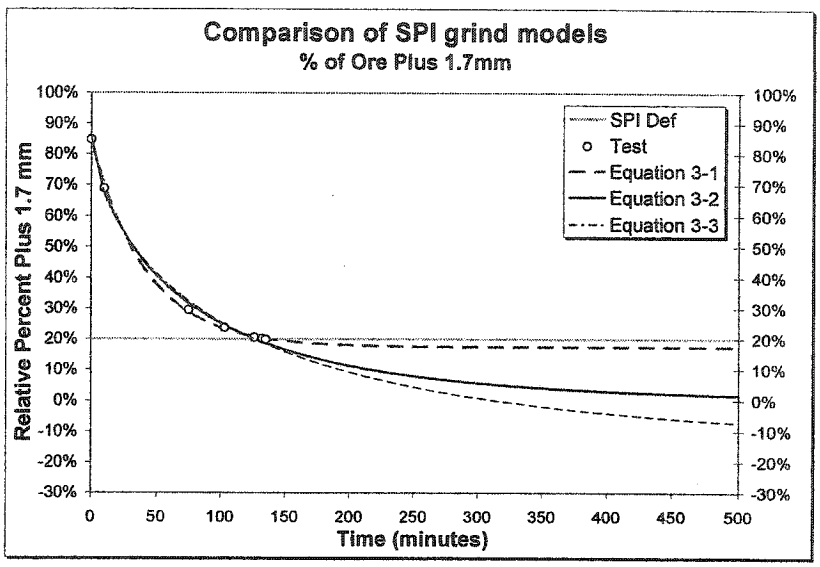

Figure 3-2 Various SPI models extrapolated past the SPI termination point

Equation 3-2 is the most-used form of equation used for modeling the SPI test, but for very soft or very hard ores it does not perform well. Soft ores undergo very rapid reduction in the plus 10-mesh fraction, which disappears after a very short grinding time. This rapid reduction is not adequately modeled by Equation 3-2 because it converges on 0%, creating a bias near test completion on very soft ores. This is not a significant source of error for the SPI test in its current form but blending studies and geostatistical concerns (discussed below) require knowledge of the grind curves of soft ores in the time range beyond the point where 20% is retained an the test stopped. In this range the errors introduced by the convergence on zero of Equation 3-2 would become significant. These errors are minimized by the use of Equation 3-3, for which the constant c_1 allows to converge on 0 – c_1. The concept that there can be a negative percent retained on the 10-mesh screen is meaningless in practice, but the mathematical modeling of such a scenario works adequately for the study of blending. The only cautionary note that applies involves the modeling of extremely soft ores (*e.g.* SPI values under 15 minutes). In this case it is necessary to use two equations to describe the behaviour of the ore in the SPI test mill: one for modeling the breakage

rate before P = 0 and one to hold P = 0 for all time values past that point on the model as shown in Figure 3-3.

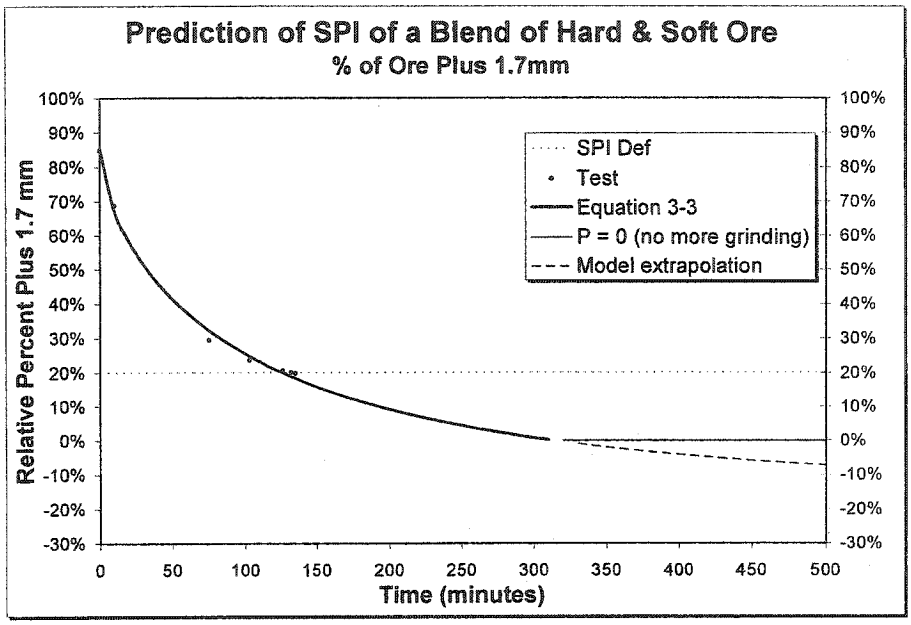

Figure 3-3 Application of Equation 3-3

The convergence of Equation 3-2 on 0% creates problems for hard ores as well as soft, but for the opposite reason. Many hard ores *never* reach 0% retained. Equation 3-1, which converges on c_1, is then used.

3.2 BEHAVIOUR OF BLENDED ORE

To predict the behavior of a blend, it is assumed that the portion of an ore that is present in the blended sample retains the same grinding characteristics that its parent ore exhibited in the unblended test. This assumption enables the use of the models of the parent ores to predict the behavior of the progeny blends.

The best way to illustrate the technique is using an example. In this case the ores blended are hard and soft copper porphyry ores (Figure 3-4) from Kennecott Minerals, Utah. The experimental points and their respective models are shown in Figure 3-4.

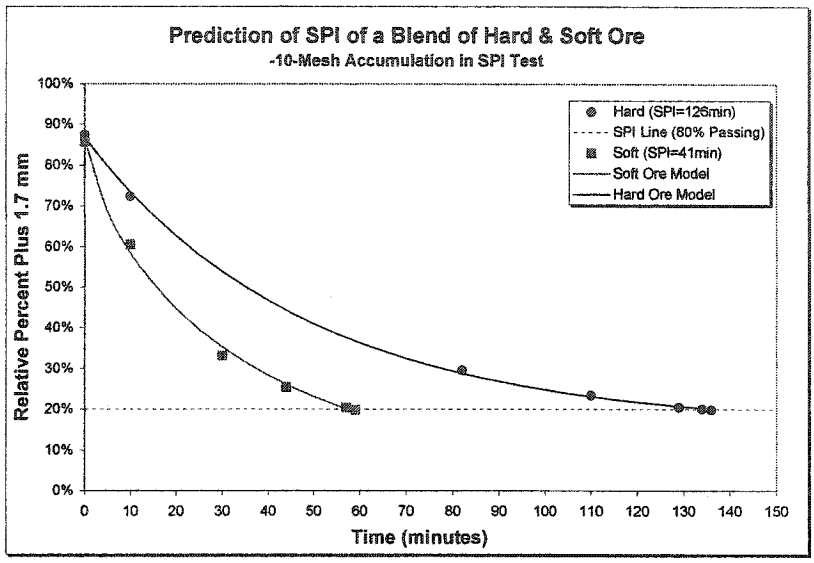

Figure 3-4 Hard (134 minutes) and soft (58 minutes) ores

The behavior of a 50% blend of the two ores shown in Figure 3-4 can be predicted as follows. Their curves are discretized into 5-minute intervals and the percentage of material remaining at the end of each interval is calculated from the models. The percentage of material remaining in the blended sample at the end of the same time interval is then calculated by arithmetic average based on the ratios of material that constitute the blend. For example, after 5 minutes of grinding there would be 80% of the hard ore remaining in the 10-mesh fraction, and 69% of the soft ore. By simple arithmetic average, there should be 74.5% of the coarse remaining after 5 minutes in the plus 10-mesh fraction of a 50% blend of these ores. The calculation steps are shown in Table 3-1.

BLEND	
Soft:	50%
Hard	50%
SPI:	85

Time	P Hard		P Soft		P Blend
(min)	% + 1.7mm	operation	% + 1.7mm	operation	% + 1.7mm
0	87%	* 50% +	86%	* 50% =	86%
5	80%	* 50% +	69%	* 50% =	74%
10	73%	* 50% +	59%	* 50% =	66%
15	66%	* 50% +	51%	* 50% =	59%
.	.	.	.	.	.
.	.	.	.	.	.
.	.	.	.	.	.
85	28%	* 50% +	12%	* 50% =	20%

Table 3-1 Method for calculating the SPI of a blend

Figure 3-5 shows the graphed prediction of the grindability of a 50% blend of the two parent ores and the experimental results of the SPI test performed on this blend. The experimental points show close correlation with the theoretical model.

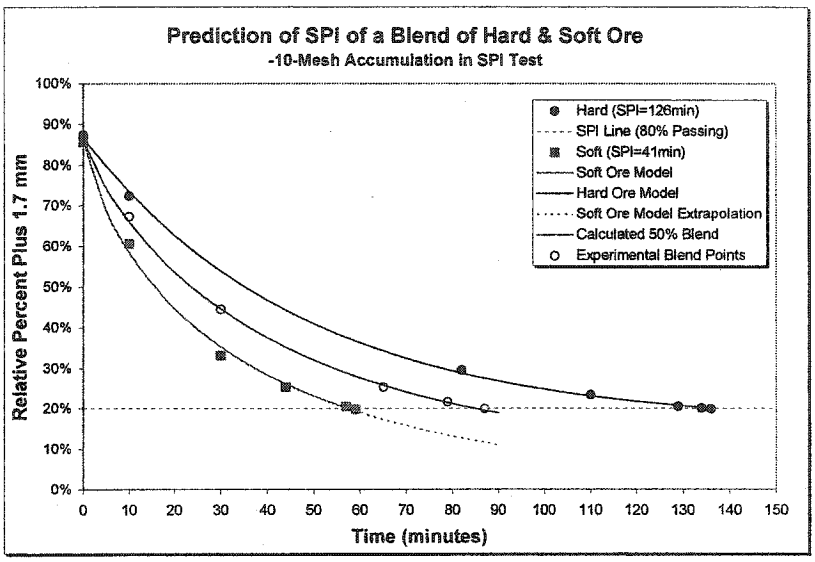

Figure 3-5 50% Blend model with experimental points

To investigate this further, experimental work was performed on blend samples created in various different ratios of parent ores. The confirming results are shown in Figure 3-6 and Figure 3-7.

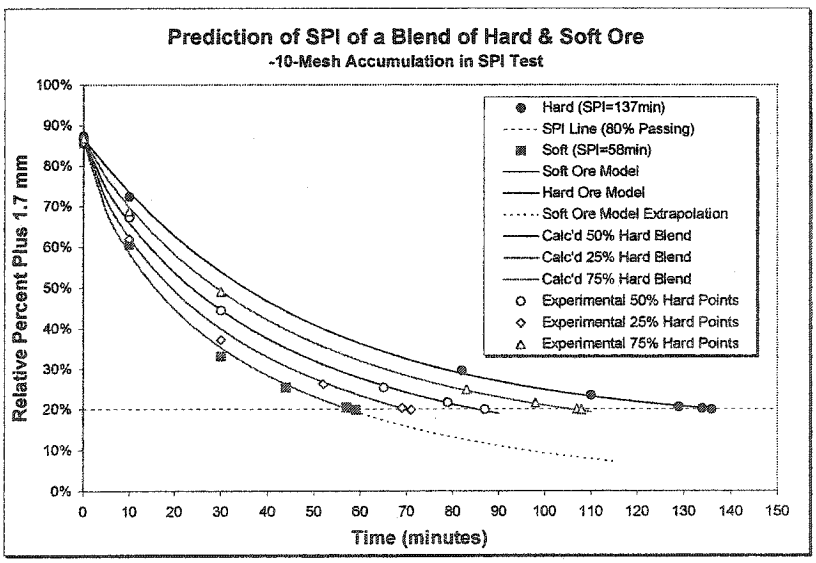

Figure 3-6 Predicted and actual grindability of two parent ores (137 and 58 minutes) and their three progeny blends.

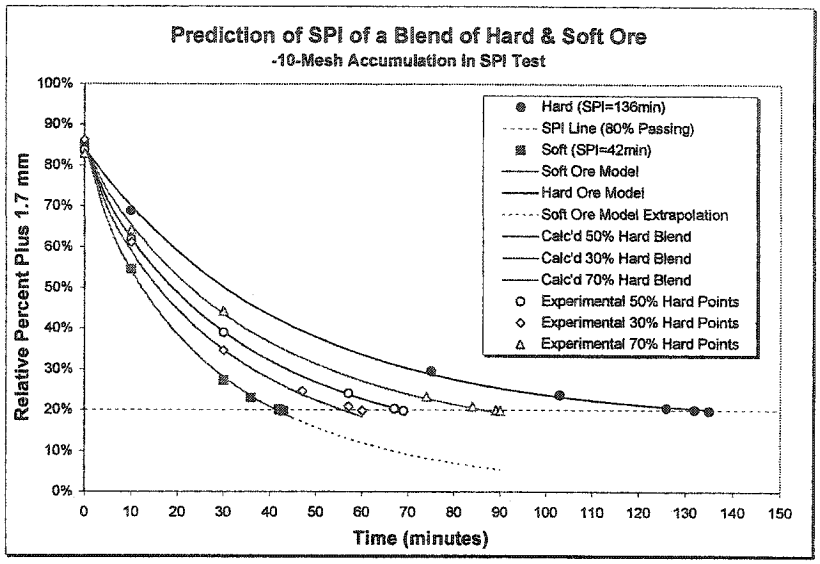

Figure 3-7 Predicted and actual grindability of two parent ores (136 and 42 minutes) and their three progeny blends.

3.3 PREVIOUS BLENDING RESULTS

The above analysis can be extended to previous blending work with the caveat that the blending techniques applied during the sample preparation for the Kennecott samples above were not applied during the blending of the samples tested in the previous work. This previous work consists of two main studies. The first, performed in 1997 under the auspices of NSERC, did not utilize the controlled blending[33] or the improved test procedures[34] developed during 1999 and 2000 for quality control purposes. The second, a 1999 study at Phelps Dodge Chino Mines, also did not use the improved test procedures (although the ores were prepared using the controlled blending methods). Therefore, it is expected that the results of this previous work would show more scatter and variability then those shown above for Kennecott.

Figure 3-8 is a simple scatterplot with the measured SPI of the blend along the x-axis and that predicted from the modeling method along the y-axis. The most recent, lower-variance test results are shown as black triangles grouping within a few SPI minutes of

[33] "controlled blending" means that the relative size distribution of the coarse material in each component of a blend is identical to those of their parent ores. See Appendix XXX.

[34] Specifically a more rigorous feed preparation procedure that includes a oven-drying stage before the test is performed.

the equality line. The previous blend studies (Chino and NSERC) show no visible bias about the equality line, although slightly higher variance (scatter) is apparent. Some statistics are shown in Table 3-2. Note that although Chino has a higher relative standard error, this is due only to one single test near the origin that skews the results. Removing the test from the sample set reduces the relative error of the Chino data set to approximately 16%.

The bias of the blending results was testing using a two-tailed t-test for paired data means. For 23 degrees of freedom (24 blending tests), the t-score is 1.15, which is much lower than the significance value of 2.07 for 2 levels of confidence. Hence, there is no significant bias between the SPI value measured on a blend of ores and the value calculated from the parent ore grinding models. Table 3-3 shows the t-test statistics.

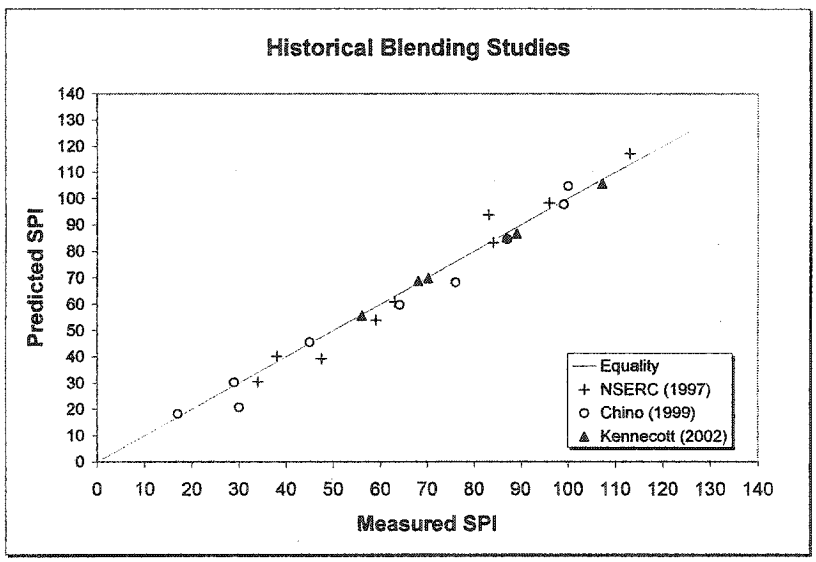

Figure 3-8 Previous blending studies in the context of the current analysis

Study	Date	Relative Standard Error (% of SPI)	Absolute Standard Error (minutes)
NSERC	1997	28%	16
Chino	1999	40%	14
Kennecott	2002	4%	4

Table 3-2 Previous blending studies

	Measured	*Calculated*
Mean	68	67
Variance	734	821
Observations	24	24
Pearson Correlation	0.99	
Hypothesized Mean Difference	0	
df	23	
t Stat	1.15	
P(T<=t) two-tail	0.26	
t Critical two-tail	2.07	

Table 3-3 t-test statistics for blending studies

3.4 RECOMMENDATIONS

Several recommendations for improvements in the test procedure can be drawn from the analysis presented in this section.

3.4.1 Extrapolation of Soft Ores

Be it for the purpose of process optimization or geostatistical interpolation, the mathematical modeling of the grinding behaviour of a blend of ores is a straightforward procedure given adequate knowledge of the grinding behavior of the parent ores. During discussion of modeling in Section 3.1 it was noted that correct blending analysis requires knowledge of the grinding curve of the soft ores beyond the point in time where the test is stopped. Use of the correct model will avoid some of the errors, but the lack of experimental points in this area will add uncertainty to the extrapolation of any model. Furthermore, because of the double-exponential nature of the Rosin-Rammler equation, minor experimental errors in the point locations would result in large errors in the extrapolated model. This in turn creates significant errors in the blend calculations[35], particularly when attempting to mathematically blend extremely soft ores with harder ones.

[35] For example it was noted in the previous section that one of the Chino tests was a significant outlier. That particular test was performed on a blend of 75% soft / 25% hard ore where the soft ore had an SPI value of 12 minutes and the hard ore had an SPI value of 127 minutes. It is strongly suspected that minor errors in the determination of the SPI of the soft ores resulted in much more significant errors in the calculated blend value due simply to the large amount of extrapolation applied to an already-limited model.

The simple solution to this is problem is to modify the SPI test such that soft ores are ground for some time after they have reached 80% passing 1.7mm (test completion). This will provide enough data in the post-completion part of the test to significantly reduce the amount of extrapolation required for soft ores.

3.4.2 Extra Grind Iterations Near Completion

Often two or three grind iterations are performed at the end of the SPI test to determine the exact location of the completion point by linear interpolation, as shown by the test example depicted in Figure 3-9. This is no longer necessary because the models developed in the previous sections can now be used to calculate the completion point. Although using the model equation instead of linear interpolation to calculate the test completion results in minor differences in SPI values, the procedural change has trivial impact on the test accuracy and zero impact on the geostatistical error[36]. This hypothesis was tested by comparing the SPI values from 939 SPI tests from Escondida to those calculated using the proposed methodology (after removing the redundant grind iterations and re-fitting the models).

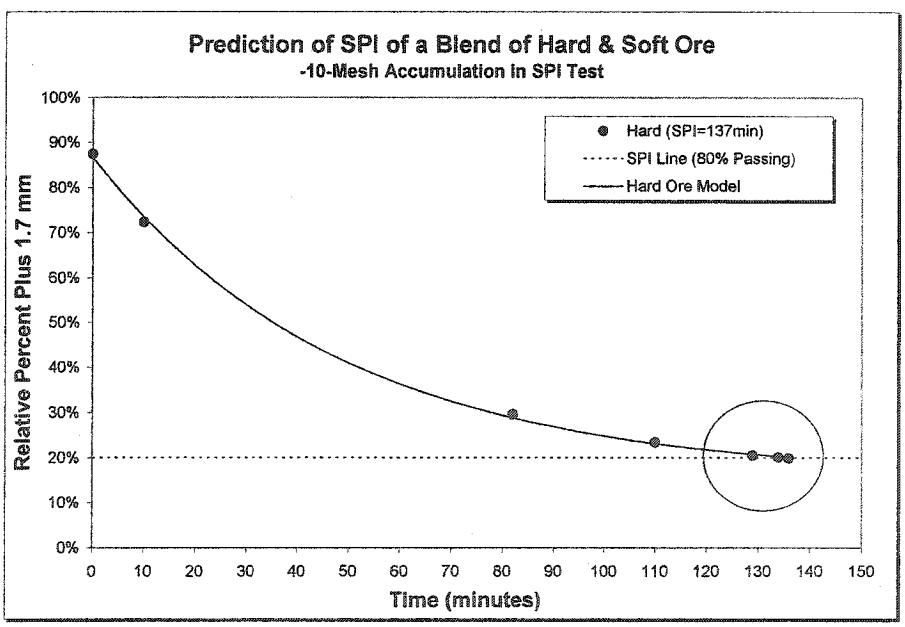

Figure 3-9 SPI test model showing redundant end-points

[36] Because in light of the current blend analysis it may become necessary to krige or distribute the entire curve.

Although some error can be seen in the scatterplot shown in Figure 3-10, this is due to differences in the lengths of the grind iterations (and hence the best-fit parameters that are derived from them) and not to an error inherent in the estimation of the SPI point. Fixing the iteration lengths to constant intervals may help to avoid these minor differences.

The bias between the two methods was investigated using a simple two-tailed z-test. Statistics are shown in Table 3-4. The z-score of -0.032 is much lower than the significance value of 1.96 for a 0.95 confidence level, indicating that there is no significant bias between the two at 2 levels of confidence.

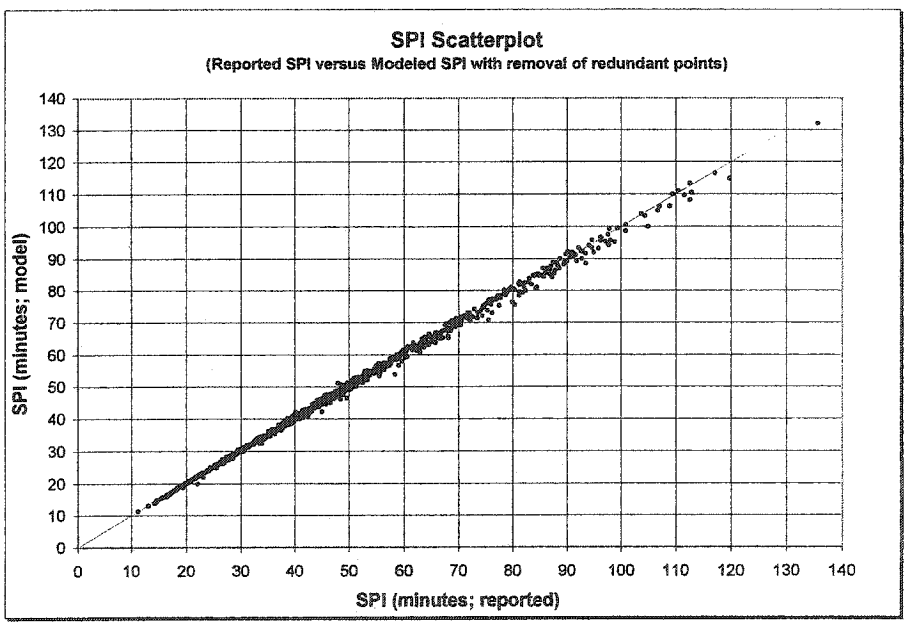

Figure 3-10 Scatterplot of deviation in SPI value when omitting redundant points near the test completion point

	Linear Int.	*Model*
Mean	49.0	49.0
Known Variance	512	493
Observations	939	939
Hypothesized Mean Difference	0	
z	-0.032	
P(Z<=z) two-tail	0.974	
z Critical two-tail	1.960	

Table 3-4 Z-test statistics for data shown in Figure 3-10

3.4.3 Geostatistical Considerations

It is worth reminding the reader again that the process of interpolating SPI values into a block model is effectively a mathematical blending of ores. The above analysis has shown that the SPI is not an additive property when the SPI is considered exclusive of its underlying grinding curve; hence, the geostatistical processes that assume additivity do so erroneously. This fact is novel—indeed, the geostatistical work presented below is itself based on the additive procedures for variogram calculation and kriging. While the general methodology described in the subsequent section still applies, some errors will result from the findings presented in this section. The magnitude of the error will be a function of ore body properties and can only be quantified with a comparative study—this will be discussed in Section 6.3. As the geostatistical studies were performed prior to the development of the blending conclusions presented above[37], a correction to the procedures described in Section 4.1 will be proposed. These corrections consist of interpolating the entire curve and then using the interpolated curve to back-calculate the SPI. This is presented in detail in Section 5.

[37] This was a result of some of the commercial implications of this research program.

4 THROUGHPUT ESTIMATION ERRORS

The throughput capacity of a plant is calculated by substituting Equation 2-4 into Equation 2-5 as follows:

$$T = \frac{P}{c_1\left(\frac{SPI}{\sqrt{T_{80}}}\right)^{C2} f_{sag}}$$

Equation 4-1

where T is the throughput in tonnes/hr and P is the mill power draw in kW. Errors in CEET throughput forecasts can be broadly attributed to two main causes:

1. Imperfect knowledge of the ore body (*i.e.* the error in SPI)
2. Imperfect knowledge of the process plant (*i.e.* all other terms in Equation 4-1)

The first error arises from the distance between samples in the ore body, the geographic variability of ore hardness, and the imperfections that cannot be eliminated from sampling protocol, sample preparation procedures, and test procedures.[38]

The second group of errors arises from the inability to design an economically-feasible sampling campaign that can perfectly capture the complexities of an industrial-sized grinding circuit. Because CEET is based on semi-empirical models that are calibrated to industrial grinding circuits using an extensive database derived from plant sampling campaigns, these errors are manifested in the form of scatter, or "noise", in the various calibration equations.

The first group of errors can be approximated through geostatistical studies performed on ore body hardness data as illustrated and exemplified in Section 4.1. Section 4.2

[38] These errors are mathematically expressed by the variogram and nugget effect.

describes a methodology and example for approximating the second group of errors through Monte Carlo simulation studies.

Two assumptions are made in the following analysis. The first assumption is that the capacity of the SAG circuit is not limited by external equipment such as the ball mills, and the second is that there is perfect knowledge of the term *P* (mill power draw) in Equation 4-1. These assumptions are discussed in Section 5.

4.1 THE ORE BODY

When designing a process plant to meet certain minimum average throughput rates, the two single most important questions that are asked by the design team are:

1. What is the average and variability of the ore hardness?
2. Given the design throughput and the answer to question 1, what size of grinding mill is required?

The complex system of natural processes that cause hardness variability in an ore body makes it a difficult task to solve the first problem. Hence, it is easy to empathize with the design engineer who historically has devoted more attention to the second question than to the first. But given the current design trends of higher grinding circuit capital costs and lower run-of-mine feed grades, the financial risks associated with undersized grinding mills no longer permit the design team to claim ignorance of the ore hardness variability in the interest of expediency.

4.1.1 Ore Classes

In past and present practice, the common approach to simplifying this task has been to divide the ore body into various "ore classes", *i.e.* categorize based on similar characteristics. These ore classes are then assigned the mean hardness value determined from test work on that ore. This section presents a discussion on the applicability of this method to ore hardness characterization. The method itself is not

original, but the data and discussion presented here are an original analysis of the method and is integral to the process of ore body hardness characterization.

The underlying assumption with this method is that ores that share similar properties (such as geology, lithology, or alteration) should also share similar hardness values. For reasons discussed below, this assumption has sometimes proven false. This is illustrated by the histograms of SPI values presented in Figure 4-1 for several rock and alteration types selected by geologists at Phelps Dodge Chino Mines, a copper porphyry deposit from the southwestern United States. Rock types shown are skarn and granodiorite. Alteration types shown are biotized and retrograde. Statistics are presented in Table 3-1.

The rock type "granodiorite" and the alteration type "biotized" show the lowest relative standard deviation of SPI, indicating that the hardness variability within these ore classes is lower than for the other two. Furthermore, it can be stated that the rock type "skarn" has a relative standard deviation that is intermediate (although the absolute standard deviation is the highest of the four), and that the alteration type "retrograde" appears to have the lowest overall SPI values but the highest relative standard deviation.

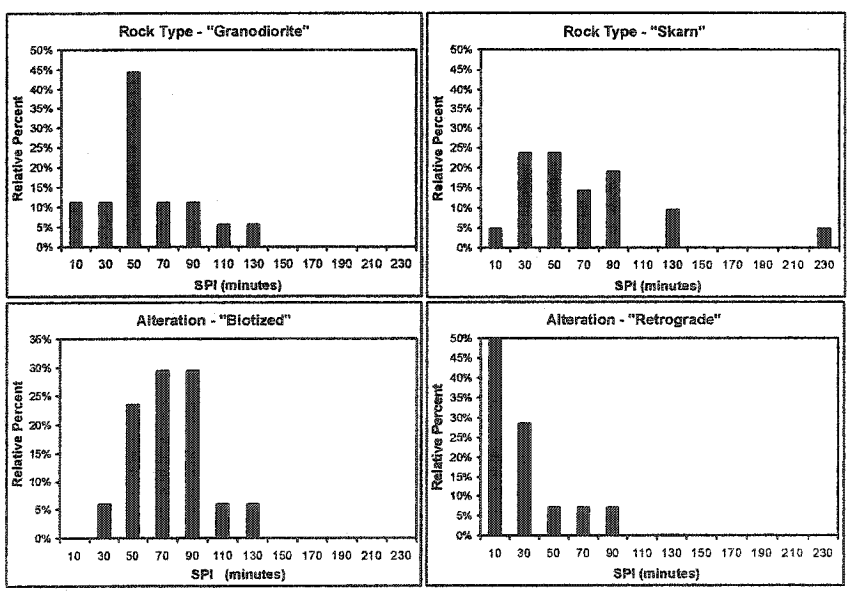

Figure 4-1 SPI histograms for selected rock and alteration types from Chino Mines.

Statistic	Rock Type		Alteration	
	Granodiorite	Skarn	Biotized	Retrograde
No. Samples	18	21	17	14
Min (minutes)	17	13	38	7
Median (minutes)	54	52	79	23
Max (minutes	125	220	135	91
Average (minutes)	58	70	77	31
St. Dev (minutes)	29	47	23	25
RSD (%)	50%	68%	30%	82%

Table 4-1 Statistics for rock and alteration types from Chino Mines

This discussion reveals an important limitation of the ore classification approach: variability within ore classes is ignored. Furthermore, it brings up another question: How does one decide that "skarn" or "retrograde" is adequate as a class definition? A skarn, for example, can have the subclasses of endoskarn or exoskarn[39]; it can be either a magnesian or calcic skarn. "Retrograde" alteration can be found in infinite degrees ranging from 0% alteration to 100% alteration.

The question of ore classification is important for two reasons. Firstly, if the class definitions are too broad then important trends in hardness might be overlooked, and if the class definitions are too narrow, then the amount and costs of sampling and test work required to generate the necessary statistical information will increase. Secondly, classification is often left to the personal interpretation of the geologist, and is affected by things such as differences in experience and vaguely defined threshold levels.

The ore classification approach offers a starting step in understanding hardness variability in the ore body. It can be used to identify areas where more hardness information is required. It can even be used exclusively for design when high confidence in the design results is not required, for example for projects with minimal capital expenditure or at the pre-feasibility stage of a high-capital project. But as a sole basis for the design of a capital-intensive, high-production grinding circuit, the relatively wide distributions shown in the histograms and/or the errors that may result from arbitrary class definitions or sample classification may lead to the improper sizing of the SAG mill. If used for the purposes of budgetary production planning for a high-production operation

[39] Indicating either a sedimentary or igneous protolith, respectively.

(which is based on a much narrower time frame) this method could prove even less robust[40].

4.1.2 Geostatistical Methods

The alternative approach to using ore classes is to use geostatistical methods to characterize the ore body. In this section a general procedure is presented for implementing a geostatistical program applied to SPI values. Practical observations made by the author during this investigation are presented with the hope of assisting the practicing geologist or geostatistician to devise a site-specific procedure. The variogram and precision curve examples were developed in collaboration with Michel Dagbert, Systèmes Géostat International Inc, as part of the research project undertaken at Chino Mines.

For grinding circuit design or production planning the engineer is interested in the error of the average throughput estimate or mill size, hence the variances of the block must be combined in a manner that generates the standard error of the mean (or "standard error"). This is then used in the Monte Carlo simulation procedures described in Section 4.2.

Before describing this method, it is worth pointing out some of its drawbacks. The first is that the method requires a variogram of ore hardness and hence the samples must be dispersed spatially throughout the ore-body. If diamond drill core of sufficient competency and quantity is not available for SPI and Bond testing, it may be necessary to drill additional drill holes, which could be an expensive prospect.

It is possible for ore bodies that lack sufficient drill core or that do not consist of one or several large, continuous mineralization zones (such as Falconbridge's Raglan[41] property in northern Canada) to combine the ore-class approach with the geostatistical approach. The result is a compromise solution that considers the estimates resulting

---

[40] because fewer ore blocks are processed and hence the propensity of the errors to "canceling each other out" is minimized

[41] Raglan consists of a series of major and minor mineralized lenses dispersed throughout a zone tens of kilometers in length.

from ore class relationships in parallel with those derived by geostatistical computation in accordance with the inverse of their estimation variance. In this case the estimation variance for the class-derived estimate will be the SPI variance in that class, and the estimation variance derived from kriging will simply be the kriging variance. The end result will be that in areas where drill core is available for sampling, the geostatistical estimations carry more weight, and in areas where ore class is the only readily available information, the estimate for that ore class will have more influence.

There are two methods for applying the general techniques for approximating the standard error of the mean kriged SPI. The first method is used when a sampling campaign has already been completed and the engineer desires to know the precision of the resultant throughput forecasts or mill sizes. A complete description of the procedure is given elsewhere (David 1988), but the general methodology is as follows. A nearest-neighbor polygon of influence surrounding each sample is identified and discretized and the elementary extension variance for each discretization point is obtained using the variogram and the classical kriging formula. The extension variances are then combined to determine the estimation variance of the polygon. Volume-variance relationships are used to combine the variance of each polygon to produce the variance of the mean hardness for that given production period.

As this work focuses on the design of sampling campaigns, we will discuss the second method in more detail. It is applied when the engineer must design a sampling campaign to achieve a minimum acceptable error of the throughput forecast or mill design. It uses the same methodology described above to estimate the variance of the average for a series of different hypothetical sampling grids. As the distance between neighboring drill core samples becomes smaller, the confidence in the hardness estimates of the ore body become greater. In this manner, a curve can be generated that shows the relationship between the distance between samples and the resultant precision of the throughput estimate. This is done for a volume of ore corresponding to a specific mining schedule or an assumed mining schedule.

Figure 4-2 shows the results of the method as applied at Phelps Dodge Chino Mines, New Mexico. Calculations were performed for four different mining periods (one month,

three months, six months, and one year). The sample spacing (in meters) is plotted on the x-axis and the precision of mean SPI (*i.e.* relative standard error).

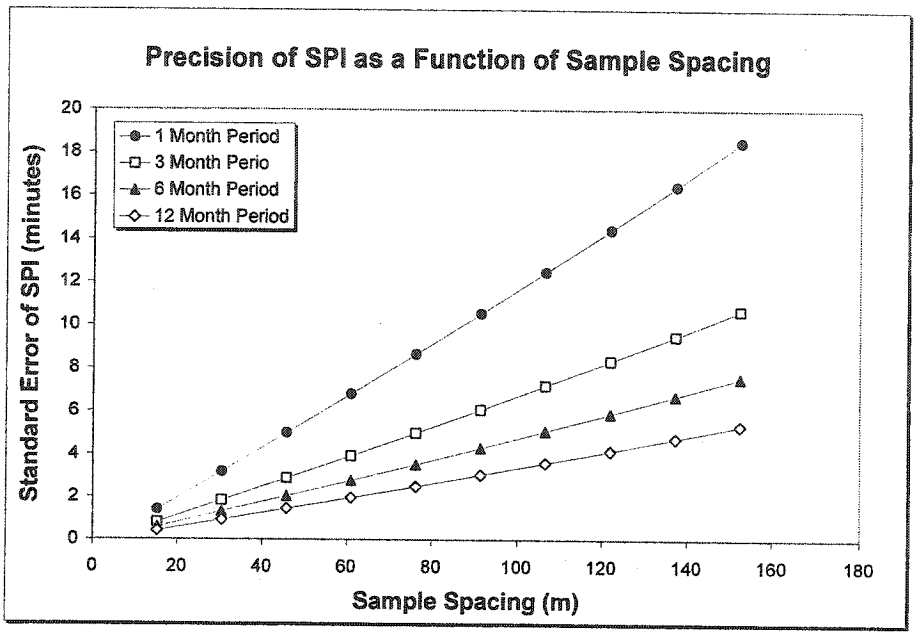

Figure 4-2 Precision curves from Chino Mines

The following steps are taken to produce the curve for a given production period.

1. Select the production period. Four production periods are shown for the comparative purposes in Figure 4-2 but for the purposes of this example, we select a one-month period.
2. For the production period, define the geometry of the active faces by assuming certain block dimensions, bulk density, mean throughput, and active benches. The active face dimensions for this period were determined from reasonable assumptions drawn from discussion with metallurgical, mining and geological personnel at Chino. In the case of the 1-month example, there are two active ore faces each 500-ft by 300-ft by 50-ft (150m by 90m by 15m), comprising a total of 120 15m-cubic ore blocks and approximately 1.1 million metric tonnes of ore.
3. Select a given sample interval. For this example we select 15 m as the distance between centers of drill core samples, and for the active face geometry defined in Step 2, 15 m sample spacing would allow for 60 individual composite samples per active face.
4. Using a geostatistical program, compute the extension variance of each composite to its cell of influence, and combine the variances to generate the

variance of the mean hardness for the entire face. For the defined face, the extension variance of a sample to its polygon of influence is 231 min^2. The combined variance as per the classical kriging equation (Equation 2-17) for 60 equally-spaced composite samples at 25 m intervals is 4 min^2. This is the variance of the mean for this face.

5. Using the standard volume-variance relationship, combine the mean variance for the active faces to generate the variance of the mean for the production period. Because in this example the faces are of equal dimension, the variance of the mean for a face can simply be divided by 2 because there are two faces. The variance of the mean SPI for a 120 composites representing one month of mine production is therefore 2 min^2.
6. Use the above procedure to calculate the variance of the mean for sequentially larger sample intervals until the curve depicted in Figure 4-2 is generated. The calculations are shown in Table 4-2.

Months in Period	Spacing (ft)	Spacing (m)	Ext. Var (min2)	#comp.in face	Est var. face (min2)	Est var. total (min2)	Standard error (min.)
1	500	152	410	1	684	342	18.5
1	450	137	400	1	541	270	16.4
1	400	122	390	1	417	208	14.4
1	350	107	380	1	311	155	12.5
1	300	91	369	2	222	111	10.5
1	250	76	358	2	149	75	8.6
1	200	61	346	4	92	46	6.8
1	150	46	331	7	50	25	5.0
1	100	30	303	15	20	10	3.2
1	50	15	231	60	4	2	1.4

Table 4-2 Variance calculations for 1 month time period and multiple sample intervals

The standard error of the mean SPI (last column in Table 4-2) is used as the estimation error of the ore body hardness (SPI) in the Monte-Carlo simulation. To this error must be added the errors due to imperfect knowledge of the process plant. This will allow the y-axis in Figure 4-2 to be converted from the units of SPI (minutes) to units of plant throughput (tonnes/hr). The model error can either be added to the individual cells of influence (in which case it must be divided by the number of composites representing the ore during the given production period) or it can be added to the mean estimation error after the Monte Carlo simulation (this is the method used in Section 4.2.2.2). Both methods yield the same result.

4.1.3 Practical Observations

Sampling Effort

The scope of the sampling effort will play a role in the method selected for modeling the hardness of the ore body. For example, Figure 4-3 shows the calculated and model variograms for Chino Mines and Figure 4-4 shows the same for BHP-Billiton's Escondida deposit. Both y-axes are in units of variance (min^2 in the case of the SPI). In each graph the unsmoothed line is the experimental variogram calculated from the raw SPI values and the smooth line is the model variogram fit with a mathematical formula. Numbers near the points on the experimental variogram from Chino show the number of sample pairs used to compute that point.

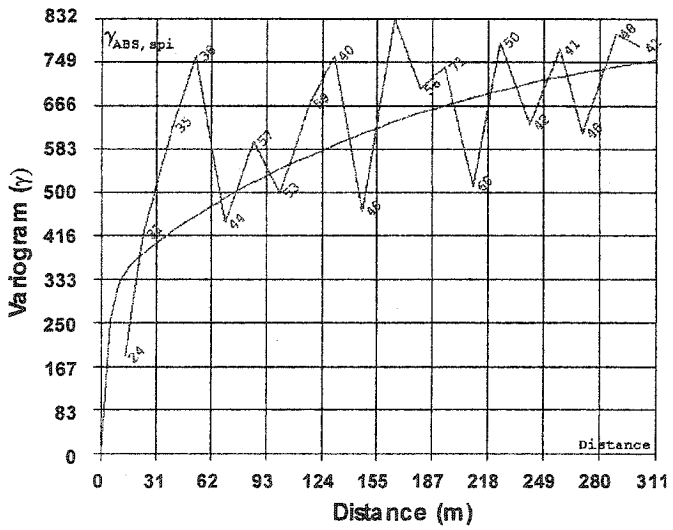

Figure 4-3 Experimental and model variograms for Chino

It is immediately apparent that the experimental variogram from Chino shows much more variability with respect to its model than that from Escondida. The difference results from differences in the number of samples used to calculate each variogram: little more than a hundred SPI composites in the case of Chino and nearly 800 in the case of Escondida. In both cases the samples were reasonably well dispersed in the ore body.

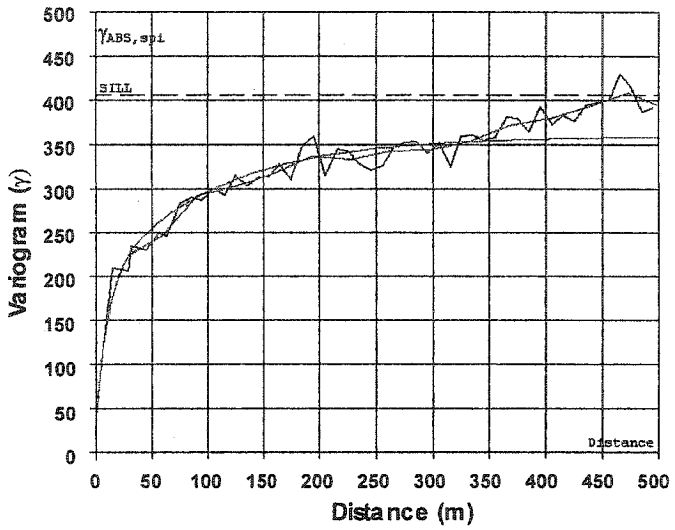

Figure 4-4 Experimental and model variograms for Escondida

The above comparison suggests that given reasonable assumptions about composite dispersion in the ore body, it will become difficult to model the shape of the variogram when fewer than approximately 100 samples are available. This threshold value is useful if a limited budget is available and one must decide between the ore-class approach and the geostatistical approach. It is also useful if there are a large number of classes identified in the ore-class approach. To collect and test sufficient samples to obtain reliable mean and variance figures for each class may greatly exceed the number of samples required to obtain a variogram. In this case the geostatistical method could be used to provide better hardness characterization, either exclusively or in combination with the ore class approach as discussed in Section 5.2.

Another obvious question that might arise from the geostatistical procedure demonstrated in Section 4.1.2 is how to begin a sampling campaign when no prior sampling work has been performed. The variogram is required to calculate the number of samples for a given precision target, but samples are required to calculate and model the variogram. The solution in this case is to propose an iterative procedure that focuses first on collecting enough information to obtain a variogram. This will permit the generation of a series of preliminary precision curves that can be use to expand the sampling effort. As the sampling campaign effort expands, more data are made available to update the variogram.

Variogram Modeling

Examination of Figure 4-3 and Figure 4-4 above shows that the general shapes of the two variograms are similar. Both have low nugget effects and variances that increase very quickly near the origin of the distance axis. The variances increase to half of the value of the sill within approximately the first 50 meters and thereafter increase less quickly. The estimates of the nugget effect for each variogram were determined experimentally from repeat sampling and test work. In the case of Escondida, for example, two, three, and sometimes four repeat tests performed on 39 composite samples. The absolute variance (specifically the average of the variances of the repeats on each sample) of the 88 repeats is an experimental determination of the nugget effect. In this case it was determined that for the suite of data analyzed (shown in Table 4-3) 15.3 min^2 was a good estimate of the nugget effect. Compared with the sill of the variogram this is a low nugget effect.

Statistic	Value	Units
No. Composites	39	
No. Duplicates	88	
Min Ave. SPI	19	min
Med. Ave. SPI	45	min
Max. Ave. SPI	77	min
Ave. SPI	47	min
Relative Variance	0.006	
Relative St. Error	7.8%	
Absolute Variance	**15.3**	min^2
Absolute St. Error	3.9	min

Table 4-3 Statistics of 39 composites tested in duplicate for SPI

It can be argued that because the nugget effect for Escondida was determined by repeat test work on the same sample, it does not contain the variability attributable to the sampling method used when collecting the composite from the drill core. To address this, experimental work was conducted at Chino in which three 15-meter core composite samples were collected from the same bench composite of drill core and tested for SPI variability. Results of SPI and Bond work index determinations on these core samples are shown in Table 4-4. They agree well with the reproducibility work presented above. Other work performed on a large copper deposit in Chile has shown similar results to those from Escondida and Chino; however, permission has not been received to publish it.

Sample	SPI	Wi
1	32	11.7
2	31	11.0
3	28	10.5
Average	30	11
Variance	4.3	0.4
RSD	7%	5%

Table 4-4 Statistics for 3 duplicate core samples from Chino Mines

From the above data it can be concluded that with careful core sampling procedures, the raw variability inherent in sampling and testing procedures for SPI is negligible. Hardness, as defined by the SPI, has a low nugget effect.

Sampling Considerations

The method used to collect core samples in the above analysis was designed to minimize the variance introduced at the sampling stage. The SPI requires one-inch (2.54 cm) pieces of drill core. The composite length is generally the bench height, thereby allowing the largest possible sample mass for the given block size. One-inch (2.54 cm) sections of core were collected every 0.5 m along the 15 m length of split core, resulting in approximately 5 to 7 kg of sample. Care was taken to avoid favoring large or intact pieces of rock. The same 2.54 cm section was collected every 0.5-meter regardless of whether fractured or friable core was encountered.

Because geostatistical methods may be used in conjunction with the ore-classification approach, it is always beneficial to record the down-hole coordinates, hole-number, rock type, lithology, alteration, RQD, and all other geological or geomechanical properties of the core.

4.2 THE PROCESS PLANT

There are various models integrated into the calculations for specific energy of an ore sample in an autogenous mill. These models were derived empirically from a database of grinding circuit surveys performed in industrial plants. Irrespective of the methods used for data reconciliation, the practical difficulties associated with the sampling of industrial grinding circuits will always result in small amounts of uncertainty in the results

of the survey. This uncertainty can be visually expressed as scatter about the 45-degree line in a scatter diagram showing the predicted value versus the actual value of the variable of interest. This section attempts to quantify the errors in specific energy estimation that result from the accumulation of these errors in the various models that compose the CEET program. The method used is Monte Carlo simulation.

The first step is to quantify the amount of error inherent in each sub-model. In the second step these errors become the statistical parameters used for creating normal distributions of the model variables. The values of the model variables are combined to calculate the specific energy and in Step 3 a statistical analysis is performed on the resulting distributions. The statistical analysis yields the estimated error of the specific energy estimates assuming perfect knowledge of the ore hardness (SPI).

Many of the models used for the Monte Carlo simulation study are protected for commercial reasons. MinnovEX provided the author with the specific forms of the models for the sole purpose of this research study.

4.2.1 Model Error

Section 2.1.4.4 described the models that are used in CEET to comprise the specific energy calculations for an autogenous mill. If the primary SPI calibration equation is considered as well, there are a total of five models that can introduce error. These are:

1. Feed Size
2. Pebble Crusher Circulating Load
3. F_{sag}
4. Transfer Size
5. Primary Calibration

The error variance of each model is calculated based on two assumptions[42,43]:

1. The variance of the distribution of y for a fixed value of x is constant.

[42] The validity of these assumptions is investigated and discussed in detail in Section 4.2.2.1

[43] With the exception of the feed size models as discussed in Section 4.2.1.1

2. For a fixed value of the x, y follows a normal distribution.

Given these assumptions, the standard error variance is given by:

$$S^2_{y|x} = \sum (x_i - y_i)^2 / (n\text{-}df)$$

Equation 4-2

Where n is the number of calibration points and *df* is the number of degrees of freedom lost in the model (*i.e.* the number of independent curve-fitting constants).

4.2.1.1 ERROR OF FEED SIZE MODEL

The feed size models described in Section 2.1.4.4 employ the SPI and crusher index test C_F in combination with the primary crusher closed-side setting to predict the feed size F_{50} and F_{80}. The graphs of the models shown in Figure 2-7 (page 27) are converted into scatter diagrams of predicted versus actual feed size (Figure 4-5).

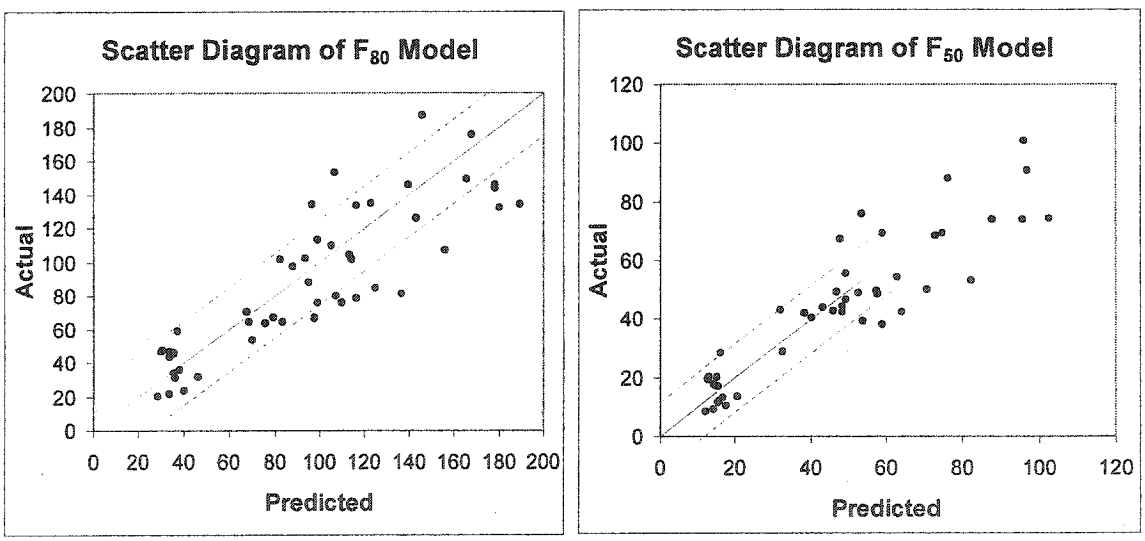

Figure 4-5 Scatter diagrams for the F_{50} and F_{80} models, in millimeters, with 1 standard error line (dashed)

The scatter is attributed to number of causes, including:

1. Sampling error introduced when mill feed sample for large-scale screen analysis was collected from the conveyor belt

2. Sampling error introduced when sample collected for SPI and crusher index determination
3. Error of mean apertures of screens used to perform screen analyses
4. Error of estimating primary crusher closed-side setting
5. Reproducibility of the SPI, crusher index, and screen analysis test procedures

Applying Equation 4-2 to the data presented in Figure 4-5 generates the error estimates presented in Table 4-5. The results show that the error sources described above introduce a combined error of approximately plus or minus 25 mm for the F_{80} and plus or minus 12 mm for the F_{50} estimates derived from the CEET models.

Statistic	F_{50}	F_{80}	units
Observations	45	50	
df	4	4	
Standard Error Variance	146	674	mm^2
Standard Estimation Error	12	26	mm

Table 4-5 Statistics of feed size model error

One additional factor must be considered for the simulation of feed size. The F_{50} and F_{80} are not independent variables; *i.e.* they are linearly correlated. This is shown by plotting measured and calculated F_{80} values against their associated F_{50} values (Figure 4-6). Because errors of the two models are partly correlated[44], a different simulation approach is required. For this study the F_{80} is simulated first using the statistical parameters shown in Table 4-5 and then the F_{50} is simulated using the linear equation and error variance that relate observed F_{50} and F_{80} values (the graph on the left of Figure 4-6). The error values for this graph are shown Figure 4-6. Like previous error models, constant variance is assumed.

[44] "partly correlated" because F_{50} estimation errors (relative to the F_{80} estimation errors) can have two causes:

1. Sampling error that affects both F_{50} and F_{80} values collected from the plant. This is analogous to a parallel shift of the size distribution curve; hence, the resulting F_{50} error is already accounted for during the simulation of F_{80}.
2. Sampling error that affects only the F_{50} or F_{80}, but not both. This is analogous to a slope shift of the size distribution curve. This error is represented by the scatter plot shown on the left of Figure 4-6.

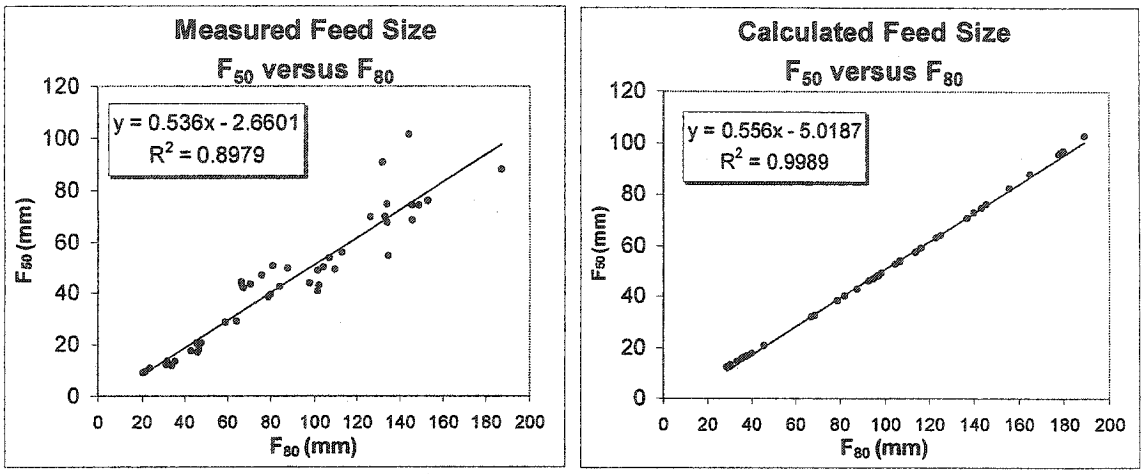

Figure 4-6 Correlation of F50 and F80 showing that the error in the F50 and F80 models are correlated

Statistic	F_{50}	units
Observations	50	
df	2	
Standard Error Variance	62	mm^2
Standard Estimation Error	8	mm

Table 4-6 Statistics for simulation of F_{50} from F_{80}

In Section 4.2.1 it was stated that the simulation assumes constant variance of y for fixed values of x. Examination of the graphs in Figure 4-5 and Figure 4-6 suggest that this assumption may be false; *i.e.* that the absolute scatter increases with feed size. This is checked by calculating the standard estimation error for different sizes. In this case, three size classes were used in order to obtain sufficient data in each one for a reliable calculation of the estimation error. Size classes were categorized by increased F_{80} values. They are 0 to 50 mm, 50 to 100 mm, and 100 to 150 mm. Results are shown in Figure 4-7. Note that the graph for F_{50} estimation error is calculated using the relationship between F_{50} and F_{80} shown in Figure 4-6.

A clear increase in estimation error is observed in Figure 4-7; therefore, the simulation study must account for increased relative model precision at small feed sizes, and vice-versa.

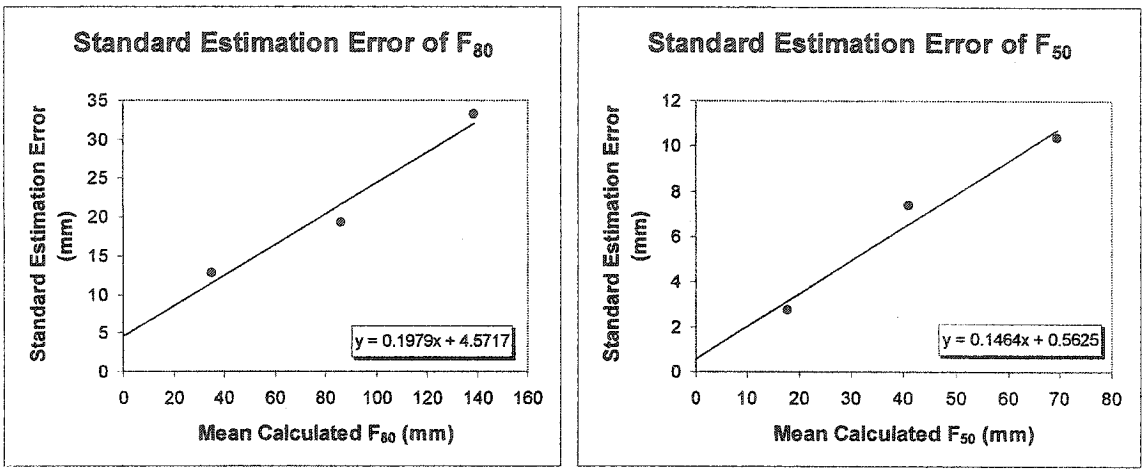

Figure 4-7 Estimation error for feed models versus mean feed size

4.2.1.2 PEBBLE CRUSHER CIRCULATING LOAD

The pebble crusher circulating load model described in Section 2.1.4.4 is based upon quantified knowledge the feed size distribution; grate and pebble port apertures; the slot width of the trommel or vibratory screen; and the ore hardness as defined by the SPI. Figure 4-8 presents a scatter diagram showing the errors in the calibration. Errors are attributable to a combination of:

1. Sampling error introduced when mill feed sample for large-scale screen analysis was collected from the conveyor belt
2. Sampling error introduced when sample collected for SPI determination
3. Error of mean apertures of screens used to perform screen analyses
4. Reproducibility of the SPI and screen analysis test procedures
5. Error attributable to imperfect knowledge of the mean pebble port and grate openings
6. Error due to imperfect knowledge of mean screen or trommel apertures

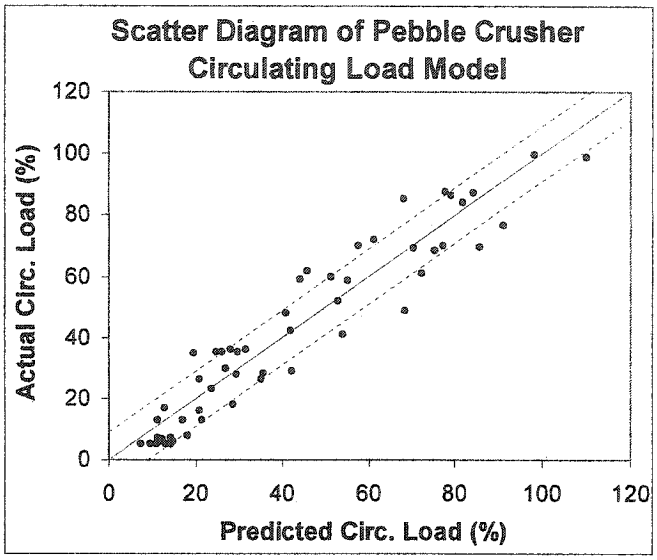

Figure 4-8 Scatter diagram of pebble crusher circulating load model

Table 4-7 shows the calculated estimation error for the model.

Statistic	PCCL	units
Observations	56	
df	6	
Standard Error Variance	88.6	$\%^2$ of Fresh Feed
Standard Estimation Error	9.41	% of Fresh Feed

Table 4-7 Statistics of pebble crusher circulating load model

The feed size distributions used to derive the model were based upon screen analyses performed on bulk samples collected from mill feed belt during the plant survey. As a result, in addition to the above errors, the Monte Carlo simulation study must consider:

7. Error attributable to the feed size distribution model

4.2.1.3 F_{SAG}

The semi-empirical F_{SAG} model is based on an unpublished equation relating the F_{SAG} to the Feed size and pebble crusher circulating load. The scatter diagram is shown in Figure 4-9.

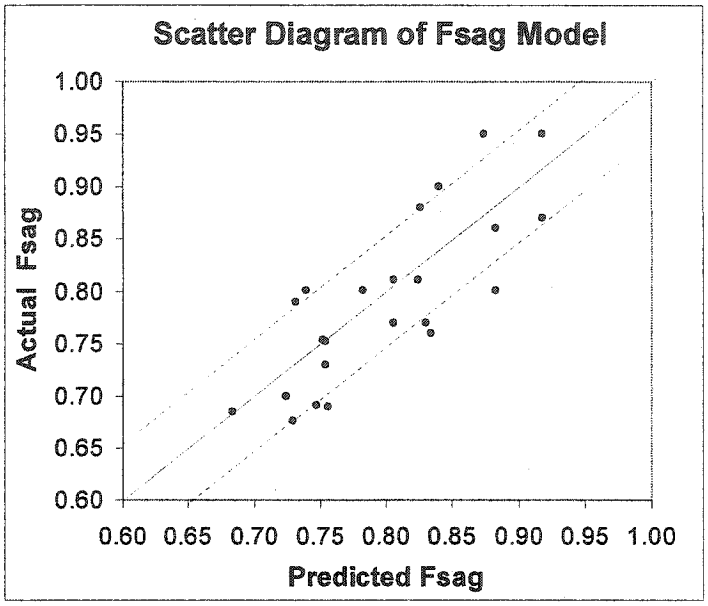

Figure 4-9 Scatter diagram of F_{SAG} model

Because the F_{SAG} model was derived using the feed size and circulating load figures determined from the plant surveys, the following error must be added to the F_{SAG} error tabulated in Table 4-8:

1. Error attributable to use of feed size model for F_{SAG} estimation
2. Error attributable to use of pebble crusher circulating load model for F_{SAG} estimation

Statistic	Fsag	units
Observations	24	
df	5	
Standard Error Variance	0.003	n/a
Standard Estimation Error	0.05	n/a

Table 4-8 Statistics of F_{SAG} model

4.2.1.4 TRANSFER SIZE

The transfer stream model described in Section 2.1.4.4 consists of a T_{80} formula, a semi-empirical model that requires quantified knowledge of:

1. The feed size distribution
2. The ore hardness as quantified by the SPI
3. The size of the grate or pebble port apertures
4. The slot width of the trommel or screen

5. The ball charge in the mill
6. The pebble crusher circulating load
7. The pebble crusher product size

The SPI calibration equation only considers the T_{80} when calculating the specific energy; hence this section is only concerned with the error introduced by the T_{80} calibration. This error is graphically represented by Figure 4-10, which shows the calibration points used to derive the models.

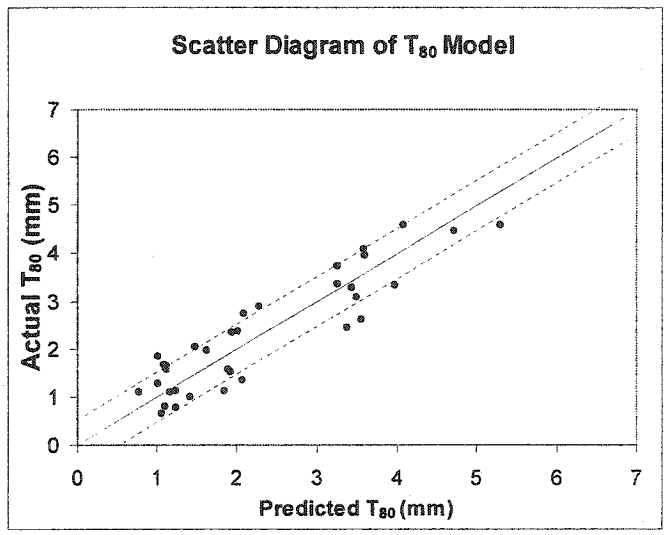

Figure 4-10 Scatter diagram of T_{80} model

Sources of the error shown by Figure 4-10 include:

1. Sampling error introduced when sampling mill feed belt for large-scale screen analysis
2. Sampling error introduced when collecting sample for SPI determination
3. Error of mean apertures of screens used to perform screen analyses
4. Error of estimating pebble crusher closed-side setting
5. Reproducibility of the SPI and screen analysis test procedures
6. Error attributable to imperfect knowledge of the mean pebble port and grate openings
7. Error due to imperfect knowledge of mean screen or trommel apertures

The sum of these errors is summarized in Table 4-9. The T_{80} model has a standard error of estimation of 0.63 mm.

Statistic	T_{80}	units
Observations	34	
df	11	
Standard Error Variance	0.39	mm^2
Standard Estimation Error	0.63	mm

Table 4-9 Statistics for T_{80} model

The calibration of the transfer stream models was performed using the screen analysis data from the bulk sample collected during the plant survey. The pebble crusher circulating load used to calibrate the model was determined from the weightometer on the recycle belt. As a result, the following errors must be considered, in addition to those presented above, when accounting for T_{80} errors during the Monte Carlo simulation:

8. Error due to feed size model, and
9. Error due to pebble crusher model.

4.2.1.5 PRIMARY CALIBRATION

The primary SPI calibration equation (Equation 2-4 on page 24) is the formula that relates the specific energy requirements of an ore in an autogenous mill to the SPI, T_{80}, and F_{SAG}. Figure 4-11 shows the specific energy calculated using the calibration equation plotted (on the x-axis) against the specific energy measured at the time of the plant survey.

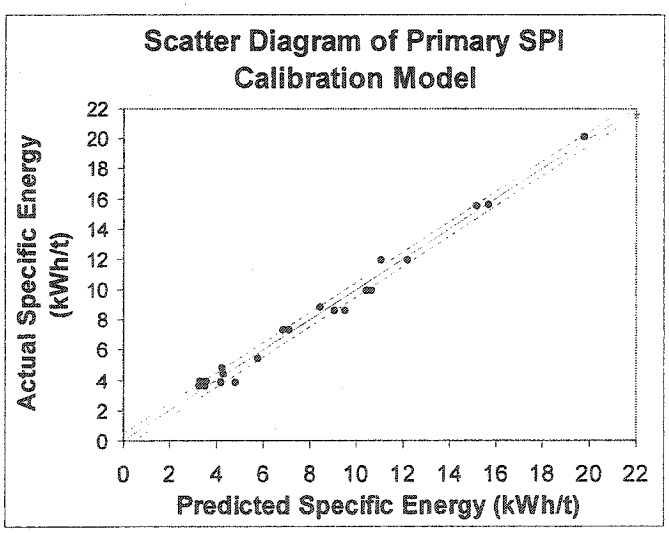

Figure 4-11 Scatter diagram of primary SPI calibration model

The error in the calibration equation shown by the scatter in Figure 4-11 is attributable to a combination of:

1. Sampling error of large-scale screen analysis sample,
2. Sampling error of SPI samples,
3. Sampling error of transfer stream sample collected from screen undersize,
4. Error of mean apertures of screens used to perform screen analyses,
5. Reproducibility of the SPI and screen analysis test procedures, and
6. Error in collection of mill feed rate and power draw and/or instrument calibration.

Table 4-10 shows the standard estimation error for the primary calibration, indicating that with perfect knowledge of the SPI, T_{80}, and F_{SAG}, there would still be an error of plus or minus 0.53 kWht/tonne in the calculated specific energy of the ore in an autogenous mill.

Statistic	PCCL	units
Observations	23	
df	2	
Standard Error Variance	0.28	$(kWh/t)^2$
Standard Estimation Error	0.53	kWh/t

Table 4-10 Statistics of primary calibration equation

4.2.2 Monte Carlo Simulations

The error values described in the previous section were used in a Monte-Carlo study that simulates the propagation of error within the CEET program. The goal of the simulation study was to determine the combined effect of the individual model errors described above on the estimate of the required specific energy of the ore in an autogenous mill. Three steps were involved:

1. Construct the Monte-Carlo simulation program
2. Simulate the estimation error of the specific energy assuming perfect knowledge of SPI
3. Integrate the estimation errors determined in Step 2 to the standard errors of SPI given in Figure 4-2.

Each step is described in detail below.

4.2.2.1 THE SIMULATION PROGRAM

The models for feed size, pebble crusher circulating load, transfer size, and F_{SAG} described in Section 2.1.4.4 are interdependent in the CEET algorithm. For example, the pebble crusher circulating load model requires knowledge of the feed size. Therefore any error in the feed size model will propagate to the pebble crusher model and increase the error of the circulating load estimate. Figure 4-12 shows a diagram illustrating the interdependency of the models and the required ore characteristics for each.

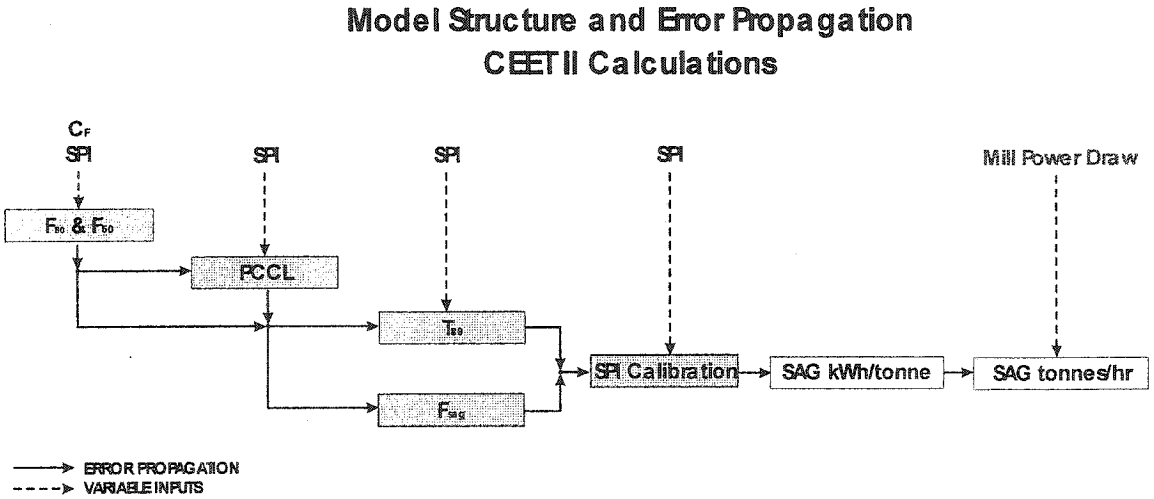

Figure 4-12 Model structure and error propagation (CEET II)

This thesis focuses on the error attributable to the CEET models and to the ore body characterization techniques. It does not address the error in estimating the power draw of the mill, but suggestions for future research in this respect are given in Section 6.2.

From Figure 4-12 it can be seen that the feed size models are inputs for the pebble crusher circulating load model. Both the feed size and pebble crusher circulating load models are inputs for the T_{80} and F_{SAG} models. The SPI calibration in turn requires only the outputs of the T_{80} and F_{SAG} models. All models except that for F_{SAG} require the SPI as a parameter input. In addition to the SPI, the feed size models require the crusher index, C_F.[45,46]

[45] Note that in Section 2.1.4.4, Equation 2-8 references the SPI test parameter P_{64} as a required input for the transfer size model. The simulation instead uses a relationship supplied by MinnovEX that relates P_{64} to

To construct the simulation program it was necessary to make assumptions about the mean values of the various parameters used in the model. The assumptions made correspond to typical values observed in industrial grinding circuits. Assumptions regarding ore characteristics and operating parameters are tabulated in Table 4-11.

Principal Assumptions		
Parameter	Value	Units
Primary Crusher CSS:	150	mm
Steel Charge:	10%	
SAG Grate Size	50	mm
Screen Aperture	9	mm
Pebble Crusher P_{80}	16	mm
Pebble Crusher P_{50}	10	mm

Table 4-11 Assumptions used for simulation program

The simulation is conducted with the same left-to-right sequence that the models are used to calculate the specific energy requirements (Figure 4-12). Specifically, the steps are:

1. Create a normal distribution of SPI values with mean of 0 and standard deviation derived from the geostatistical methods described by Section 4.1.2 and expressed by Figure 4-2. These are the SPI errors that are added to the mean SPI designated for the study. Also create a normal distribution of correlated C_F values. [47]

SPI. This relationship is often used by MinnovEX to represent the P_{64} when the P_{64} is not available (internal correspondence, MinnovEX Technologies, 2002).

[46] Note that the general forms of some of the equations used in the CEET II algorithm and summarized in Section 2.1.4.4 are proprietary to MinnovEX Technologies Inc., and are unpublished for competitive reasons. The same applies to the values of the curve-fitting constants used in many of these equations and in the primary SPI calibration equation. MinnovEX has provided the specific forms of all equations for the sole purpose of conducting the error analysis described herein. These are not published in this report but can be obtained with permission from MinnovEX for the purposes of duplication and clarity of this thesis.

[47] The investigation of the precision of the crusher index test for C_F is beyond the scope of this thesis but is identified as an area meriting future work. There is a correlation between C_F and SPI. This correlation, provided by MinnovEX, was used to ensure that realistic C_F values are used at different SPI values; however, quantification of the C_F precision would require detailed investigation into the reproducibility of the test procedures used to derive it.

2. Create a normal distribution of F_{80} error values with a mean of 0 mm and standard deviation as per Figure 4-7 in Section 4.2.1.1. For the F_{50} simulation, create a standard normal distribution (mean of 0 and standard deviation of 1). Calculate for each SPI and C_F pair generated in Step 1 the corresponding F_{80} values using the proprietary CEET II model. For each F_{80} value determine the estimated F_{50} using the equation relating observed F_{80} and F_{50} (Figure 4-6). For each F_{50} value calculate the estimation error using the regression equation from the right side of Figure 4-7 and multiply it by the simulated standard normal values. To each pair of F_{50} and F_{80} values add the simulated F_{50} and F_{80} scatter to generate a distribution of F_{50} and F_{80} values that include the model error.
3. Simulate the scatter of the pebble crushing model by creating a normal distribution of pebble crusher circulating load values (PCCL values) with a mean of 0 % (of the fresh feed rate) and a standard deviation as per Table 4-7. For each set of SPI, F_{80}, and F_{50} values calculate the estimated pebble crusher circulating load using Equation 2-7. For each point add the simulated scatter to the estimated circulating load to generate a distribution of circulating load values that include the model error.
4. Simulate the scatter of the F_{SAG} model by creating a normal distribution of F_{SAG} values with a mean of 0 and a standard deviation as per Table 4-8. Estimate the F_{SAG} value for each pair of PCCL and F_{80} values using the unpublished equation described in Section 2.1.4.4 on page 29. For each F_{SAG} value, add the simulated scatter to the estimated value to create a distribution of F_{SAG} values that includes the estimated model error.
5. Simulate the scatter of the T_{80} model by creating a normal distribution of T_{80} values with a mean of 0 mm and a standard deviation as per the estimation error given in Table 4-9. For each set of values of SPI, PCCL, and feed size calculate the estimated transfer size T_{80}. Add the simulated scatter to the estimated T_{80} value to create a distribution of T_{80} values that includes the model error.
6. Simulate the scatter due to the primary SPI calibration equation by creating a normal distribution of specific energy values with a mean of 0 kWht/tonne and standard deviation as per the model error described in Table 4-10. For each set of SPI, T_{80} and F_{SAG} values, calculate the estimated SAG mill specific energy requirements, and add to it the simulated model error to create a distribution of specific energy values that accounts for the model error

The table of specific energy calculations that results from Step 6 represents the hypothetical specific energy values that would be observed in the plant if the same ore sample were independently collected and test many times for specific energy requirements. Furthermore, by setting the standard error of the SPI distribution created in Step 1 equal to zero, the errors that are attributable to CEET can be analyzed exclusively of the geostatistical errors. In this fashion, the estimation error of the specific energy can be expressed assuming perfect knowledge of the ore hardness (SPI). This is useful because it allows us to check some of the assumptions that were made to construct the simulator. For example, the simulation was conducted assuming that the mean SPI is 70 minutes. Does the error change if the mean SPI changes? Another question relates to the simulation error itself: How many times should we simulate the variable in each distribution? These questions are discussed below.

Number of Simulation Points

To investigate the number of individual simulations that should be conducted for each variable, the following procedure was devised.

1. Perform the simulation study[48] described above 20 times for the same ore parameters, plant parameters, and error parameters.
2. For each of the 20 studies, calculate the mean specific energy by averaging the calculated specific energy for each simulation point.
3. Calculate the standard deviation of the mean specific energy values determined in Step 2.
4. Repeat steps one to three for an increasing number simulation points in each study.

The standard deviation calculated in Step 3 is the standard error of the mean specific energy value. The central limit theorem dictates that the standard error of the mean specific energy will converge on zero as the number of simulation points in the study increases. This can be shown by performing the above steps with an increasing number

[48] For clarity, in this report a "simulation study" refers to an entire Monte Carlo simulation consisting of thousands of independently simulated points. A "simulation point" refers to a data set consisting of a single simulated SPI, F_{80}, F_{50}, PCCL, T_{80}, Fsag, and specific energy (kWht/tonne).

of simulation points. The number of simulation points selected for this study was 1000, 2000, 4000, and 8000. Results are graphed in Figure 4-13.

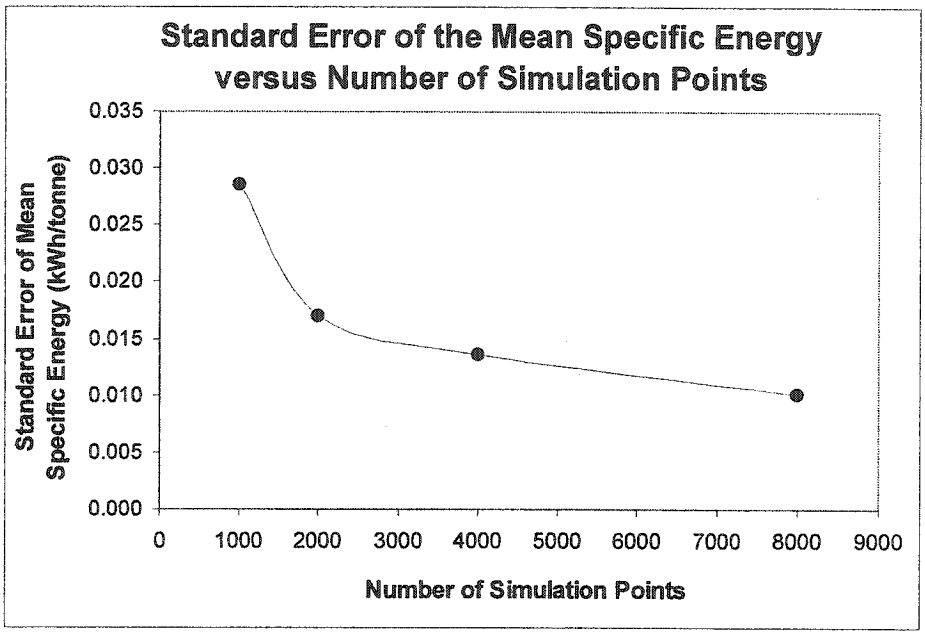

Figure 4-13 Specific energy error versus simulation points

Figure 4-13 shows that standard error of the mean kWh/tonne decreases as the number of simulation points increases. At 8000 points, the standard error of the mean specific energy is approximately 0.01 kWh/tonne. This is an acceptable level of precision for the investigative studies detailed below. For available computing resources, increasing CPU requirements becomes an obstacle to conducting simulation studies involving more than 8000 points.

Error Correction Rules

When simulating thousands of SPI associated model parameters, there is a small probability that the random number generator gives negative or otherwise unrealistic values for some variables[49]. It was found that error correction rules were required to

[49] These unrealistic values are probably due to the fact the error models do not always follow normal distributions; i.e. they are "bounded" normal distributions in some cases. For example, by definition the feed size F_{80} can never be lower than the F_{50}. The simple error models used imply that when generating thousands of random variables there may be very rare occasions at extremely small (an unrealistic) feed sizes when this may occur. Hence error correction is unavoidable.

ensure that the simulation programs functions properly and realistically. These rules are:

- F_{80} must be greater than 15 mm and the F_{50} must be greater than 5 mm
- The pebble crusher circulating load must be between 3% and 100% of the feed rate.
- The transfer size T_{80} must be larger than 200 μm
- SPI must be greater than 10 minutes

Average SPI Value

Simulations studies, each consisting of 8000 points, were conducted for mean SPI values of 30 minutes, 70 minutes, and 110 minutes. These are the general values for "soft", "medium", and "hard" ores. The relative standard errors of the specific energy estimates are given by the last column on the right of Table 4-12.

SPI mean	F80 mean	F50 mean	PCCL mean	Fsag mean	T80 mean	kWht/onne mean	kWht/onne RSD
30	41	19.2	13	0.78	3.30	3.22	20%
70	71	35.4	28	0.74	2.45	5.33	20%
110	96	48.7	37	0.72	1.73	7.57	26%

Table 4-12 Error analysis for various mean SPI values

The relative standard error is approximately 20% for mean SPI values of 30 minutes and 70 minutes, but climbs to 26% for the mean SPI case of 110 minutes. This is due primarily to the inter-relationships between feed size, transfer size and vibrating screen slot size. At larger feed sizes there is increased error in the transfer size calculations. This is not a significant factor for throughput forecast precision, however, given the significantly larger errors attributable to SPI interpolation. This will be discussed below.

Figure 4-14 shows the relative contributions of the various CEET II sub models to the total error of the specific energy estimates for a soft ore.

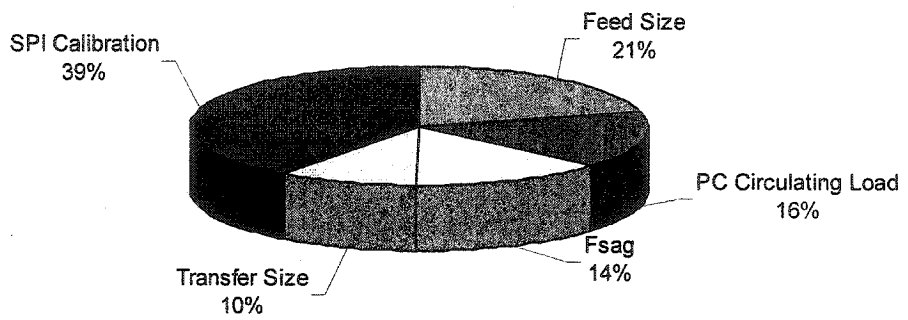

Figure 4-14 CEET II error contributions for a "soft" ore

The two largest error contributions are from the feed size sub-model and the primary SPI calibration model (37% and 38% of the error, respectively). This is expected because the F_{50} and F_{80} derived from the feed size model are required input parameters for the three models for pebble crusher circulating load, transfer size, and F_{SAG}. Errors in the feed size model therefore have a higher degree of propagation.

The SPI calibration error, also a large contributor in Figure 4-14, is significant for a different reason. The standard estimation error for the SPI primary calibration is constant at 0.53 kWh/tonne (see Table 4-10) for all values of specific energy[50]. For soft ores, the specific energy is lower, therefore the constant 0.53 kWh/tonne is a more significant source of error than it would be for hard ores with higher mean specific energy requirements. Figure 4-15 and Figure 4-16 show the error contributions for the medium (70 minutes) and hard (110 minutes) ores in. It can be seen that at 70 minutes the feed size model comprises approximately 45% of the error, and at 110 minutes it contributes 58% of the error, with the primary calibration error reduced to only 4% of the total error.

[50] *see* assumptions one and two on page 78

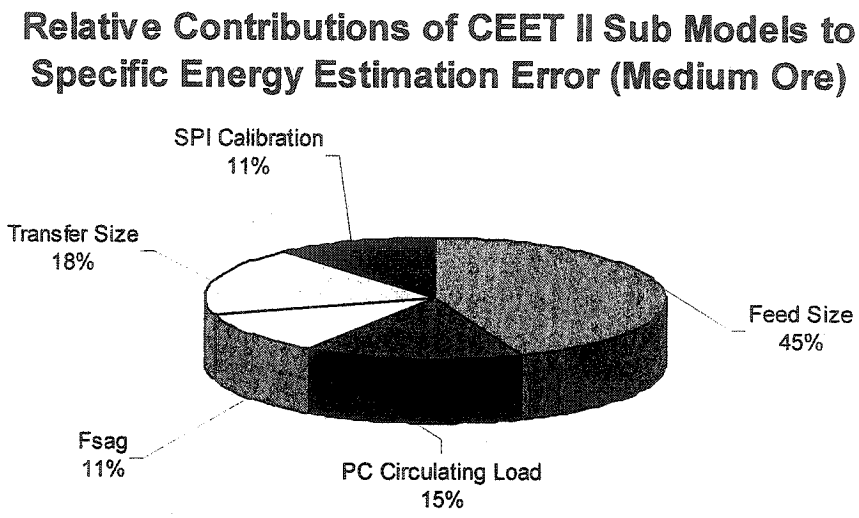

Figure 4-15 CEET II error contributions for "medium" ore

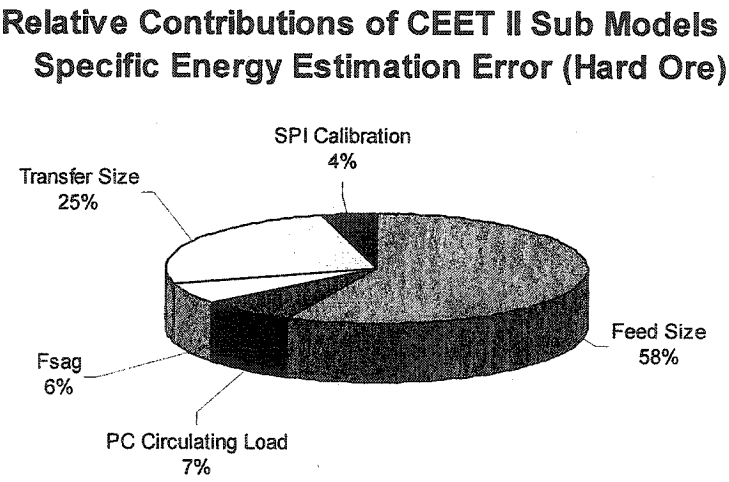

Figure 4-16 CEET II error contributions for "hard" ore

4.2.2.2 INCLUDING SPI ESTIMATION ERROR

In Section 4.1 a method was presented for quantifying the expected error of the geostatistical interpolations as a function of the distance between samples. An example of the calculations for a one-month time period was illustrated and the results presented in Table 4-2 on page 73. In this section the standard error of the mean SPI (the y-axis in Figure 4-2) is converted into the standard error of the mean specific energy. Because the specific energy is linearly correlated with throughput (by simple multiplication with

power draw), the relative error of the specific energy estimates is the same as the error of the resulting throughput estimates.

When integrating the SPI model errors (CEET errors) with the geostatistical errors, an important assumption must be made. Because the objective of this study is to determine the standard error of the mean specific energy, the error variance must be divided by the number of points used to calculate the error variance as per Equation 4-3.

$$S^2 = \frac{\sigma^2}{n}$$

Equation 4-3

With SPI calculations this is straightforward—one simply divides the error variance by the number of samples in the face or faces—but the CEET models were developed from 1-hour sampling campaigns conducted on operating grinding circuits. The correct number of points for error variance calculations is thus related to the number of unique or independent operating conditions experienced by the grinding circuit during the time frame that it would be processing the ore represented by the SPI samples. This, in turn, is related to the frequency of ore type changes and the autocorrelation properties of grinding mill variables like feed size, transfer size, and circulating load.

A series of sampling campaigns on a single grinding circuit over a large, continuous time frame would provide a definitive answer, but for the limited scope of this thesis the number of SPI samples was used as an estimate of the number of independent grinding line conditions. It is thought that this assumption is very conservative given the large amount of ore represented by a single SPI sample. Hence, the specific energy errors presented in this section should be considered maximum errors.

The first step in the process of integrating the model errors with the geostatistical errors is to estimate the standard error for each SPI sample collected in the faces. For each sample interval the variance of the mean SPI is multiplied by the number of samples in the ore volume. Taking the square root yields the estimated standard deviation of each equally spaced SPI sample. This standard deviation becomes the SPI error used in Step 1 of the simulation algorithm (recall that it was set to 0 for the analysis presented in the previous section). Calculations for the one-month period of the Chino example are shown in Table 4-13.

Months in Period	Spacing (ft)	Spacing (m)	Ext. Var (min2)	#comp.in face	Est var. face (min2)	Total # Comps	Est var. total (min2)	Standard error (min.)	**Error per Composite (min)**
1	500	152	410	1	684	2	342	18.5	**26.2**
1	450	137	400	1	541	2	270	16.4	**23.2**
1	400	122	390	1	417	2	208	14.4	**20.4**
1	350	107	380	1	311	2	155	12.5	**17.6**
1	300	91	369	2	222	4	111	10.5	**21.1**
1	250	76	358	2	149	4	75	8.6	**17.3**
1	200	61	346	4	92	8	46	6.8	**19.2**
1	150	46	331	7	50	14	25	5.0	**18.7**
1	100	30	303	15	20	30	10	3.2	**17.3**
1	50	15	231	60	4	120	2	1.4	**15.5**

Table 4-13 SPI errors per composite (last column on right) for 1-month period at Chino Mines

The second step is to input the errors for each composite into the simulation program. In doing so, it was observed that for the very large composite errors (*i.e.* the 152 m spacing scenario in Table 4-13 that yields a 26.2 minute SPI composite error) the simulations would generate occasional negative values for SPI. This was corrected by setting a minimum acceptable value of 10 minutes for SPI. The floor value is consistent with observed SPI values from the Chino deposit and is not deemed to significantly affect the overall error calculations.

The simulation program was run for the four operating periods. The resulting standard deviations of the specific energy, when divided by the mean, yield the relative standard estimation error of the specific energy. This equates to the estimated throughput error as per Equation 2-5 on page 25.

The new precision curves are shown in Figure 4-17.

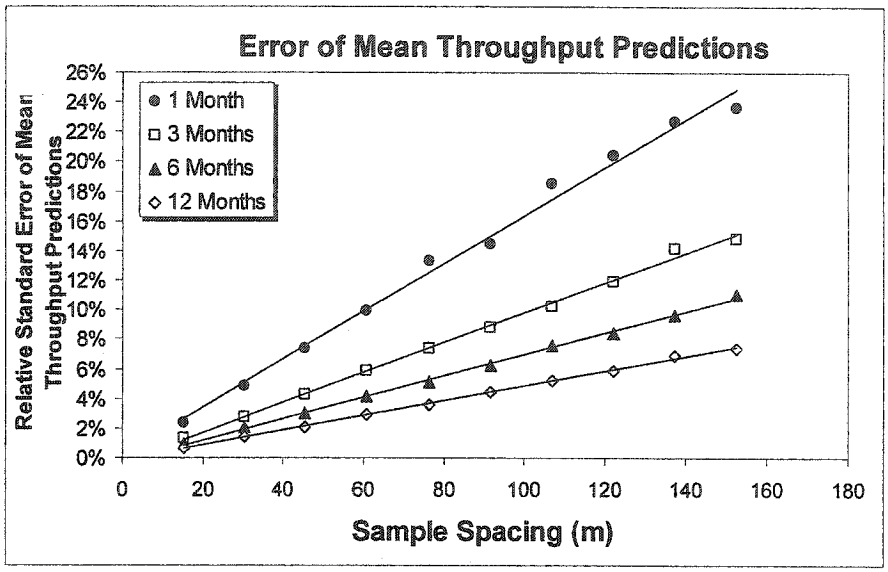

Figure 4-17 Error of mean throughput predictions versus sample spacing – CEET error included

At Chino Mines, the increase in throughput precision with decreasing sample spacing is due almost entirely to the central limit theorem; *i.e.* the increased geostatistical knowledge of the hardness properties resulting from smaller sample spacing does not significantly improve the throughput error for a single sample. To illustrate this, simulation studies were performed for different spacing intervals (30-meters, 100-meters, and infinite spacing; *i.e.* a pure nugget effect[51]). The relative contributions of the CEET sub-models to the total specific energy errors are shown in Figure 4-18 for the case of no spatial correlation (pure nugget effect). Approximately three quarters (76%) of the error is due to imperfect knowledge of the ore hardness and the rest is due to the SPI models. This error drops to 65% for the case of 100 m sample spacing (Figure 4-19), and to 61% for the case of 30 m sample spacing (Figure 4-20).

This trend is attributable to the fact that the variogram for Chino increases rapidly from a low nugget effect. This rapid increase means that the hardness can change very quickly within the ore body (an observation supported by the experience of plant personnel at Chino).

[51] "pure nugget effect" means that no spatial correlation exists between SPI values. In this case the variogram would be a horizontal line equal to the variance of all SPI samples in the ore body. For this simulation study, the standard deviation of SPI in the ore body was used as the SPI estimation error.

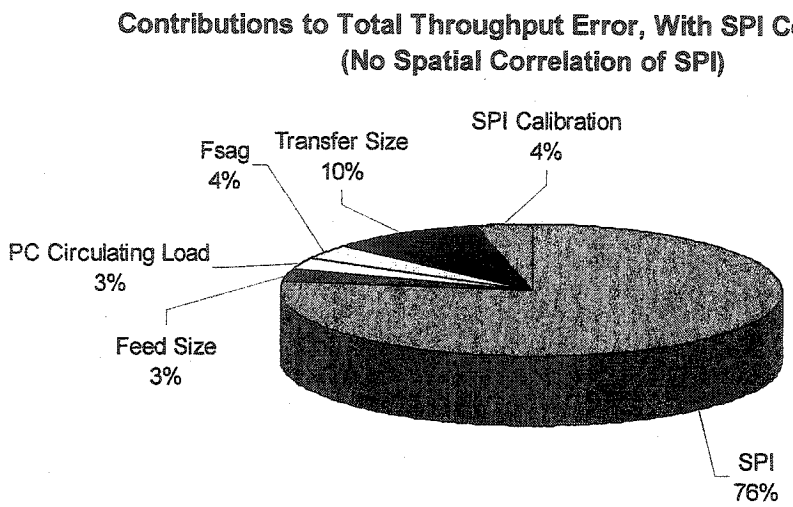

Figure 4-18 Contribution to error assuming no spatial correlation of SPI

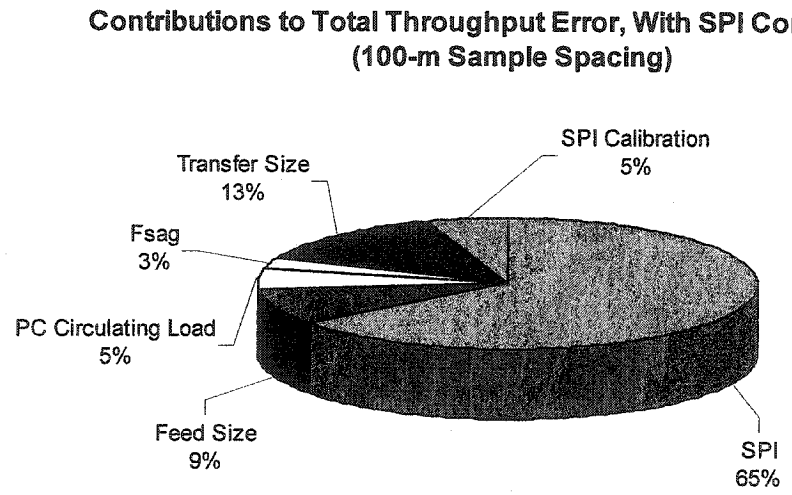

Figure 4-19 Contributions to error for 100-meter spacing

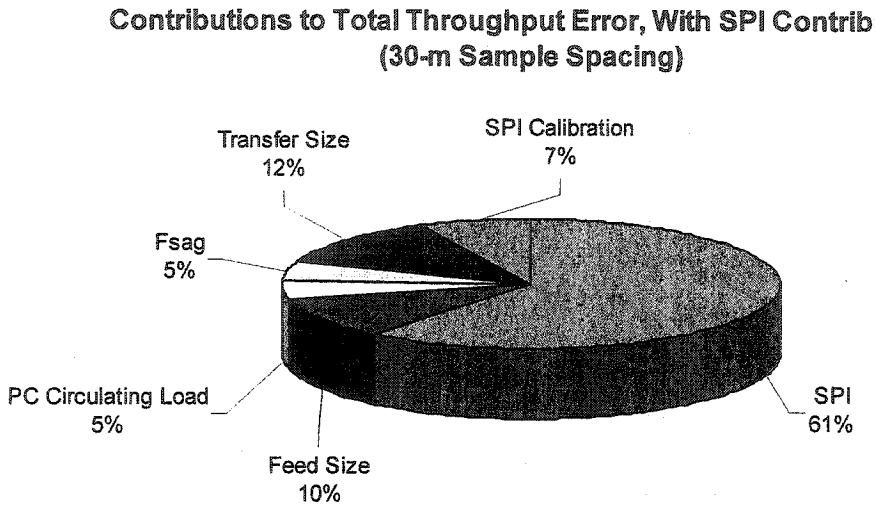

Figure 4-20 Contributions to error for 30-m spacing

This is not to say that the benefits of increased test work are muted. The error of the mean specific energy estimates for a one-year period is reduced from nearly 5% to 1.3% by reducing the sample spacing from 100 m to 30 m (and increasing the number tests from 28 to 360). Figures are shown in Table 4-14.

F80 mean	PCCL mean	Fsag mean	T80 mean	Sp. Energy mean	Sample Spacing	SPI Composites	St. Erro
(mm)	(%)		(mm)	kWh/tonne	(m)	#	%
70	27	0.74	2.6	5	100	28	5.3%
70	27	0.74	2.6	5	30	360	1.4%

Table 4-14 Standard error of mean specific energy estimates for 100-m spacing and 30-m spacing cases

5 DISCUSSION

This section is a discussion of questions that arose during this research project. It is divided into four sections:

- Discussion of the blending and modeling work on the SPI test,
- Discussion of the analysis of the geostatistical properties of the SPI and methods for interpolating the values
- Discussion of the CEET error analysis
- Discussion and interpretation of the Chino example

5.1 BLENDING

Previous work has suggested (Section 2.3.2) that the SPI is not an additive parameter. The analysis presented in Section 3 has shown that the blending of ore can be mathematically predicted by considering the entire curve of percent retained (10-mesh) versus time. The curves are additive even if the SPI (a single point on a curve) is not.

Modeling of the SPI grind curve is necessary for mathematical blending studies. The improper modeling of an SPI curve results in errors in the blending model. For example, it was mentioned that soft ores are difficult to model because the cut-off point of the test is too close to the origin for proper extrapolation of the model, particularly when attempting to blend the soft ore with a harder ore. This is a source of error in blending studies; however, the error can be minimized by use of the correct models for soft, medium, and hard ores. It can be further minimized by instituting the recommended changes in the SPI test procedure discussed in Section 3.4.1.

5.2 GEOSTATISTICS

The geostatistical investigations were performed at Chino Mines before the blending studies were undertaken in Toronto, Canada. For economic and commercial reasons,

the development of the geostatistical methodology for ore body characterization at Chino Mines was completed before the question of SPI additivity was resolved. As a result, the geostatistical analysis described was developed using the raw SPI, which, as shown and explained in Section 3, is not an additive parameter.

While a comparative study is the only way to quantify the errors associated with the method used at Chino, it is thought that the resulting error is not significant for several reasons.

1. The geostatistical estimations resulting from use of the raw SPI values will result in *positive* estimation error; *i.e.* the true value is lower than the estimated value. This means that the corresponding throughput estimates will err slightly on the side of caution.
2. The SPI is raised to a power between 0 and 1 in the primary SPI calibration equation (Equation 2-4), thereby reducing the magnitude of the error due to the SPI value.
3. Significant error only arises when very hard samples are blended with very soft samples. This would be analogous to estimating the SPI value of an unknown point in the ore body between a hard and soft composite sample. Geographic trends in ore hardness, as quantified by the variogram, reduce the likelihood of this scenario.

The correct geostatistical methodology incorporates the blending conclusion in the geostatistical process as follows:

1. Variograms should be created for various points along the time axis of the grind curve. For example 10 minutes, 30 minutes, 60 minutes, and 120 minutes, producing a set of four variograms.
2. Each point should be kriged using its respective variogram and the resulting grind curve estimated using one of the models described in Section 3.1.
3. The resulting SPI value should be estimated from the kriged grind curve.

It may be possible to use only a single variogram if the four variograms described in Step 1 show significant similarities. An investigative study should be conducted in this regard.

The procedure for the geostatistical estimation of the entire grind curves adds to the effort required to produce the precision curves. Whether this is justified by the additional accuracy thus obtained should be investigated.

If variograms are created for several points along the time axis of the SPI grind curve, it would be useful to change the SPI test procedure to fixed-length iterations instead of the variable-length used in the current procedures. This would allow the use of the measured value for variogram analysis and kriging, instead of a value estimated from a model. Continuing the test on soft ores to well past the SPI point would also diminish the error resulting from model extrapolation.

The geostatistical properties of the crusher index were not investigated or included in this study. The large contribution of the feed size model to the total estimation error indicates that the crusher index errors could contribute significantly to overall errors. It also indicates that better methods for estimating feed size would decrease the error. Such methods may include image analysis on exposed faces in the pit and/or consideration of mine blast patterns and powder factors.

5.3 CEET ERROR ANALYSIS

The CEET error analysis considers all errors caused by the scatter of the various sub-models used to return a specific energy value from the SPI, crusher index, and various operating and plant parameters. It was based on the assumption that the variance of the predicted variable is constant for fixed values of the calculated variable. The only exception is the feed size model used, which shows increasing absolute variance with mean feed size.

The error analysis study has shown that the calculation of specific energy from a single drill core sample is subject to an error of approximately 20 – 26 percent (at the 68%

confidence interval). This includes all errors attributable to the model calibration scatter. It does not include errors due to SPI or mill power draw.

It is worth commenting on this error. When a plant is surveyed, the resulting analysis is based on the observed values of feed size distribution, transfer size distribution, and pebble crusher circulating load. In this case the error is substantially lower (actually equivalent to the 0.51 kWh/tonne of the primary SPI calibration). The 20 – 26 percent error described above is based on the SPI obtained from a single 2-kg composite sample collected from the pit. This SPI value is then used to estimate the F_{80}, F_{50}, PCCL, T_{80}, F_{SAG}, and specific energy as illustrated in Figure 4-12.

5.4 THE CHINO EXAMPLE

The Chino example has shown that the improvement in the throughput error that results from a larger sampling effort is entirely explained by the central limit theorem. In other words, the benefits of using an approach based exclusively on kriging are non-existent for economically viable sample intervals at Chino.

This is a natural result of the hardness continuity expressed by shape of the variogram at Chino: a low nugget effect followed by a sharp increase near the origin of the distance axis. It is thought that one reason the variogram shows this shape is because it was created from sample pairs that have been select irrespective of geologic or lithologic zoning. The shape of the variogram might improve by respecting structural boundaries within the ore body when pairing points for variogram calculation. Another option is to create individual variograms for lithologic zones. In either case, more accurate variogram modeling of the spatial continuity of SPI will result in greater possible sample spacing for the same nominal forecast errors.

The difficulty with the above suggestions is that the number of required sample points starts to increase quickly as the new criteria eliminate possible composite pairs. One alternative is to calculate the global omni-directional variogram as exemplified by the Chino variogram, and then to scale the sill according to the variance of SPI values within each specific lithologic zone. This would effectively lower the sill of the variogram (and

hence the estimation error of the SPI) for lithologic zones that have relatively minor hardness variations.

Another alternative is to use rock type, alteration, grade, and any other secondary information to improve the geostatistical estimates. In this method a principal component analysis is performed to identify the variables that have the highest correlation with SPI value. These variables are then used in a multi-regression analysis to estimate SPI values. The estimated values are combined with the geostatistical results according to the inverse of the estimation variance for each method. The result is an estimate lower than either method would give independently.

All of these suggestions are options for improving the estimation error of the mean specific energy. Obviously each one entails an economic expenditure. Assuming that the variogram and secondary correlations are not improved substantially by more sampling and testing (a questionable assumption), the above example from Chino suggests that only marginal improvements in the geostatistical estimates would result from increasing the sampling program from 28 to 360 SPI samples for a 1-year program. This indicates that for short-term periods and/or low-production operations the diminishing returns of the geostatistical approach make it an undesirable alternative to the standard ore-class approach described in 4.1.1. In fact, in this situation performing one or a few tests on a sample composite or composites will give the same indication of the mean specific energy (but with all the smoothing problems associated with sample compositing). Note that this result is specific to Chino Mines. Other ore bodies sampled, particularly from South American copper porphyry deposits, have shown much greater degrees of hardness continuity within the ore body.

6 CONCLUSIONS

6.1 GENERAL

This research project has developed a methodology for characterizing the hardness, in terms of the SAG Power Index, of an ore body for grinding circuit design and optimization through the following steps:

1. Studying through ore blending experiments the additivity of the SPI and its implications for geostatistical or geometrical interpolation procedures
2. Adapting in collaboration with a geostatistical advisor the geostatistical procedures used for ore grade estimation to hardness estimation, and using them to quantify the error of the resultant estimates based on the distance between samples in an ore body
3. Using the error determined in step two in a Monte-Carlo simulation study that quantifies the propagation of error through the complex CEET II calculations that are used to convert SPI to required specific energy of an ore in an autogenous mill.

Conclusions specific to each step in the procedure are summarized below.

6.1.1 Blending

- The SPI test can be adequately modeled by representing the percent retained in the plus 10-mesh fraction (1.7 mm) versus time as one of several exponential curves.
- The use of these models enables the prediction of the behaviour of a blend of ores based solely on the models of its parent ores.
- The SPI is not an additive parameter. Geostatistical and blending studies should consider the entire curve of grind versus time if an additive parameter is desired.

6.1.2 Geostatistics

- Geostatistical methods can be used to estimate the standard error of the mean SPI value in a face or faces.
- For low-production operations or short time periods, an ore characterization approach based on ore classes may offer the most attractive cost/benefit ratio
- The SPI variogram at Chino mines suggests that the SPI has a low nugget effect, followed by a steeply increasing variance very close to the origin of the distance axis, reflecting high variability over short distances in the ore body
- At economically feasible sampling efforts, there is little improvement in error resulting from the kriging of closely spaced SPI values; instead, the improvements are due to the statistical implications of the central limit theorem and the larger sampling efforts involved. This is a result of the high hardness variability as shown by the variogram of SPI.
- Consideration of variability within ore zones and relationships between SPI and secondary variables such as lithography, alteration, assay, *etc.*, may improve the geostatistically-caused error of the throughput estimate. Methods for doing so were discussed in Section 5.4.

6.1.3 CEET Error Analysis

- The combined error of a specific energy estimate using the CEET II models accounting for the effects of feed size, circulating load and transfer size within the primary SPI calibration equation is approximately 20 to 26 percent.
- The majority of the error inherent in the CEET II calculations can be attributed to scatter in the feed size model and the propagation of this scatter throughout the other sub-models that require knowledge of the feed size
- As the value of the SPI decreases the percentage of the specific energy error attributable to scatter in the primary calibration model increases and that attributable to the feed size model decreases.
- For the work conducted at Chino mines, it was determined that the error attributable to the precision of CEET II accounts for approximately one third of the estimation error for SPI cell of influence, with the remainder attributable to geostatistical considerations.

6.2 RECOMMENDATIONS

- Perform SPI interpolation in an ore body respecting the entire curve of grind versus time instead of only a single point (*i.e.* the SPI).
- Modify the SPI test procedures to fix the lengths of the grind iterations at constant periods. This will facilitate the modeling of the SPI grind curve and the geostatistical or geometrical interpolation methods used to model the ore body. It will also eliminate duplication of points near the test completion point, thereby decreasing the time required to perform a test.
- Extend the SPI grinding time on soft ores to beyond the current SPI-defined completion time. This will eliminate errors caused by the extrapolation of models on soft ores.
- To reduce the error of the geostatistical interpolations, perform variogram calculation and kriging such that ore zone boundaries are respected and use correlation with secondary variables. Methods for doing so are proposed in Section 5.4.
- For low-production or short-term time frames consider the ore-class approach to modeling or compositing samples due to the diminishing benefit/cost ratio of the geostatistical methodology

6.3 FUTURE WORK

- Study the geostatistical properties of the crusher index C_F and the effects on the precision of the mean specific energy forecasts that result from geostatistical estimation of the crusher index in the ore body.
- Investigate the error of the mill power draw estimates used to calculate the final throughput values. The power draw is related to size of the mill shell relative to the installed motor power; the liner, grate, and pebble crusher configurations; the size and competency of the ore feeding the mill; its density and rheology inside the mill; and the operating practices used to control the mill. Because the power draw is directly proportional to the throughput (refer to Equation 2-5), the error attributable to power draw is a significant one and in the opinion of the author has not been adequately investigated. It would be an interesting research project to

attempt to characterize mill power draw as a function of ore characteristics. Models exist for characterizing material transport and mill load in autogenous mills. If these can be adopted for ore body characterization, a significant source of error would be removed from the CEET calculations.

- Perform a comparative study to quantify the differences between direct geostatistical interpolation of SPI and the interpolation of the entire SPI grind curve. If the differences are insignificant, it may not be necessary to interpolate the entire curve grind versus time. This would greatly simplify the development of the precision curves. If the differences are significant, it may be necessary to develop a methodology for developing the precision curves such that the entire SPI grinding curve is accounted for in the face calculations.
- Develop and exemplify the procedure for incorporating the relationships between SPI and secondary variables in the interpolation procedures.
- Investigate alternative methods for improving the feed size models. Because the feed size models comprise the largest portion of the CEET II error, reductions in the feed size models will lead to reductions in the specific energy predictions. Options for consideration include considering ore blasting practices and/or image analysis of exposed faces.

7 ACKNOWLEDGEMENTS

The author wishes to thank the following individuals and organizations for their support and contributions to this research project.

- McGill University, in particular Dr. André Laplante for his advising role
- MinnovEX Technologies Inc., and in particular Dr. Glenn Dobby for his advising role
- Geostat Systems International, in particular Mr. Michel Dagbert for development of the Chino variograms and precision curves and education regarding all geostatistical matters. Mr. Dagbert is also an advisor to this Masters program.
- Phelps Dodge Chino Mines, in particular Mr. James Vanderbeek, for the commercial support without which this project could not have been done
- NSERC, for the financial assistance that enabled this research work to proceed.
- The author's parents Roger and Annemarie in Squamish, B.C., for the reference sources (Roger) and cappuccinos (Annemarie) generously provided during the writing of this thesis

8 BIBLIOGRAPHY

Amelunxen, P., "Minnovex SPI Grind-Time Variations in Hard/Soft Ore Combinations", MinnovEX Technologies / NSERC study, Toronto, Ontario, 1997.

AMMTEC (Australian Metallurgical and Mineral Testing Consultants) website, Comminution Services, http://www.ammtec.com.au, 2002

Barratt, D.J., and Sochocky, M.A., "Factors Which Influence Selection of Comminution Circuits", Design and Installation of Comminution Circuits, Mular, A.L., and Jergensen, G.V., editors, American Institute of Mining, Metallurgy, and Petroleum Engineers, Inc., 1982.

BMHB (British Materials Handling Board), Particle Attrition, State-of-the-Art Review, Trans Tech Publications, Belgium, 1987.

Bond, F.C., 1985. SME Mineral Processing Handbook, SME-AIME 1985, Ch. 4., pp 3C-57 to 3C-59.

Custer, S., Garretson, P., McMullen, J., Bennett, C., and Dobby, G., "Application of CEET at Barrick's Goldstrike Operation", Proceeding of the 33rd Annual Meeting of the Canadian Mineral Processors, Ottawa, 2001.

Dagbert, Michel, Geostatistics for Ore Reserve Estimation and Grade Control, Seminar Notes, Geostat Systems International, Toronto, Ontario, 2001.

David, Michel, Handbook of Applied Advanced Geostatistical Ore Reserve Estimation, Elsevier Science Publishing Company Inc., New York, 1988.

Deister, R.J., "How to Determine the Bond Work Index Using Lab Ball Mill Grindability Tests", **E and MJ**, February 1987, pp 42-45.

Digre, Marcus, "Testing for AG/SAG Circuits", Proceedings of the Conference on International Autogenous and Semi-autogenous Grinding Technology 1989 (SAG 1989), Vancouver, British Columbia, 1989.

Dobby, G., Bennett, C., and Kosick, G., "Advances in SAG Circuit Design and Simulation Applied to the Mine Block Model"., Proceedings of the Conference on International Autogenous and Semi-autogenous Grinding Technology 2001 (SAG 2001), vol. 4, Vancouver, British Columbia, 2001.

Farrow, C.J., and Smith, M.J., "Bench and Pilot-Scale Test Programs to Specify Autogenous Grinding Programs", 14th Annual Meeting of the Canadian Mineral Processors, Ottawa, 1982.

Frohling, Edward S., and Lewis, Milton F., "Fesibility Study", Mineral Processing Plant Design, 2nd Edition, Ch. 1, Mular and Bhappu, Editors, American Institute of Mining, Metallurgical, and Petroleum Engineers, Inc., 1980.

Hart S., Valery W., Clements B., Reed M., Song M., and Dunne R., "Optimisation of the Cadia Hill SAG Mill Circuit", Proceedings of the Conference on International Autogenous and Semi-autogenous Grinding Technology 2001 (SAG 2001), vol. 1, Vancouver, British Columbia, 2001.

Isaaks, Edward H., and Srivastava, R Mohan, An Introduction to Applied Geostatistics, Oxford University Press, New York, 1989.

Jones, Stuart M., "Appendix of AG-SAG Installations Worldwide", Proceedings of the Conference on International Autogenous and Semi-autogenous Grinding Technology 2001 (SAG 2001), vol. 1, Vancouver, British Columbia, 2001.

JKMRC, "The JK Drop Weight Tester; Test Procedure", Adobe Acrobat download, www.jktech.com, 2003.

Kosick, G., Dobby, G., and Bennett, C., "CEET (Comminution Economic Evaluation Tool) (For Comminution Circuit Design and Production Planning)", Proceedings of the SME, Colorado, USA, 2001.

Kosick, Glenn, "Philosophy of SPI/CEET Arrangement with CEET Partners", internal correspondence, 2000

Kosick, G.A., and Bennett, C, "The Value of Ore body Power Requirement Profiles for SAG Circuit Design", Proceedings of the 31st Annual Meeting of the Canadian Mineral Processors, Ottawa, 1999.

Lane, G., Bennett, C., and Villanueva, C., "Cerro Corona Grinding Circuit Design", Proceedings of the Conference on International Autogenous and Semi-autogenous Grinding Technology 2001 (SAG 2001), vol. 4, Vancouver, British Columbia, 2001.

Leung, K., Morrison, R.D., and Whiten, W. J., "En Energy Based Ore Specific Model for Autogenous and Semi-Autogenous Grinding", Mineral Processing and Process Control, Mular, A., Gonzalez, G., and Barahona, C., editors, Copper '87, volume 2, Universidad de Chile, Santiago, Chile, 1987

Rowland, Chester A., "Rod and Ball Mills", Mineral Processing Plant Design, 2nd Edition, Mular and Bhappu, *ed.*, Ch. 9, pp 239-278, SME of the AIME, New York, 1980

Rowland, Chester A., "Testing for Selection of Autogenous and Semi-Autogenous Grinding Mills and Circuits", Proceedings of the Conference on International Autogenous and Semi-autogenous Grinding Technology 1989 (SAG 1989), Vancouver, British Columbia, 1989.

Lynch, A.J., and Lees, M.J., "Simulation and Modeling", SME Mineral Processing Handbook, Vol 1., Ch. 6., SME of the AIME, New York, 1985

McLaren, D., Mitchell, J., Seidel, J., and Lansdown, G., 2001. "The Design, Startup, and Operation of the Batu Hijau Concentrator", Proceedings of the Conference on

International Autogenous and Semi-autogenous Grinding Technology 2001 (SAG 2001), vol. 4, Vancouver, British Columbia, 2001.

McPherson, Arthur R., and Turner, Robert R., "Autogenous Grinding From Test Work to Purchase of a Commercial Unit", Chapter 13, Mineral Processing Plant Design, vol 2, Mular and Bhappu, editors, Society of Mining Engineers of the AIME, New York, 1980.

McPherson, A.R., Knight, Doug A., Medina, V. G., and Spiller, D. Erik, "Case Histories of Using Small-Scale Tests to Design SAG Mill Circuits", Proceedings of the Conference on International Autogenous and Semi-autogenous Grinding Technology 1989 (SAG 1989), Vancouver, British Columbia, 1989.

McPherson, Arthur R., "The Development of Autogenous Grinding and Semi-Autogenous Grinding", Proceedings of the Conference on International Autogenous and Semi-autogenous Grinding Technology 1989 (SAG 1989), Vancouver, British Columbia, 1989.

Mitchell, J., and Holowachuk, N.V., "Ore Blending at Highland Valley Copper Its Necessity, Effects, and Benefits" Proceedings of the Conference on International Autogenous and Semi-autogenous Grinding Technology 1996 (SAG '96), vol. 1., Vancouver, British Columbia, 1996.

MinnovEX Technologies Inc., "Hard Ore Methodology for Falconbridge-Raglan", Internal Correspondence with Glenn Dobby, 2001.

MinnovEX Technologies Inc., "MinnovEX SPI Standard Test Procedures", internal documentation, 2001.

MinnovEX Technologies Inc., "Determination of the Best Block Model Estimation Method for SPI and Bond Wi Data for the Escondida Ore body (Edited for CEET Partner Distribution)", June 2001, Toronto

MinnovEX Technologies Inc., "Justification for Benchmarking a Grinding Circuit," Internal Documentation, May, 2001, Toronto

Mosher, John, and Bigg, Tony. "SAG Mill Test Methodology For Design and Optimization", Proceedings of the Conference on International Autogenous and Semi-autogenous Grinding Technology 2001 (SAG 2001), vol. 1, Vancouver, British Columbia, 2001.

Napier-Munn, T.J., Morrell, S., Morrison, R.D., Kojovic, T. "Mineral Comminution Circuits Their Operation and Optimisation". Julius Kruttschnitt Mineral Research Centre, University of Queensland, 1999.

Sherman, Mark, "Optimization of the Alumbrera SAG Mills", Proceedings of the Conference on International Autogenous and Semi-autogenous Grinding Technology 2001 (SAG 2001), vol. 1, Vancouver, British Columbia, 2001.

Starkey, J., and Dobby, G., "Application of the Minnovex SAG Power Index at Five Canadian SAG Plants", Proceedings of the Conference on International Autogenous and Semi-autogenous Grinding Technology 1989 (SAG 1989), Vancouver, British Columbia, 1989.

Starkey, J., "Getting more from Drill Core - Preliminary SAG Design", Randol Gold Forum, Monterery, California, 1997

Starkey, J., Dobby, G. and Kosick, G., 1994, "A New Tool for SAG Hardness Testing", Proc. Canadian Mineral Processor's Conference, Ottawa.

Taggart, Arthur F., Handbook of Mineral Dressing, Ores and Industrial Minerals, John Wiley and Sons, Inc., New York, 1945.

Wyslouzil, D.M., "Standard Laboratory-Pilot Plant Tests for Equipment Selection", Design and Installation of Comminution Circuits, Mular, A.L., and Jergensen, G.V., editors, American Institute of Mining, Metallurgy, and Petroleum Engineers, Inc., 1982.